Taxonomic and Palaeobiological Assessment of the South African Mosasaurids

Megan Rose Woolley

University of Cape Town, South Africa

DISSERTATION

Presented for the degree of Master of Sciences in the Department of Biological Sciences,

University of Cape Town

2020

Supervisor: Anusuya Chinsamy-Turan (UCT)
Co-supervisor: Michael Wayne Caldwell (UA)

PLAGIARISM DECLARATION

I understand the meaning of plagiarism and I declare that all of the work in the following dissertation, expect for that which I have properly acknowledge, is my own.

Signed by candidate

Megan Rose Woolley

10 August 2020

Contents

List of Figures

List of Tables

Acknowledgements

I would like to extend a huge thanks to the following people and organisations for the successful completion of my Masters dissertation:

- The National Research Foundation Grantholder linked bursary (AOP fund number 117716) for funding this project.
- Prof. Anusuya Chinsamy-Turan for welcoming me into her research group and giving me the opportunity to work on something I am so passionate about. I thank her for her endless support, encouragement, patience, enthusiasm and guidance throughout my time as her student.
- Dr Michael Caldwell for his encouragement and guidance throughout the duration of this project. His knowledge and passion of these animals is inspiring!
- Zaituna Erasmus and the staff of Karoo Palaeontology at the Iziko Museum of Cape Town for access to the SAM-PK-5265 specimens. A huge thanks to the preparators who spent long hours preparing the fossils.
- The staff at the Council for Geoscience for access to the CPG/1/2265 specimen.
- Kholisile Nzolo, Ragna Redelstorff and Zaituna Erasmus for permission to perform analyses on the specimens.
- Dr Roopam Dey, Dr Aaron Le Blanc, Paul Keanly, Dr Petrus Le Roux, Dr Kevin Rey, Dr Julie Luyt, Miranda Waldron, Petra Muller, Dr Lynn Harrel Jr., Dr Romain Amiot, Dr Nathalie Bardet for their contributions and for sharing their knowledge.
- The students and postdocs of the UCT Palaeobiology Research Group for their friendship, assistance and support.
- My friends in the Biological Sciences Department and UCT for making the early mornings and late evenings enjoyable, and for their constant encouragement and understanding.
- My friends and family from afar for their kindness and motivation.
- Finally, my family - Sami, Denise and Andy Woolley and my boyfriend - Ivan Poulter for their endless love and support in everything I do. I am so grateful.

Abstract

South African mosasaur remains consist of a frontal with articulating portions of the parietal and postorbitofrontals (SAM-PK-5265); two dentary fragments (SAM-PK-5265) assigned to '*Tylosaurus capensis'* by Broom in 1912 (SAM-PK-5265); an undescribed muzzle unit and associated isolated teeth (CGP/1/2265) from Pondoland and a more recently discovered isolated partial vertebra from St Lucia. Some research has been done on the material, but there is still uncertainty concerning their relationships and taxonomy. This research aims to provide a taxonomic assessment of all the SA mosasaurid material to better understand their phylogenetic relationships and to place them in the context of mosasaurs from other parts of Africa and globally. In addition, isotopic analyses, micro-computed tomography (micro-CT), mineralised tissue histology and scanning electron microscopy (SEM) are applied to the SA mosasaur remains to decipher various aspects of their palaeobiology. This study identifies three mosasaur taxa from SA: *Mosasaurus sp., cf. M. hoffmannii.*, cf. *Taniwhasaurus*, and cf. *Prognathodon*. The isolated vertebra is assigned to *Mosasaurus sp., cf. M. hoffmannii.* The frontal and dentary fragments (SAM-PK-5265) originally described as *Tylosaurus* appears to be a mix of two taxa: One of the dentary fragments possesses replacement teeth with enamel ornamentation that resembles, *Ta. mikasaensis*, but is tentatively assigned to cf. *Taniwhasaurus* based on tooth recurvature. The other dentary fragment and a frontal with articulated elements are suggested to belong to the same individual as the muzzle unit for which the suggested assignment is cf. *Prognathodon.* Strontium analysis of tooth enamel dated the cf. *Prognathodon* material to the end of the Maastrichtian ($^{87}Sr/^{86}Sr = 0.707817$; age = 66.85Ma). The cf. *Taniwhasaurus* dentary fragment is likely Santonian-aged, as originally indicated in 1901. SEM of enamel from cf. *Prognathodon* reveals a complex array of prismless enamel types and pervasive aggregations of

fossilised bacteria in the underlying dentine. The $\delta^{18}O_{PO4}$ derived body temperature estimate (T_b) of the cf. *Prognathodon* (T_b = 33.21°C) compares well with previously reported T_b for mosasaurs and may indicate that the mosasaur was capable of maintaining a T_b higher than that of the surrounding seawater.

Keywords: mosasaur, *Tylosaurus capensis, Prognathodon, Taniwhasaurus, Mosasaurus,* SEM, fossilised bacteria, Sr isotopes, O isotopes.

Chapter 1: Introduction

1.1) Overview: Mosasaurs

Mosasaurs were a large group of extinct marine reptiles of the order Squamata that arose in the Cenomanian, approximately 95 million years ago [Ma] (Russell, 1967). A drastic rise in sea level during the mid-Cretaceous flooded the continents forming large intercontinental seas (Ellis, 2003). It is hypothesised that small, limbed semi-aquatic lizards commonly referred to as aigialosaurs colonised these shallow intercontinental seas and then rapidly evolved into diverse lineages of obligatorily aquatic, often colossal, marine predators that are known as mosasaurs, which reached peak diversity just before their extinction at the end of the Maastrichtian around 66.0Ma (Ellis, 2003; Russell, 1967; Simões *et al*., 2017; chronology follows Cohen *et al.*, 2018).

1.1.1) Phylogeny and palaeobiogeography

The presence of remains from Late Cretaceous deposits of every continent suggests that mosasaurs achieved a global distribution during their relatively short reign (Bell, 1997). The mosasaur fossil record is relatively well-studied and a generally accepted broad phylogeny exists. Mosasauroidea is a superfamily, which includes the Aigialosauridae, small semi-aquatic stem mosasaurs that were basal to the Mosasauridae, which were more derived and are more widely-known mosasaurs (Bell, 1997; Simões *et al*., 2017). The Mosasauridae is divided into six subfamilies: Halisaurinae, Yaguarasaurinae, Tethysaurinae, Tylosaurinae, Plioplatecarpinae, and Mosasaurinae (Simões *et al.*, 2017). Each of the aforementioned subfamilies are briefly discussed with regards to their palaeobiogeographical distribution and temporal range in this section. Diagnostic features of the subfamilies are summarised in Appendix A.

Halisaurinae

Halisaurinae was established as a clade by Bardet *et al.* (2005). This group is relatively rare and poorly understood but is suggested to be the most basal clade within Mosasauridae (Polcyn *et al.*, 2012). The group shares plesiomorphic characters with those marginally modified squamates such as *Varanus* and *Aigialosaurus* (Bardet *et al.*, 2005; Polcyn *et al.*, 2012) but also exhibits characters unique to more derived mosasaurs (Fernández and Talevi, 2015). Despite the apparent rarity of halisaurine mosasaurs, the fossil record suggests that they had a wide palaeobiogeographical distribution with remains recovered from North America (Polcyn *et al*., 2012), South America (Caldwell and Bell, 1995; Fernández and Talevi, 2015), Europe (Lingham-Soliar, 1996; Lindgren and Siverson, 2005), Morocco (Bardet *et al.*, 2005), and Japan (Konishi *et al.*, 2016); as well as a wide stratigraphic range from the Santonian to the Maastrichtian (86.3±0.5 – 66.0Ma) (Lindgren and Siverson, 2005; Fernández and Talevi, 2015; Konishi *et al.*, 2016).

Yaguarasaurinae

Yaguarasaurus columbianus from the Turonian beds of Columbia, South America is considered to have one of the most primitive mosasaur morphologies and shares more skull characteristics with aigialosaurs than any other mosasaur (Páramo-Fonseca, 2000). Originally it was placed in the Plioplatecarpinae (Páramo-Fonseca, 2000); however, a new clade called Yaguarasaurinae (Palci *et al.*, 2013) was established and it was reassigned there with *Russellosaurus* (Polcyn and Bell, 2005a) and a new genus from Turonian deposits in Italy, *Romeosaurus,* which was erected at the same time (Palci *et al.*, 2013).

Tethysaurinae

Like the Yaguarasaurinae, the Tethysaurinae was established as a new clade relatively recently by Makadi *et al.* (2012). It is comprised of only two basal genera namely *Tethysaurus* (Bardet, Suberbiola and Jalil, 2003) and *Pannoniasaurus* (Makadi *et al.,* 2012) with one species representing each genus. *Tethysaurus nopcsai* was recovered from Early Turonian aged deposits in Morocco and is considered a basal mosasauroid (Bardet, Suberbiola and Jalil, 2003). *Pannoniasaurus inexpecticus* (Makadi *et al.,* 2012) was described and named based on a number of individuals of varying ontogenetic stages recovered from a Santonian-aged freshwater deposit in Hungary. It was found to possess a plesiomorphic pelvis, a pontosaur-like tail structure, a crocodile-like skull and limbs that resembled those of a terrestrial lizard, thus making it a basal mosasauroid (Makadi *et al.*, 2012).

Tylosaurinae

The Tylosaurinae (Williston, 1897) is a large clade of mosasaurs that achieved a wide palaeobiogeographical distribution. Members of this clade have been discovered on every continent, including Antarctica. Its current stratigraphic range is from the Turonian to Maastrichtian (93.9 – 66.0 Ma) (Jiménez-Huidobro, 2016), although they appeared to reach peak abundance in the Coniacian (89.8 – 86.3 Ma) (Polcyn *et al.*, 2014). This clade historically includes three genera, namely *Tylosaurus* (Marsh, 1872), *Taniwhasaurus* (Hector, 1874) and *Hainosaurus* (Dollo, 1885). However, a fairly recent mosasaur discovery from the Marambio Island of Antarctica has led to the formation of a new genus *Kaikaifilu,* of which there is only one species, *K. hervei* (Rubilar-Rogers *et al.*, 2016). Jimenez-huidobro and Caldwell (2016) reassessed the *Hainosaurus* type species, *Hainosaurus bernardi* (Dollo, 1885) from the early Maastrichtian deposits of Belgium, and determined that *Hainosaurus* should be included in the

Tylosaurus genus. Therefore, Tylosaurinae (Caldwell *et al.*, 2003) now comprises of *Tylosaurus, Taniwhasaurus* and *Kaikaifilu.*

Plioplatecarpinae

Plioplatecarpinae (Dollo, 1884) is typically placed as sister group to the Tylosaurinae (Jiménez-Huidobro, 2016) and is comprised of seven genera: *Ectenosaurus, Selmasaurus, Angolasaurus, Plioplatecarpus, Platecarpus, Latoplatecarpus* and *Plesioplatecarpus* (Konishi and Caldwell, 2009). There have been numerous changes to the nomenclature within and among the genera and tribes, which has led to much confusion and debate (Lingham-Soliar, 1994; Polcyn and Bell, 2005; Jacobs *et al.*, 2009). Novel genera such as *Latoplatecarpus* and *Plesioplatecarpus* have been added (Konishi and Caldwell, 2009). Despite this clade being considered one of the more derived, plioplatecarpines first appeared in the Turonian, and then sustained a relative abundance till the end Maastrichtian (Polcyn *et al.*, 2014). A new genus and species from the Maastrichtian of Morocco has since been added to this clade (Strong *et al.* 2020). This discovery allowed for a re-evaluation of the '*Platecarpus*' *ptychodon,* a problematic taxon and the validity of which is rejected by the authors. The new plioplatecarpine is named *Gavialimimus almaghribensis* (Strong *et al.* 2020).

Mosasaurinae

Mosasaurinae is the largest and the most diverse clade, particularly with regards to body sizes and forms within the group (Bell and Polcyn, 2005b; Polcyn *et al.*, 2014). They first appear in the Middle Turonian (~92 Ma) and are represented by the small and primitive forms such as *Dollosaurus* (Bell and Polcyn, 2005b). They appear to have remained endemic to the Western Interior Seaway in North America until the Middle Campanian (~83.6 Ma) (Polcyn *et al.*, 2008). Only during the Coniacian did their derived hydropedal morphology emerge (Bell and Polcyn,

2005b; Polcyn *et al*., 2014). This meant that their limbs were adapted to a life in water. Thereafter, mosasaurines became increasingly abundant and widespread throughout the Late Cretaceous, and by the Maastrichtian they were the most abundant clade (Polcyn *et al.*, 2014).

1.1.2) Evolution and palaeobiology

Mosasaurids are secondarily aquatic organisms, meaning their evolutionary origins begin on land. Complex physiological and morphological adaptations have to occur for terrestrial organisms to become successful in aquatic environments (Houssaye and Fish, 2016). Many of the modern secondarily aquatic reptilian clades are not fully aquatic because they still depend on land for important aspects of their lifestyles such as reproduction, feeding and thermoregulation. These semi-aquatic reptiles include turtles, crocodiles, marine iguanas and snakes. Mosasaurs are one of the few reptilian lineages along with ichthyosaurs (Superorder: Ichthyopterygia) and plesiosaurs (Superorder: Sauropterygia) to have achieved the biological adaptations needed for a fully aquatic lifestyle (Ellis, 2003)

Adaptations for a fully aquatic lifestyle

Locomotion

The basal mosasauroids, such as the aigialosaurs possessed morphological features suggesting both terrestrial and aquatic adaptations, and they inhabited shallow nearshore environments, and were likely semi-aquatic (Russell, 1967; Carroll and Debraga, 1992). The mosasaurid body plan had to undergo a number of adaptations to make the transition to a fully aquatic lifestyle in a more pelagic setting. These adaptations included the development of paddle-shaped flippers for rotation and stability; an elongated, laterally flattened tail with a bifurcated terminal fin (Lindgren *et al*., 2010; 2013), powered by strong muscles for propulsion

via lateral undulations (Russell, 1967); an elongated and streamlined body (Massare, 1988); and the development of small, keeled body scales that are suggested to have reduced frictional drag when swimming (Lindgren *et al.*, 2009).

The early mosasaurs were anguilliform swimmers like their hypothetical ancestors, meaning propulsion involved lateral undulations of the body that originated at the head and were passed down the length of the body, increasing in amplitude towards the tail (e.g. in eels and sea snakes) (Russell, 1967; Massare, 1988; Lindgren *et al.*, 2011). However, through mosasaur evolutionary history, their body plans became increasingly adapted to carangiform and even early thunniform swimming in the highly derived forms (e.g. *Plotosaurus*) (Lindgren *et al.,* 2007). A progression towards a more piscine body form, as well as the development of a high-aspect-ratio hypocercal tail is noted in the derived mosasaurs (Lindgren *et al.,*2007; Konishi *et al.* 2012; Lindgren *et al.* 2013). Changes that facilitated a stiffening of vertebral column for more energy-efficient axial swimming include an increased number of pygal vertebrae; an increase in the size of the interarticular surfaces of the vertebral centra and a relative shortening of the vertebral centra (Lindgren *et al.*, 2011). Many of the locomotory adaptations in the derived mosasaurs were shared with the apex predators before them – the ichthyosaurs, suggesting a trend towards convergent evolution (Harrell *et al.*, 2016).

Lingham-soliar (1992a) suggested an alternative (and rather controversial) mode of propulsion to lateral undulation for some mosasaurs: based on unique characteristics of the pectoral girdle and limbs, Lingham-Soliar (1992a) proposed subaqueous flight in *Plioplatecarpus marshi*. Apparently, the pectoral propulsion would have been beneficial for sudden and intricate manoeuvres in a complex environment, e.g. shallow water with seaweeds or coral reefs (Lingham-Soliar, 1992a). He further noted that similar modes of locomotion are used

by fish in confined reef environments, e.g. Embiotocidae (surfperches) (Dorn *et al.*, 1979), because the use of paired fin (pectoral) propulsion in fish provides them with a means of braking (Webb, 1982).

Massare (1988) discussed mosasaur swimming capabilities and its influence on their predatory strategy and success. Adaptations for locomotion in the aquatic environment follow two trends of specialisation in fish, which would have had a direct impact on the types of organisms they could have hunted (Massare, 1988). The first trend is toward a more energy-efficient periodic motion, which would have been beneficial for continuous swimming and for chasing prey over long distances (Massare, 1988). The second trend is toward a more efficient transient motion, i.e. agility and fast acceleration for ambush predation (Massare, 1988). Therefore, assessing body shape, as well as tooth morphology (see section on *Feeding*) is important for making deductions about feeding strategies and prey selection.

Reproduction

There are no modern or extinct aquatic amniotes that lay eggs in the water (Ellis, 2003), and the structure of the mosasaur body i.e. the large size and presence of flippers, was not conducive to effective movement on land. Early palaeontologists quickly recognised this and realised that the probability of the fully aquatic mosasaurids going ashore to lay eggs, as do turtles, was extremely low (Williston, 1904; Maxwell and Caldwell, 2003).

The scarcity of young mosasaurs in regions such as the Niobrara Chalk of Kansas, which is known for its copious mosasaur fossils (Russell, 1967) led early researchers like Williston (1904) to suggest that female mosasaurs left pelagic environments to breed and give birth elsewhere that was safer for their offspring. Williston (1904) further suggested that mosasaurs and aigialosaurs were occasional occupants of freshwater and that they may have swam up rivers

to give birth in safer freshwaters, where the young mosasaurs would remain until they grew large enough to move into pelagic marine environments. Although, Field *et al.* (2015) suggest that toothed jaws of Niobrara stem birds such as *Ichthyornis* and *Hesperornis* belong to baby mosasaurs. It is not possible to know exactly where and how female mosasaurs birthed and cared for their young, there is evidence to suggest that mosasaurs were viviparous (Ellis, 2003).

Viviparity (giving birth to live young) has evolved a number of times in secondarily aquatic animals, suggesting that it is an important adaptation for life in an aquatic context (Caldwell and Lee, 2001). Despite the high number of terrestrial reptiles that have developed this reproductive strategy, evidence for viviparity is only found in the marine reptiles (Maxwell and Caldwell, 2003).

Bell *et al.* (1996) reported the mosasaur embryos associated with the fragmentary remains of an adult belonging to the species *Plioplatecarpus primaevus* in South Dakota (Bell *et al*. 1996 in Ellis, 2003). In that same year, Caldwell and Lee re-examined a *Carsosaurus marchesetti* specimen initially described by Kornhuber (1893) who interpreted extra skeletal elements in the body cavity as undigested remains of fish, amphibians and lizards. Caldwell and Lee (2001) described the skeletal elements in the posterior two-thirds of the trunk region as belonging to four large, highly ossified and fully formed embryos (Caldwell and Lee, 2001).

The orientation of the embryos, i.e. head facing anteriorly and the curvature of the bodies, was considered evidence against the gut contents hypothesis because prey are expected to be swallowed head first in order to reduce the risk of injury during acquisition and handling (Caldwell and Lee, 2001). This evidence supported the embryo hypothesis by suggesting the baby mosasaurs were born tail first, as is seen in modern cetaceans and sirenians in order to minimise the risk of drowning during birth (Caldwell and Lee, 2001). Evidence for viviparity in

a semi-aquatic basal mosasauroid, such as the aigialosaur *C. marchesetti*, suggests that viviparity evolved early in the mosasauroid lineage. Therefore, it not only implies that the larger, more derived mosasaurids were also viviparous, it provides a mechanism for the transition from a semi-aquatic to fully aquatic lifestyle (Caldwell and Lee, 2001).

Thermoregulation

The thermoregulatory behaviours observed in modern terrestrial reptiles would not have been accessible to fully aquatic marine reptiles in open ocean environments. This led researchers to suggest that they may have been able to regulate their body temperature via metabolic control, which may have contributed to their evolutionary success (Bernard *et al.,* 2010). The temperature at which embryos are incubated can have major impacts on the development and viability of the young. Therefore, viviparity in marine reptiles provided a potential clue to their thermoregulatory capabilities (Ellis, 2003). In viviparous reptiles the thermoregulatory behaviour (e.g. sunning) of the pregnant female needs to be attuned to meet both her physiological needs and those of her developing offspring (Beucheat, 1988). It is widely agreed that mosasaurids were viviparous therefore regulating their body temperature would have been beneficial to their evolutionary success, especially in an open ocean environment. The discovery of plesiosaur and ichthyosaur remains from Early Cretaceous (Aptian) southern high latitude deposits of White Cliffs, southeastern Australia (Kear, 2005; Bernard *et al.*, 2010) generated a lot of interest in the possibility of thermoregulation in marine reptiles. Palaeoclimate indicators of that deposit suggested cold year-round temperatures to near-freezing temperatures in the winter (Kear, 2005). These conditions would be intolerable for modern reptiles such as turtles and crocodiles, which are generally found in more tropical climates (Bernard *et al.*, 2010). Thus, palaeontologists became intrigued by how the marine reptiles coped with these cold temperatures.

It has been shown that the $\delta^{18}O$ values from phosphate of bone and teeth of known ectotherms can be used as a palaeothermometer for seawater temperature (Longinelli and Nuti, 1973; Kolodny *et al.,* 1983). In the same sense this methodolgy can be used to detect endothermy in marine organisms as the $\delta^{18}O$ value is dependent on the ambient body temperature of the animal and the composition of the water it ingested (Longinelli and Nuti, 1973). Tooth enamel is used in these analyses because it is least susceptable to diagenetic alteration (Hillson, 2005). The phosphate derived $\delta^{18}O$ is used because postdepositional isotope exchange between the phosphate ions (PO_4^{3-}) and aqueaous inorganic solutions (i.e. seawater) is negligible, even over geological time scales; however, it is highly sensitive to changes that occur during life (Kolodny *et al.,* 1983; Kolodny and Raab, 1988).

Longinelli and Nuti (1973) came up with a $\delta^{18}O_{phosphate}$ vs $\delta^{18}O_{water}$ temperature scale, which could be expressed as a linear equation (1). Data included by Kolodny *et al.* (1983) resulted in slight variations to both the intercept and slope, which lead to the use of equation (2) for estimating temperature (°C).

$$T(°C) = 111.4 - 4.3(\delta^{18}O_{phosphate} - \delta^{18}O_{ocean}) \quad (1) \quad \text{(Longinelli and Nuti, 1973)}$$

$$T(°C) = 113.3 - 4.38(\delta^{18}O_{phosphate} - \delta^{18}O_{ocean}) \quad (2) \quad \text{(Kolodny } et\ al.,\ 1983\text{)}$$

Intrigued by the findings of Kear (2005), Bernard *et al*. (2010) assessed phosphate-derived-oxygen isotope ($\delta^{18}O_{PO4}$) values from tooth enamel belonging to ichthyosaurs, plesiosaurs and mosasaurs and compared these values to those of coexisting marine fishes from the same sedimentary bed in order to find evidence for thermoregulation in the marine reptiles. Bernard *et al.* (2010) made use of equation (2) set out by Kolodny *et al*. (1983) and the results suggested that the three groups of marine reptiles were able to maintain constant and high body temperatures in ocean environments that ranged from cold to tropical. Whilst the plesiosaur and

ichthyosaur results were very clear, the results from the mosasaur tooth enamel were less conclusive and it was suggested that the mosasaurs may have been more influenced by the surrounding seawater temperature (Bernard *et al.*, 2010).

Motani (2010) suggested that a slightly elevated body temperature for mosasaurs may be due to the fact that they were so large, thus they maintained heat within the body by gigantothermy. Harrell *et al.* (2016) noted that Bernard *et al.* (2010) did not rule out the possibility of gigantothermy in their study and that they lacked an endothermic representative with which to compare the results of the mosasaurs. Therefore, they conducted a study whereby they tested the $\delta^{18}O_{PO4}$ in tooth enamel and bone belonging to *Enchodus,* a coexisting small poikilothermic fish; *Toxochelys,* a medium sized marine turtle to represent an air-breathing ectotherm; *Cladistes, Platecarpus* and *Tylosaurus,* mosasaur genera of varying body size; and two genera of extinct toothed seabirds namely *Hesperonis* and *Ichthyornis,* which represented endotherms (Harrell *et al.*, 2016).

The results showed that the bone and enamel samples correlated well with each other and were therefore averaged together. They used equation (3) outlined by Pucéat *et al.* (2010), which differed slightly from those by Longinelli and Nuti (1973) (1) and Kolodny *et al.* (1983) (2) because it included a correction value, i.e. $(22.6 - \delta^{18}O_{NBS120c})$. Oxygen isotope analyses of phosphate are most commonly standardised using NBS120c (a natural Miocene phosphorite from Florida), for which there are slightly different values (Pucéat *et al.*, 2010). The two most frequently used NBS120c values are 21.7‰ (Lécuyer *et al.*, 2003) and 22.6‰ (Vennemann *et al.*, 2002), thus the correction value minimises variation in results from calculations using different values for the NBS120c standard (Pucéat *et al.*, 2010).

$$T(°C) = 118.7 - 4.22[(\delta^{18}O_{phosphate} + (22.6 - \delta^{18}O_{NBS120c})) - \delta^{18}O_{ocean}] \quad (3)$$ (Pucéat *et al.*, 2010)

They did the calculations using different values for $\delta^{18}O_{ocean}$ (i.e. $\delta^{18}O_{ocean}$ = -1.37‰; -0.36‰; 0.00‰; 0.23‰) and found that the mosasaurs they sampled had body temperature values closer to those of modern and fossil birds and higher than the measured body temperatures of the fish and turtles (Harrell *et al.,* 2016). The differences in the body temperatures of the three mosasaur genera were independent of size, therefore refuting Motani's (2010) suggestion that they were gigantotherms.

Remains of mosasaurs have been found in Maastrichtian deposits at high latitudes such as the Antarctic Peninsula (Novas *et al.*, 2002; Fernandez and Martin, 2009; Rubilar-Rogers *et al.*, 2016; Reguero *et al.*, 2019). This indicates that at least some derived mosasaurids were able to exploit cooler polar waters. The Late Cretaceous ocean temperatures also underwent a general cooling trend, with a cold and even glacial period during the Early Maastrichtian (Friedrich *et al.,* 2012). Therefore, as was highlighted by Harrell *et al.* (2016), such an increase in diversity and abundance of mosasaurs during the Maastrichtian would be unlikely if they were not able to maintain an elevated body temperature (Polcyn *et al.*, 2014). Furthermore, convergent trends towards endothermy in other non-mammalian marine predators such as lamnid sharks and tuna (Bernal *et al.*, 2001) lends itself to the possibility of similar trends in mosasaurids.

Feeding

Hunting methods for mosasaurs have been hypothesised based on their morphological features, gut contents and the methods adopted by modern ecological counterparts such as large predatory sharks and cetaceans (e.g. Kauffman and Kesling, 1960; Konishi *et al.*, 2018). Unlike the ichthyosaurs and plesiosaurs, which are suggested to have been pursuit predators (Massare, 1988) the early mosasaurids are generally thought to have relied more on ambush predation as a means of acquiring prey. For example, it has been suggested that the tylosaurines used their

edentulous rostrum to ram and stun or even kill their prey, similar to the way modern killer whales hunt other large cetaceans (Visser *et al.*, 2010; Konishi *et al.*, 2018). It is not possible to know exactly how mosasaurs hunted different prey items, but the preservation of gut contents provides more concrete evidence for the kinds of prey mosasaurs were hunting. By understanding what a predator eats it is easier to speculate about how it hunted it.

Russell (1967) suggested that medium-sized fish would have made up the bulk of the diet of mosasaurs, but that larger and more pelagic species may have fed on other marine reptiles, large fish, cephalopods and sharks. Russell (1967) further said that other species were adapted to feed on shallow water and/or benthic organisms such as bivalves, echinoderms, and shelled cephalopods like ammoniodes and belemnoids. Massare (1987, Table 1, p.128) summarised the prey of different marine reptile taxa based on studies that specifically utilised gut contents to provide evidence of what those marine reptiles were eating. The mosasaurs represented had a variable diet that included most of the prey items that Russell (1967) had speculated, with the exception of an extinct flightless bird, *Hesperornis,* which was preserved in the stomach region of a *Tylosaurus* (Bjork, 1981 cited in Massare, 1987).

Konishi *et al.* (2014, Table 1, p.816) provides the most up-to-date summary of mosasaur gut contents from a number of other publications. It shows that mosasaurs fed on marine reptiles including sea turtles (Konishi *et al.* 2011; Konishi *et al.*, 2014), plesiosaurs (Sternberg, 1918; Everhart, 2004) and were even cannibalistic (Bjork, 1981 cited in Massare, 1987). However, taphonomic evidence such as tooth marks in the skull (Massare, 1987) and gut contents suggests that mosasaurs rarely preyed on their own kind (Polcyn *et al.*, 2014). The record of cannibalism amongst mosasaurs is interpreted as more opportunistic than obligatory, and perhaps only among the larger species because their diet would have been fairly indiscriminate (Polcyn *et al.*, 2014).

Much like some species of *Varanus* lizards, early generalised mosasaurs had increased intracranial mobility, meaning that the individual bones in the skull were movable enabling them to hunt and eat larger prey items (Callison, 1967; Russell, 1967). Teeth would have been used for capturing and manoeuvring the prey in order to get them into a position so that they could be swallowed whole (Massare, 1987). Interestingly, the larger more derived mosasaurs lost their intracranial mobility (Russell, 1967) and were able to feed on prey items that were larger than they could swallow because of adaptations in tooth morphology that enabled them to cut and tear the flesh of larger organisms into bite size pieces that could then be swallowed (Massare, 1987), much like the large predatory sharks (Whitenack and Motta, 2010). Massare (1987) characterises these cutting teeth as being large and pointed at the apex and having at least two cutting edges (or carinae), sometimes with serrations. Other tooth morphologies described by Massare (1987) include the crush, crunch, smash, pierce and general guilds. A number of studies have attempted to use to tooth morphology to provide insights into the diets of the marine reptiles in the absence of direct evidence, such as gut contents (e.g. Foffa *et al.*, 2018).

Mosasaurid dentition

Mosasaurid tooth development and replacement

Mosasaurid dentition has been a topic of much interest and debate with many disagreements on the topic of replacement and tooth attachment (e.g. Lee, 1997; Zaher and Rieppel, 1999; Caldwell, 2007). Much of this interest stems from the difficulties in defining the relationships between the mosasauroids and the other members of Squamata i.e. snakes and lizards. Tooth development and replacement patterns have been used to argue the affinities of mosasauroids with both snakes and lizards, which show very distinct patterns.

According to Lee (1997), the snake tooth replacement pattern involves a recumbent replacement tooth that swings upwards ninety degrees to a vertical functional tooth position (see Lee, 1997, Figure 5, p.309). Lee (1997) argued that this is one of the two major features that made mosasaur dentition and tooth replacement like that of snakes. The other feature that he used to support his argument was that mosasaurs demonstrated a thecodont tooth attachment (Lee, 1997), meaning the teeth are rooted and set in sockets (Caldwell, 2007).

Conversely, Zaher and Rieppel (1999) argued that mosasaurs have a more typical reptilian pattern of tooth replacement (see Lee, 1997, Figure 5, p.309) because most of the descriptions, figures and personal observations that they made showed the replacement teeth in upright position, apart from a few that appeared to be 'recumbent'. These 'recumbent' teeth, however, were all lying outside of their respective resorption pits, and were suggested to have been displaced therefore having an unnatural orientation (Zaher and Rieppel, 1999). They also argued against Lee's (1997) thecodont tooth attachment for mosasaurs and stated that only acrodonty and pleurodonty exists in squamates.

Caldwell (2007) presented a model for the movement path of a developing tooth crown with eight ontogenetic stages of tooth development and replacement. The simplified movement path of the replacement teeth is first horizontal, then down into resorption pit and then upwards as it grows and pushes out the functional tooth. However, despite this initial horizontal movement, throughout all the stages the replacement teeth are in an upright position (see Caldwell, 2007, Figure 6, p.697), which agrees with Zaher and Rieppel's (1999) and Kearney and Rieppel's (2006) interpretation of a typical reptilian tooth replacement for mosasaurids.

Zaher and Rieppel (1999) suggested that mosasaurids did not have thecodont tooth attachment patterns, but rather a type of pleurodonty, which means that the teeth are ankylosed

by their sides to the lingual surface of the dentary/maxilla. This interpretation was only based on gross morphology, but Caldwell *et al.* (2003) used histological analysis to confirm the presence of the thecodont condition in mosasaurids. They made vertical and horizontal thin sections through the left dentary of a *Platecarpus* sp., which revealed various tooth and bone tissues analogous with those found in thecodont amniotes (mammals and archosaurs), such as alveolar bone, periodontal ligaments and cementum (Caldwell *et al.,* 2003; Caldwell, 2007).

Dental histology

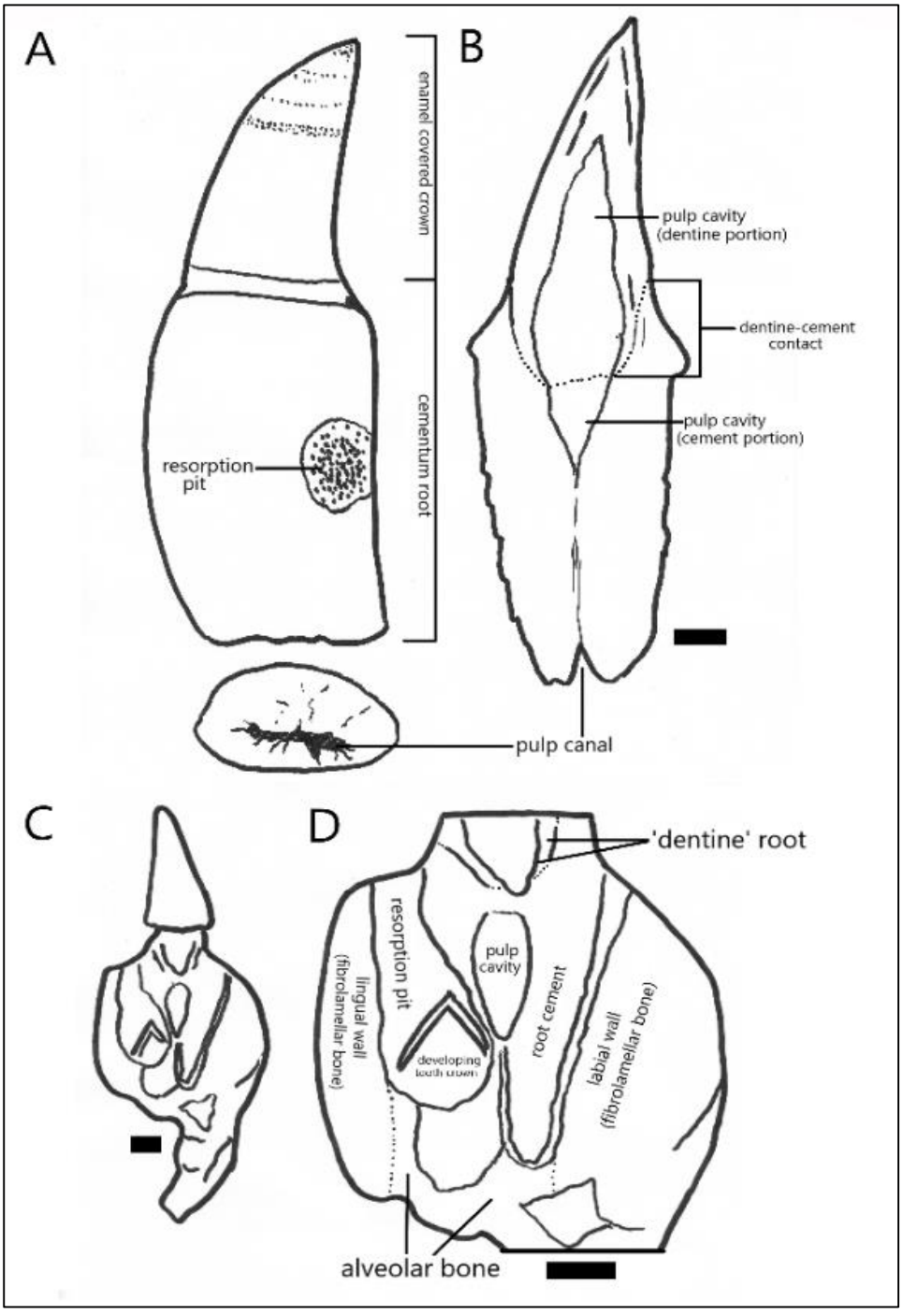

Figure 2. Drawings adapted from figures in Caldwell (2007) showing the parts of the tooth and the various tooth tissue types. (A) External features of a tooth belonging to Mosasaurus sp. *(NHMM 002459-1) in medial and ventral view. (B) Longitudinal section of the tooth in A. (C) Longitudinal section through a right dentary of Prognathodon waiparensis (CM-ZFR108) with tooth crown, (D) High magnification drawing of B showing various tissues and features involved in tooth attachment and replacement. Scale bars = 10mm.*

Mosasaur teeth consist of an enamel-covered crown and a cementum root, which is implanted into the alveolus of the tooth bearing element. The tooth bearing element is comprised of an endosteal bone on the inside and periosteal bone forming the outer layer (Budney *et al.,* 2006). The alveolus can be thought of as the bony tooth socket and consists of an outer cortical plate, a spongious bony layer and the lining bone at the base of the alveolus, which is in contact with the root cementum (Caldwell *et al.*, 2003). The lining bone is also known as the cribriform plate and contains small holes for nerves and blood vessels to pass through the alveolus into the cellular root cementum via the periodontal ligaments (Caldwell *et al.*, 2003). These periodontal ligaments are responsible for the fibrous attachment of the cementum tooth base, but there are also dense clusters of Sharpey's fibres present at the cementum-alveolar bone contact, which presumably function as a means of attachment (Caldwell *et al.,* 2003; Luan *et al.,* 2009).

The cement portion of the root is a massive tooth base and is made of two types of cementum i.e. cellular and acellular cementum (Luan *et al.,* 2009), which surrounds the 'dentine' root, partial pulp cavity and the pulp canal (Figure 2B). Cellular cementum is the main component of the cementum root and is composed of a generalised cementum matrix that contains cementoblasts, which become entrapped during cementum formation. These are referred to as cementocytes that support the cementum. Similar to osteons in bone, there are also cementeons in cementum, which can have concentric laminae around their endosteal margins (see Caldwell *et al.,* 2003, Figure 3, p.627 for image of cementum, cementocytes and cementeons). Acellular cementum is avascular and contains no cementeons or cementocytes. It forms a very thin, dense layer around the dentine root from the enamel-dentine contact towards the root apex and is more lamellar in structure (Carlson, 1990; Caldwell *et al.*, 2003).

Chinsamy *et al.* (2012) provided a detailed characterisation of the dentine and enamel of *Mosasaurus hoffmannii* from the Late Cretaceous of Turkey. Upon thin sectioning a functional tooth they found a small replacement tooth within it. Both the functional and replacement tooth showed a thin outer layer of enamel surrounding a thick layer of dentine, but a pulp cavity was only noted within the functional tooth.

The dentine belonging to the functional tooth was well-preserved. A thin layer of predentine immediately surrounded the pulp cavity and dentinal tubules were clearly seen, which appear as thin, tightly packed, parallel lines running perpendicular to the pulp cavity (see Chinsamy *et al.,* 2012, Figure 1, p.87). Lines of von Ebner were also noted, which are concentric lines that run parallel to the pulp cavity and are formed daily (Hillson, 2005), thus by counting the number of lines of von Ebner one can estimate the time taken (in days) for a particular section of dentine to form (Erickson, 1996; Chinsamy *et al.*, 2012). The *M. hoffmannii* tooth sectioned by Chinsamy *et al.* (2012) took approximately 511 days to deposit dentine at the measured level. Contour lines of Owen were also noted, which are incremental lines (similar to lines of von Ebner) that have been emphasised by a disruption in mineralisation and therefore appear darker under a microscope (Hillson, 2005; Chinsamy *et al.,* 2012). The thick dentine layer supports a very thin outer layer of enamel.

Enamel architecture

Chinsamy *et al.* (2012) histologically described the *M. hoffmannii* tooth enamel as having a distinctive birefringence under polarised light, which they interpreted as prismatic enamel after Cooper and Poole (1973). This finding is unexpected since reptilian enamel is typically prismless in structure, while prismatic enamel is typically a mammalian feature (Carlson, 1990; Stern and Crompton, 1995; Sander, 2009). However, prismatic enamel is known in the agamid lizards of

the genus *Uromastyx* (Cooper and Poole, 1973; Alazem and Abramyan, 2019), where thin sections of the enamel under polarised light showed a typical "striped appearance" which was attributed as a characteristic of prismatic enamel seen in mammals. (Cooper and Poole, 1973, p.96)

There is only one other study that claims to have found prismatic enamel in mosasaurids: Torii (1998) assessed tooth enamel from a *Mosasaurus* sp. using scanning electron microscopy (SEM). Torii (1998) interpreted the micrographs to reveal enamel crystallite groups of varying shapes and sizes with distinct boundaries between them. In longitudinal view these boundaries corresponded to fissures in tangential view (Torii, 1998). The micrographs were not detailed, but the vague description partially supported their suggestion that the *Mosasaurus* sp. had prismatic enamel. Chinsamy *et al.* (2012) assessed the *M. hoffmannii* tooth using SEM and they also resolved that it supported their prediction that it may be prismatic.

Chinsamy, Tunoglu and Thomas (2012) described parallel enamel crystallites that were arranged perpendicular to the enamel dentine junction (EDJ) and spanned the entire distance between the EDJ and the outer enamel surface (OES). However, the figures and descriptions are not detailed enough to make deductions about the nature of the enamel with regards to it being prismatic or prismless. When compared to the hierarchical levels of structural complexity and diversity of amniote enamel outlined by Sander (2009), this description only covers the level of crystallite orientation to the EDJ. Furthermore, it seems like their description matches that of parallel crystallite enamel, which is a type of prismless enamel (Sander, 2009). However, it should be noted that there can be different enamel types within one tooth (Schmelzmuster; e.g. Hwang [2009]) and it could be that the birefringence seen using polarised light was indicative of prismatic enamel that was simply not seen in the SEM micrographs.

Therefore, there is scepticism around the claims of prismatic enamel in mosasaurs. M. Caldwell and A. LeBlanc have previously looked at mosasaurid enamel using SEM and failed to note any prism structures (personal communication, January 2020). Additionally, given their carnivorous diets and relatively rapid tooth replacement, there is no obvious biological or ecological reason for mosasaurids to have possessed prismatic enamel, as described for *Uromastyx* lizards (Cooper and Poole, 1973).

1.1.3) Mosasaurs from Africa

Presently, mosasaurid remains are known from seven African countries, namely Morocco, Egypt, Niger, Nigeria, Democratic Republic of Congo [DRC], Angola and South Africa [SA] (Jiménez-Huidobro *et al.,* 2017). Lingham-Soliar (1994, p.259) described the first record of mosasaurs from the Maastrichtian of Zaire (now DRC), wherein he says that '…the picture therefore is that of an almost continuous band of mosasaur localities stretching from Egypt, across to Morocco and Algeria then southwards to Niger, Nigeria, Zaire, Angola and South Africa.' and optimistically suggested that mosasaur fossils in Africa may match or even exceed the records in some of the primary mosasaur bearing regions of the world. Ellis (2003) put forward that mosasaurs may have even originated in Africa and then spread across the world.

Unfortunately, due to factors such as political instability, wars, poverty and limited funding available to support palaeontologists, there is less determination for new mosasaur discoveries in Africa than elsewhere in the world. This is particularly true for countries and regions where mosasaur remains have not already been found. Generally the North African countries like Morocco, receive more attention probably due to its proximity to Europe and the French-Moroccan programme of collaboration. Camille Arambourg, a French palaeontologist initiated a long and diverse recording of mosasaurs in Morocco between the 1930s and 1950s

(Bardet *et al.*, 2010), which continues to increase with on-going discoveries and research. Little work has been done on mosasaurs from Egypt after Zdansky (1935, bibliographic reference not included) published his descriptions of eight different mosasaur species (Ellis, 2003). In Niger and Nigeria, Lingham-Soliar (previously Soliar) did much of the research after Swinton (1930) first discovered mosasaurs in west Africa (Lingham-Soliar, 1998) and suggests that the diversity of mosasaur fauna in this region may rival that of Niobrara Chalk of Kansas, which is considered to be one of the chief mosasaur bearing regions of the world (Russell, 1967). Lingham-Soliar (1994) also contributed to research on the mosasaurs from the DRC. In southern Africa there are a number of palaeontologists doing on-going research and field work in Angola (e.g. Jacobs *et al.*, 2006; Polcyn *et al.*, 2010; Schulp *et al.*, 2013), many of which are members of Projecto PaleoAngola (Mateus *et al.*, 2019). However, the research regarding SA marine reptiles is limited to a few older studies of plesiosaurid (Rogers and Schwarz, 1902; Andrews, 1911; McGowran and Moore, 1971) and mosasaurid remains (Rogers and Schwarz, 1902; Broom, 1912).

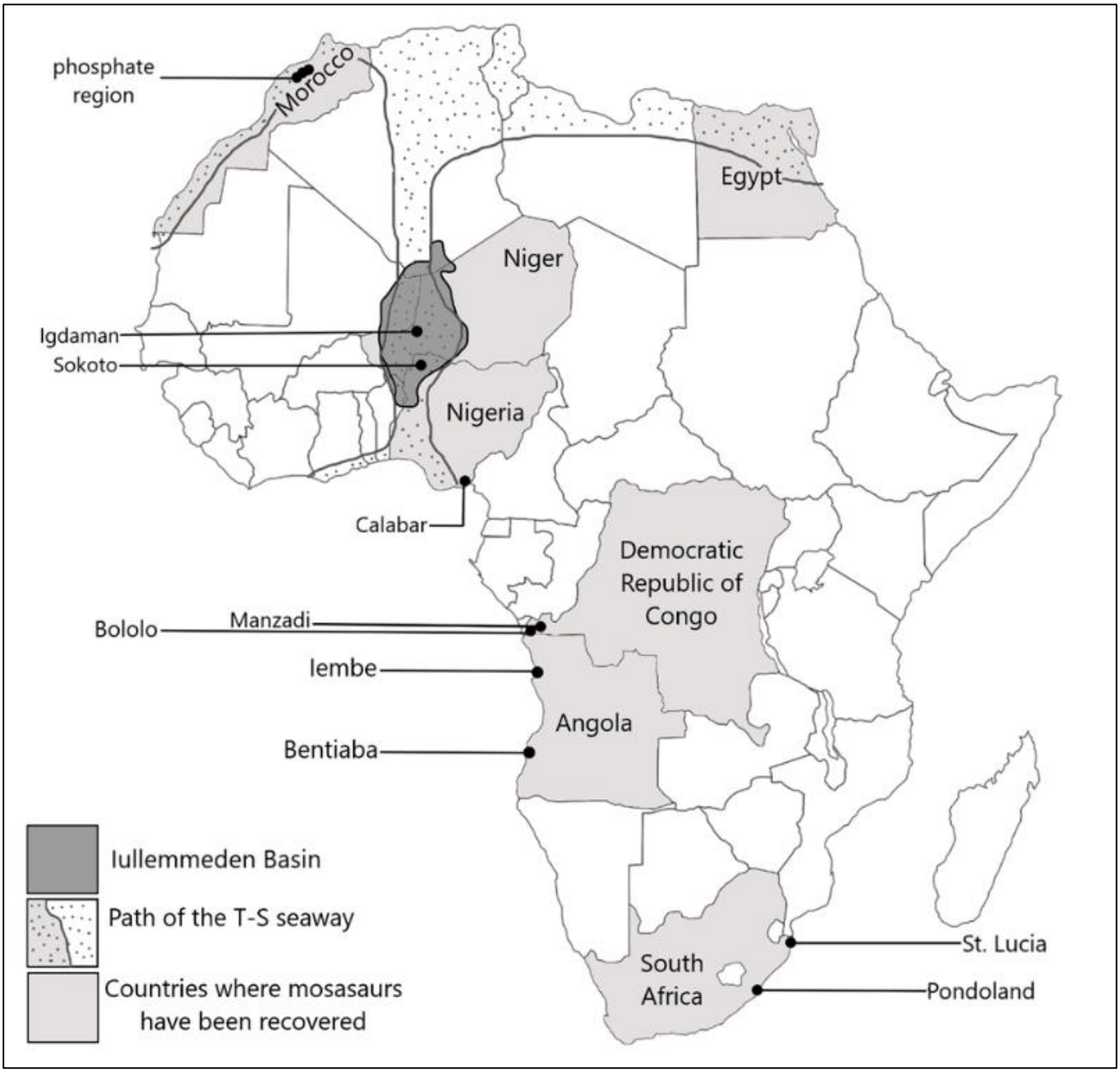

Figure 3. Map of Africa showing the countries where mosasaur remains have been found and the approximate geographical locations of the mosasaur localities discussed in this study. The path of the Trans-Saharan (T-S) seaway (dotted area) and the extent of the Iullemmeden Basin across West Africa (dark grey) is indicated.

Morocco

Bardet *et al*. (2010) published a summary of the reptilian assemblages from the latest Cretaceous-Palaeogene phosphates of Morocco, which also included the history of the diverse fossil discoveries made there. The main phosphatic basins are in the north-eastern regions of Morocco, they are slightly inland between the cities of Casablanca in the north and Agadir in the south (Bardet *et al.*, 2010; Le Blanc *et al.*, 2012). According to Bardet *et al.* (2010) the phosphate deposits of Morocco have been exploited for exportation purposes since the early 1920s, and still play a key role in the country's economy. The phosphate deposit stratigraphic range spans the Maastrichtian to the middle Eocene and is characterised by its quantity and diversity of fossil remains (Bardet *et al.*, 2010). The deposits are predominantly marine, therefore the fossil remains include those of selachians, squamates (mosasaurids), plesiosaurs, marine chelonians, marine avifauna (only from Palaeogene deposits of Oulad Abdoun Basin) and crocodyliforms. Non-avian dinosaurs and pterosaurs are also present, but are more scarce in the Moroccan Maastrichtian phosphates (Bardet *et al.*, 2010).

The diversity and abundance of mosasaur remains in the Maastrichtian deposits of Morocco suggests that they were the most important predatory group during this time and after they went extinct at the end of the Cretaceous, the crocodyliforms took over that predatory niche and became a diverse group in the Palaeogene (Bardet *et al.*, 2010). According to Jiménez-Huidobro *et al.* (2017) there are 13 species of mosasaurs from Morocco representing four subfamilies, namely Halisaurinae, Tethysaurinae, Plioplatecarpinae and Mosasaurinae. There are two species present within Halisaurinae, *H. arambourgi* and '*H. walkeri',* although the latter taxon has not been definitively identified (Bardet *et al.*, 2015). *Tethysaurus nopcsai* is a basal mosasauroid from the Early Turonian deposits and represents the tethysaurines (Bardet *et al.*,

2003). *'Platecarpus' ptychodon* (Arambourg, 1952), was initially described and named based on isolated teeth and Bardet *et al.* (2015) suggested that it is in fact a relatively abundant taxon in the Maastrichtian phosphates of Morocco despite it being the only representative member of Plioplatecarpinae. They also propose that *'Platecarpus' ptychodon* may be a new genus as its unusual morphology is different from other members of the genus *Platecarpus* (Bardet *et al*., 2015). However, Strong *et al.* (2020) considered '*Platecarpus' ptychodon* invalid and established a new species under a new genus with a new holotype, which they named *Gavialimimus almaghribensi.*

Mosasaurinae is the most prevalent subfamily from Morocco with 9 of the 13 species belonging to this group. There are at least three species of the genus *Prognathodon,* a frequent taxon from the Maastrichtian phosphate deposits (Bardet *et al.*, 2010) namely *P. giganteus* (Dollo 1904), *P. currii* (Christiansen and Bonde, 2002) and an undescribed new species, the latter two of which are the largest of the Moroccan mosasaurids (Bardet *et al.*, 2015). Two species of *Mosasaurus* are present, namely the *M. beaugei* (Arambourg, 1952) and *M. (Leiodon)* cf. *anceps* (Owen, 1845; Arambourg, 1952). Two species of the durophagous mosasaurid, *Carinodens* are present, one of which is the extremely rare, *C. belgicus* (Woodward, 1891; Bardet *et al.,* 2015) and *C. minalmamar* (Schulp *et al.,* 2009). *Globidens phosphaticus* (Bardet *et al.*, 2005) and the more recently described *Globidens simplex* (LeBlanc *et al.,* 2019) are the only *Globidens* from the Maastrichtian outside of North America. *G. phosphaticus* is fairly common in the Moroccan phosphates (Bardet *et al.*, 2005; Bardet *et al.*, 2015). *Eremiasaurus heterodontus* was described and named from nearly complete specimens from Upper Maastrichtian deposits of Morocco and is characterised by its high degree of heterodonty (Le Blanc *et al.,* 2012).

Revisions of the older publications have led to the reassignment of several specimens to different species and for new species to be established. For example Arambourg (1952) assigned a number of isolated teeth with different morphologies to *G. aegyptiacus* (Zdansky, 1935); however, it was found that these teeth that were lumped under one species actually belonged to three separate species: *G. phosphaticus* (Bardet *et al.*, 2005)*, C. belgicus* (Woodward, 1891) and *C. minalmamar* (Schulp *et al.*, 2009; Bardet *et al.*, 2010)*.* These kinds of revisions are important for bringing the older literature and material up-to-date and relevant for use with new literature. They also caused problems because if *G. aegyptiacus* is in fact an invalid taxon, it means that any other material assigned to *G. aegyptiacus* potentially needs to be reassigned. According to Jiménez-Huidobro *et al.* (2017) *G. aegyptiacus* is present in both Niger and Egypt; and in Egypt it is supposedly the only mosasaurid present.

Egypt

G. aegyptiacus is suggested to be the only mosasaurid present in Egypt (Jiménez-Huidobro *et al.,* 2017), which is contrary to Zdansky (1935), where he describes ten species of mosasaur, eight of which are from Egypt (Ellis 2003). The problem with *G. aegyptiacus* is that any material assigned to this species could in fact be representative of one, two or potentially three species, as was the case in Morocco (Bardet *et al.*, 2010).Bardet *et al.* (2015) suggested that the *G. phosphaticus* is synonymised with *G. aegyptiacus.* However, the alpha taxonomy for *G. phosphaticus* is based on a single tooth crown. Therefore, until all the material is properly reassessed and it has been established that *G. aegyptiacus* is invalid, it is treated here as though it is a valid taxon.

Niger

There are extensive Maastrichtian and Palaeocene marine deposits across West Africa due to a rise in sea level during the Cretaceous (Petters, 1978), which led to the formation of the Trans-Saharan (T-S) seaway, which supposedly linked the Gulf of Guinea and the Tethys Sea and passed through the western parts of modern day Niger and Nigeria (Elewa, 2002) (Figure 3). Due to its position in the path of the ancient T-S seaway, the Iullemmeden Basin, which incorporates northwest Nigeria and southwest Niger (Figure 3), is rich in marine fossils (e.g. Petters, 1978; Lingham-Soliar, 1991; Elewa, 2002). It would have provided one of the richest environments in the world for mosasaur evolution and diversification from the Late Campanian to Maastrichtian (Lingham-Soliar, 1998).

According to Jiménez-Huidobro *et al.* (2017), there are six species of mosasaurid represented in Niger from four main groups, namely Halisaurinae, Plioplatecarpinae, Mosasaurinae and the enigmatic genus *Goronyosaurus.* Most of the mosasaurid material comes from Maastrichtian deposits near the town of Igdaman in the south-western corner of Niger (Lingham-Soliar, 1991). Lingham-Soliar (1991) described a fragment of a large tooth crown, which he referred to as *Mosasaurus* cf. *hoffmannii.* This is still a significant specimen because it represents the only *Mosasaurus* remains from Niger and Nigeria (Lingham-Soliar, 1991). *G. aegyptiacus* is also included as one of the Nigerien species (Jiménez-Huidobro *et al.*, 2017). In 1991, Lingham-Soliar erected a new genus, '*Igdamanosaurus'* to which he assigned *G. aegyptiacus* because he agreed with Russell's (1975, bibliographic reference not included) observation that the teeth of *G. aegyptiacus* were unlike those of other *G. alabamaensis* and *G. dakotensis*. However, '*Igdamanosaurus'* is not a widely accepted genus.

The plioplatecarpines from Niger were also described and identified by Lingham-Soliar (1991). A mid-cervical vertebra from Mount Igdaman and numerous vertebrae from the '*Mosasaurus* Shales' in Tahout, were assigned to *Plioplatecarpus* sp. A dorsal vertebra with inflated heart-shaped condyles and cotyles were assigned to *Platecarpus* sp. (Lingham-Soliar, 1991). Lingham-Soliar (1991) also described four vertebrae, one of which belonged to a younger individual that he assigned to *Angolasaurus* (Antunes, 1964). He later suggested that *Angolasaurus* was the earliest member of *Platecarpus* (Lingham-Soliar, 1994), which has since been refuted (Jacobs *et al.*, 2006, 2009, 2016; Mateus *et al.*, 2011). Therefore, the material is referred to here as *Angolasaurus* (Table 1); however, it is noted that the Maastrichtian-age of the Nigerien specimen is inconsistent with other Turonian-aged material from Angola, North America and Brazil (Antunes, 1964; Bengtson and Lindgren, 2005; Jacobs *et al.*, 2009).

Lingham-Soliar (1991) described several cranial elements, probably from two individuals from Mt. Igdaman, which he referred to as *Goronyosaurus* sp., which was named after the Goronyo District of the Sokoto State (Azzaroli *et al.,* 1972). This is a problematic genus and is yet to be placed within the mosasaurids due to several unique and unusual cranial modifications (Lingham-Soliar, 2002). These unique characteristics include the presence of interdental pits, which would have allowed their jaws to fit tightly together; a large number of teeth, exceeding those of any other mosasaur (Lingham-Soliar, 1991); and the presence of caniniform teeth. These characteristics were thought to be unique among mosasaurids. However, Strong *et al.* (2020) noted that *Gavialimimus almaghribensis* also possesses interdental pits and that *Goronyosaurus* may not have as many unique characteristics as once thought, due to the incompleteness of the holotype and limited specimens (Strong *et al.* 2020).

Lingham-Soliar (1991) described several isolated vertebrae, which he likened to *Halisaurus* sp. However, upon formally describing the material in 1998, he erected a new genus and species and named it *Pluridens walkeri.* This genus represented another unique and specialized taxon in West Africa and *P. walkeri* specimens from both south-western Niger and southern Nigeria (near Calabar) indicated that the T-S seaway was open-ended and not a marine embayment of the Tethys Sea that reached the south-western borders of Niger (e.g. Petters, 1978).

Lindgren and Siverson (2005) reassessed the '*Pluridens'* material from Niger and found that many of the characters suggested to be unique to *Pluridens* were shared with *Halisaurus,* thus they suggested that *Pluridens walkeri* should be referred to as *Halisaurus walkeri* (Lindgren and Siverson, 2005; Jiménez-Huidobro *et al.,* 2017). Conversely, Longrich (2016) supported Lingham-Soliar's (1998) assignment of the Nigerien material to *P. walkeri.* Upon closely analysing the *Pluridens* material from Niger and Nigeria, he concluded that there were two distinct *Pluridens* species present.

Nigeria

The first mosasaur from Nigeria was discovered by Swinton (1930) who described and named the mosasaur *Mosasaurus nigeriensis* (Ellis, 2003) based on postcranial elements and jaw fragments from the Cretaceous '*Mosasaurus* Shales' (Soliar, 1988). In 1970 more material was discovered and assigned to the same species; however, the presence of a number of unusual characters led Azzaroli *et al.* (1972) to assign it to the newly erected genus, *Goronyosaurus*. In Jiménez-Huidobro *et al.* (2017, Table 2, p.358), *G. nigeriensis* is considered the only species of mosasaur from Nigeria, but the literature suggests that there is another taxon namely *Pluridens. calabaria* from the Campanian section of the Campanian-Maastrichtian Nkporo Shale near

Calabar Nigeria (Longrich, 2016). According to Longrich (2016) the Nkporo mosasaur, *P. calabaria* was recovered from Campanian strata, making it older than the Maastrichtian-aged *P. walkeri* from Niger. Longrich (2016) also noted that *P. calabaria* did not share many of the derived features seen in *Pluridens walkeri,* which demonstrates the rapid evolution of mosasaurs during the Late Cretaceous. Therefore, based on this more recent interpretation of the *Pluridens* material from Niger and Nigeria (Longrich, 2016). *P. walkeri* from Niger and *P. calabaria* from Nigeria are considered valid taxa in this study (Table 1).

Angola

Antunes (1964) was the first to do thorough research on the palaeontology and fossil vertebrates of Angola. Unfortunately, little work was done thereafter due to the Angolan war of Independence during the 1970s and the civil war, which broke out in 1975 and continued until 2002 (Mateus *et al.*, 2011; Pearce, 2012). Once it was possible to re-establish fieldwork in Angola, Projecto PaleoAngola was initiated and commenced in 2005, forming a collaboration of researchers from Angola, United States, Portugal, Netherlands and Sweden (Mateus *et al.*, 2011). The vertebrate fossil record in Angola has a temporal range from the Triassic to the Holocene and there are extensive remains of fishes, turtles, crocodiles, cetaceans as well as plesiosaurs and mosasaurs (Jacobs *et al.*, 2016). The rocks on the Angolan coast record the Early Cretaceous split between South America and Africa, which severed the east-west terrestrial dispersal route. However, it created a new north-south dispersal route for marine organisms by opening the South Atlantic to the North Atlantic Ocean (Jacobs *et al.*, 2009, 2016). There are two main Cretaceous localities near the coastline that have yielded a large quantity of fossils. Namely, the Turonian Itombe Formation of Iembe in Bengo Province and the Maastrichtian Mocuio Formation of Bentiaba in Namibe Province (Figure 3) (Mateus *et al.,* 2011). The north-

south dispersal of marine organisms in the Atlantic Ocean is not only supported by the presence of northern fossil ammonites and invertebrates at the aforementioned localities, but also by the presence of much larger amniotes, such as the mosasaurids (Jacobs *et al.*, 2016).

According to Jiménez-Huidobro *et al.* (2017, Table 2, p.358), there are six mosasaur taxa present in Angola, representing the subfamilies Mosasaurinae, Tylosaurinae and Plioplatecarpinae. All of the mosasaurines are from Maastrichtian-aged deposits, whereas the tylosaurine and plioplatecarpine are from the much earlier Turonian-aged deposits of Iembe (Mateus *et al.*, 2011). Representing the tylosaurines is *Tylosaurus iembeensis* from the Upper Turonian Chalk of Iembe, which was described and named in 1964 by Antunes, who referred to it initially as *Mosasaurus iembeensis* (Lingham-Soliar, 1992b). Lingham-Soliar's (1992b) reassigned *M. iembeensis* to *Tylosaurus,* consequently making it the oldest member of the Tylosaurinae subfamily. The poorly preserved and incomplete remains of *T. iembeensis* were not well-understood and the original holotype was lost in a fire in Lisbon (Lingham-Soliar, 1992b; Jacobs *et al.*, 2006; Mateus *et al.*, 2011). However, a new specimen has been recovered from Angola and although it is fragmentary and yet to be figured or formally described it is said to consist of a preserved quadrate with a poorly developed infrastapedial process, which is similar to that of '*T. kansasensis'*[1] but larger, making it a relatively basal tylosaurine (Mateus *et al.*, 2011).

Angolasaurus bocagei (Antunes 1964) was also recovered from the Upper Turonian deposits of Iembe in the northern parts of Angola and is a member of Plioplatecarpinae. The more recent fieldwork has uncovered additional specimens belonging to this species thus

[1] It should be noted that *'T. kansasensis'* has been named a junior synonym for *T. nepaeolicus* (Jiménez-Huidobro *et al.,* 2016).

providing new anatomical details of this mosasaur (Jacobs *et al.*, 2006). Lingham-Soliar (1994) suggested that *A. bocagei* is in fact the earliest member of the genus *Platecarpus* and its inclusion as *P. bocagei* in Jiménez-Huidobro *et al.* (2017) suggests that they agree with this reassignment. However, published literature from researchers working closely and consistently with the Angolan material (e.g. Jacobs *et al.,* 2006, 2009, 2016; Mateus *et al.,* 2011) continues to consider *Angolasaurus* a valid taxon within Plioplatecarpinae as shown by (Polcyn and Bell, 2005), therefore in this study it will also be considered valid (Table 1).

Mateus *et al.* (2011) briefly highlights additional specimens of known taxa from Angola, as well as several new taxa that had previously not been recovered from the Maastrichtian Mocuio Formation of Bentiaba; however, few of these have been formally described and named. These taxa include mosasaurines such as a species of *Mosasaurus* that has affinities with *M. hoffmannii,* but is indistinguishable from either *M. hoffmannii* or *M. maximus; Prognathodon kianda,* which was described and named by Schulp *et al.* (2008) based on material from the same locality and is also suggested to be the most basal species of the clade; new material referred to *Prognathodon saturator* (Dortangs *et al.*, 2002)*;* Polcyn *et al.* (2010) described material belonging to the durophagous species initially described from Morocco, *Globidens phosphaticus* (Bardet *et al.*, 2005). The new plioplatecarpine material from Angola, which was collected in 2010 is probably represented by *Gavialimimus almaghribensis* (Strong *et al.,* 2020) as '*Platecarpus' ptychodon* (Arambourg, 1952) has since been rejected as a valid taxon. There is also material representing Halisaurinae, including a species of *Halisaurus,* which is suggested to be referable to *H. arambourgi* (Polcyn *et al.*, 2007)*; Phosphorosaurus* sp. (Dollo, 1889), which was synonymised with *Halisaurus* (Lingham-Soliar, 1996), but Mateus *et al.* (2011) and Konishi *et al.* (2016) suggest that there are enough differences between the two genera to separate them.

There are also vertebrae belonging to a small (approximately 1.5m long) *Halisaurus* sp. that were collected from Santonian-aged deposits near Iembe, this is a significant find because if the age of the specimen is accurate it could be as old as the holotype and it would also be the oldest halisaurine outside of North America (Mateus *et al.*, 2011).

Jiménez-Huidobro *et al.* (2017) included *Carinodens belgicus* and *Prognathodon saturator* as mosasaurs from Angola, which were reported by Schulp *et al.* (2013). The remains of these two species were both recovered from the Maastrichtian deposits. *P. saturator* was recovered from Tzimbio locality, about 15km northeast of the Bentiaba locality and *C. beligicus* from the Bentiaba locality (Schulp *et al.*, 2013). Interestingly, both species are found in Northern Europe (Dortangs *et al.*, 2002) and *P. saturator* was previously thought to have been restricted in its range to the Netherlands and surroundings. These findings suggest that both species achieved a much wider geographical range than previously thought (Schulp *et al.*, 2013).

Democratic Republic of Congo

In western DRC there are two fossil-rich Maastrichtian localities from which mosasaurs have been recovered, Manzadi and Bololo, which are in relatively close proximity to each other along the Congo River (Figure 3) (Lingham-Soliar, 1994; Jiménez-Huidobro *et al.,* 2017; Solé *et al.*, 2019). Lingham-Soliar (1994) provided the first report of the mosasaur fauna from DRC (previously Zaire).

He reported eight potential taxa mostly based on isolated teeth, isolated vertebrae and in one case fragments of a dentary (Lingham-Soliar, 1994). Six of the eight taxa reported belong to the Mosasaurinae, namely teeth from Mazandi referable to *Prognathodon* cf. *giganteus*, *Mosasaurus* cf. *lemonnieri, Mosasaurus* cf. *hoffmannii*; three vertebrae referable to *Mosasaurus* sp. from Mazandi; another two from Bololo also referable to *Mosasaurus* sp. and teeth belonging

to an indeterminate mosasaurine from an unnamed locality (Lingham-Soliar, 1994). Other subfamilies include a halisaurine, *Halisaurus* sp. based on a poorly preserved vertebra from Bololo and a plioplatecarpine, *Plioplatecarpus* sp. from Mazandi based on isolated teeth probably from different individuals (Lingham-Soliar, 1994).

In their summary of mosasaurs from Africa, Jiménez-Huidobro *et al.* (2017, Table 2, p.358) include *Carinodens* cf. *belgicus* and *Globidens phosphaticus,* which Polcyn *et al.* (2010) noted in a collection of reptile teeth in the Royal Museum for Central Africa in Tervuren, Belgium. However, the labels associated with these teeth did not include exact information about the locality and stratigraphic age of the specimens, and they are thought to be from localities along the Congo River (Polcyn *et al.*, 2010). Jiménez-Huidobro *et al.* (2017, Table 2, p.358) did not include some of the taxa reported by Lingham-Soliar (1994). This is likely due to vague descriptions, poor preservation of the specimens and lack of any reassessments of the material, making the assignments by Lingham-Soliar (1994) somewhat tentative.

Table 1. Chrono-geographic distribution of mosasauroid squamates in Africa adapted from Jiménez-Huidobro et al. (2017) with additional taxa included from other sources. The names in bold were not included in Jiménez-Huidobro et al. (2017), likely because the descriptions of these mosasaurs are vague or are unpublished. Names in inverted commas are tentative.

	Angola	**DRC**	**Egypt**	**Morocco**	**Niger**	**Nigeria**	**South Africa**
Maastrichtian 72.1 ± 0.2 - 0.66 mya	*Carinodens belgicus* (Schulp et al., 2013) *Globidens phosphaticus* (Polcyn *et al*., 2010) *Prognathodon saturator* (Schulp *et al*., 2013) *Prognathodon kianda* (Schulp *et al*., 2008) ***Mosasaurus* sp. *aff. Hoffmannii*** (Mateus *et al*., 2011) ***'Platecarpus' ptychodon*** (Mateus *et al*., 2011) ***Halisaurus* sp.** (Polcyn *et al*., 2007) ***Phosphorosaurus* sp.** (Mateus *et al*., 2011)	*Carinodens* cf. *belgicus* (Polcyn *et al*., 2010) *Globidens phosphaticus* (Polcyn *et al*., 2010) *Halisaurus* sp. (Lingham-Soliar, 1994) *Plioplatecarpus* sp. (Lingham-Soliar, 1994) Cf. *Prognathodon giganteus* (Lingham-Soliar, 1994) *Mosasaurus* sp. cf. *hoffmannii* (Lingham-Soliar, 1994) ***Mosasaurus* sp. *cf. lemonnieri*** (Lingham-Soliar, 1994)	*'Globidens' aegyptiacus* (Zdansky, 1935)	*Carinodens belgicus* (Arambourg, 1952) *Carinodens minalmamar* (Schulp *et al*., 2009) *Eremiasaurus heterodontus* (LeBlanc *et al*., 2012) *Halisaurus arambourgi* (Bardet *et al*., 2005) *Pluridens (=Halisaurus) walkeri* (Bardet *et al*., 2015 pers. obs) *Prognathodon currii* (Bardet *et al*., 2005) *Prognathodon giganteus* (Bardet *et al*., 2005) *Prognathodon nov.* sp. (Bardet *et al*., 2015)	*Globidens aegyptiacus* (Lingham-Soliar, 1991) *Goronyosaurus* sp. (Lingham-Soliar, 1991) *Mosasaurus* cf. *hoffmannii* (Lingham-Soliar, 1991) *Plioplatecarpus* sp. ((Lingham-Soliar, 1991) *Platecarpus* sp. (Lingham-Soliar, 1991) *Angolasaurus* sp. (Lingham-Soliar, 1991) ***Pluridens walkeri*** (Lingham-Soliar 1991; Longrich, 2016)	***Pluridens calabaria*** (Longrich, 2016) *Goronyosaurus nigeriensis* (Soliar, 1988)	

	Angola	DRC	Egypt	Morocco	Niger	Nigeria	South Africa
		Mosasaurus sp1. (Lingham-Soilar, 1994) ***Mosasaurus sp2.*** (Lingham-Soilar, 1994) **Mosasaurinae** indet. (Lingham-Soilar, 1994)		*Gavialimimus almaghribensi*.(Strong *et al*, 2020) *Globidens phosphaticus* (Bardet *et al*, 2005) *Globidens simplex* (LeBlanc *et al*. 2019)			
Campanian 83.6±0.2 – 72.1±0.2 mya **Santonian 86.3±0.5 – 86.3±0.2 mya** **Coniacian 89.8±0.3 – 86.3±0.5 mya**	**Halisaurinae sp.** (Mateus *et al*., 2011)						*'Tylosaurus 'capensis'* (Broom, 1912)
Turonian 93.9-89.8±0.3 mya	*Angolasaurus bocagei* (Antunes, 1964) *Tylosaurus iembeensis* (Antunes, 1964)				*Tethysaurus nopcsai* (Bardet *et al*. 2003)		

South Africa

Pondoland mosasaurid remains

The first South African mosasaurid remains were discovered in 1901 on the coast of Pondoland, Eastern Cape, SA by geologists Dr. Arthur William Rogers and Dr. Ernest Hubert Lewis Schwarz (Rogers and Schwarz, 1902). According to the geological report written in 1902, a set of lower jaws resembling those belonging to *Mosasaurus* were discovered in Santonian-aged marine deposits south-west of the Mzamba River mouth (Rogers and Schwarz, 1902), approximately 3.5km from the border of KwaZulu-Natal. A decade later in 1912, Broom described this material as an almost complete frontal bone and the articulated anterior portion of the parietal and portions of both postorbitofrontals, herein referred to as the frontoparietal complex (Figure 4). He also mentioned that the specimen included jaw fragments with teeth but did not describe these.

According to Broom (1912) the large frontal had a length of 304mm and was triangular in shape with an almost straight line between the anterior end and the outer corner of the bone margin; a moderately flat and smooth dorsal surface and a conspicuous groove running down the

midline of the ventral surface (Broom, 1912) likely the olfactory lobe (Russell, 1967), and a slight depression on the midline of the dorsal surface near the parietal suture. The anterior portion of the frontal was said to be more rounded than any other frontal he had seen figured, suggesting that the nostrils were wider apart and distinct nasal bones were present (Broom, 1912).

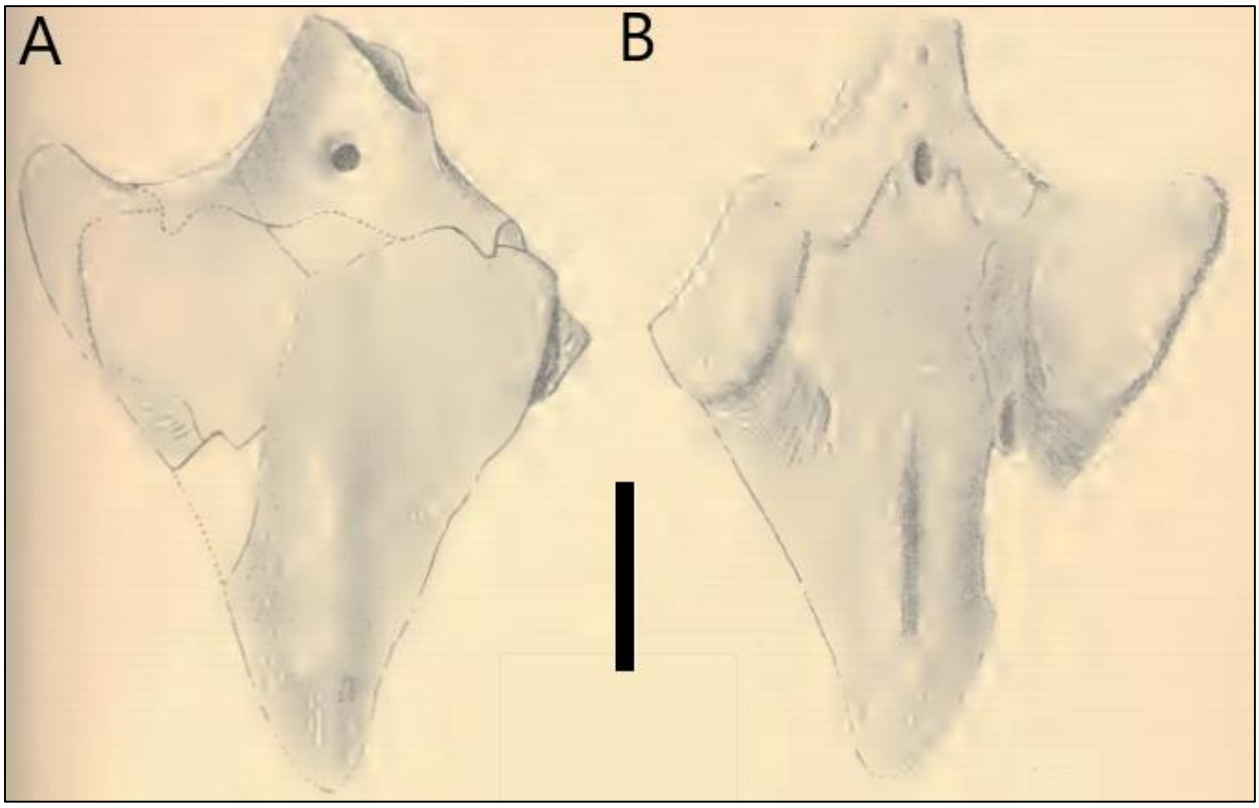

Figure 4. Drawings of SAM-PK-5265 frontoparietal complex in dorsal (A) and ventral (B) views adapted from Broom (1912). Scale bar = 100mm.

Broom (1912) noted that the suture between the postorbital and the frontal bone was like that of *Tylosaurus proriger* (Marsh, 1872). However, the frontoparietal suture is more like that of *Mosasaurus horridus* (Williston, 1895), which was later reassigned to *Mosasaurus missouriensis* (Russell, 1967). Only the frontal portion of the postorbital is preserved and Broom (1912) suggested that it agreed closely with *T. proriger*, though it was slenderer. Broom (1912) also indicated that the broad upper surface of the parietal was exactly as it is in *T. proriger*. Broom

(1912) noted that the pineal foramen is situated behind the plane that passes through the front of the [superior] temporal fossa, and that this differs from the position of the pineal foramen in *T. proriger,* leading Broom (1912) to propose a different species within the genus *Tylosaurus*: He named this holotype *Tylosaurus capensis.*

Lingham-Soliar (1992b) noted that *T. capensis* is likely more closely related to the earlier occurring *Tylosaurus nepaeolicus* (Merriam, 1894) rather than *T. proriger,* as suggested by Broom (1912), due to the fact that the parietal foramen is positioned behind the frontoparietal suture in *T. capensis* and *T. nepaeolicus,* whereas it is positioned on the frontoparietal suture in the later form *T. proriger* (Lingham-Soliar, 1992b). The position of the parietal foramen was long considered a diagnostic feature for species recognition in mosasaurs (Lingham-Soliar, 1992b). However, Jimenez-Huidobro and Caldwell (2016) suggested that it and the frontoparietal suture shape can vary through ontogeny and has been shown to vary within adult individuals and species of tylosaurines, e.g. *T. proriger* (Jiménez-Huidobro *et al.*, 2016; Stewart and Mallon, 2018).

Jiménez-Huidobro (2016)[2] provided the first thorough description of the SAM-PK-5265 dentary fragments and suggested that *T. capensis* be reassigned to the genus *Taniwhasaurus* (Hector, 1874). The proposed reassignment was based on facets and grooves in the crowns of two replacement teeth in one of the dentary fragments. This enamel ornamentation is said to be like that observed on the teeth of *Ta. oweni* and *Ta. antarcticus,* but have not been observed in *Tylosaurus* (Jiménez-Huidobro, 2016). Furthermore, it has been noted that deep vertical

[2] It should be noted that the isolated vertebra figured by Jimenez-Huidobro (2016) with the other SA material is not associated with SAM-PK-5265. There is no record of this isolated vertebra in the collections of Iziko Museums South Africa and it is suggested that it was included in error.

striations on the tooth crowns are unique to *Taniwhasaurus* (Martin and Fernandez, 2007), therefore providing additional support for the reassignment of *T. capensis* to *Taniwhasaurus.* The reassignment of SAM-PK-5265 frontoparietal complex and dentary fragments to *Taniwhasaurus* was published (Jiménez-Huidobro and Caldwell, 2019); however, further investigation of the material as well as other potentially associated remains will be conducted in the current study.

In addition to the material described by Broom (1912) and Jimenez-Huidobro (2016), an unprepared set of jaws (CGP/1/2265) was recently rediscovered in Geoscience Museum collections in Pretoria, SA by A. Chinsamy-Turan. It was realised that the jaws may be the 'lower jaws' that Rogers and Schwarz (1902, p.41) referred to in their geological survey report. The 'lower jaws' remained undescribed and unprepared until 2019, when it was taken to Iziko South African Museum where it was prepared out, and identified as upper jaws with other articulated elements forming a muzzle unit. Based on the Rogers and Schwarz (1902) report, the jaws were suggested to have been associated with the other '*T. capensis'* material (SAM-PK-5265) from Pondoland (Chinsamy-Turan *et al.,* 2018).

St Lucia mosasaurid material

In addition to the remains from Pondoland another indeterminate mosasaurid partial vertebra was recovered by Chris Shelton in 2016 from St Lucia, KwaZulu-Natal approximately 355km north-east of the other mosasaurid locality in Pondoland, Eastern Cape (Chinsamy-Turan *et al.,* 2018). The vertebra was recovered from south-western tip of the Nibela Peninsula, Lake St Lucia (27°59'09.2'' S 32°24'38.1'' E). The modern Lake St Lucia estuary seen today originated during the mid-Holocene when flood waters carved rivers into the Cretaceous bedrock (Gomes *et al.*, 2017). The geological changes that occurred in this region are poorly understood, as is the chronostratigraphy. According to Wright *et al.* (2000), this is due to a lack of outcrop, the

haphazard, scant fossil remains in the region and the widespread reworking of old sand and sediment (Wright *et al.,* 2000). Geological maps of KwaZulu-Natal published by Geology Education Museum, University of KwaZulu-Natal (n.d) suggests Cretaceous-aged deposits but does not provide specific details.

1.2) Rationale of this study

It has recently been shown that the mosasaur remains from SA are more extensive than previously realised (Jimenez-Huidobro, 2016; Chinsamy *et al.,* 2018) and the scope of knowledge of mosasaurs as an extinct group has been greatly expanded and improved in the last century (Ellis, 2003). The phylogenetic affinities of the SA mosasaurid remains are unclear and it is therefore essential that a thorough assessment of all the material is made and old assignments (e.g. Broom, 1912) be revised with more recently acquired knowledge.

The SA material is interesting as it represents the only record of mosasaurs on the east coast of Africa. Therefore, identifying the mosasaur taxa in SA could provide insights into possible dispersal or migration routes of mosasaurs during the Late Cretaceous. Another interesting feature of the SA mosasaurid remains from Pondoland is that they are said to have been recovered from Santonian strata (Rogers and Schwarz, 1902), making it one of only two known African taxa from the Santonian and one of the very few earlier African mosasaurs (see Table 1).

This study will provide a taxonomic assessment of the SA mosasaurid remains. Firstly, this work will provide a revised description of the SAM-PK-5265 specimen described by Broom (1912) i.e. the frontal with the attached parietal and postorbitofrontals (frontoparietal complex); and the associated lower jaw fragments with replacement teeth described by Jiménez-Huidobro (2016). Secondly, this work will encompass a full anatomical description of the recently prepared

specimen from Pondoland (CGP/1/2265), i.e. the muzzle unit and associated isolated teeth that were removed from the matrix around the muzzle unit during preparation. The third aspect of the taxonomic assessment will be an anatomical description of the isolated vertebra from St Lucia (Chinsamy-Turan *et al.,* 2018).

Geochemical analyses will also be done in order to confirm the age of the mosasaur material from Pondoland. Since the only publication about the Pondoland specimens dates to nearly 120 years ago (Rogers and Schwarz, 1902) there is much uncertainty around the stratigraphic location and exact age of the SA mosasaurid material. Thus, this research will provide some clarity as to the age of these fossils by considering the fact that the strontium isotope composition ($^{87}Sr/^{86}Sr$) of enamel belonging to marine organisms will have the same composition as the seawater at the time of enamel mineralisation (Veizer *et al.*, 1999; Harrell *et al.,* 2016). Strontium isotope analysis of the enamel of an isolated tooth (CGP/1/2265) from Pondoland will follow methods applied by Chinsamy *et al.* (2012) to a *M. hoffmannii* tooth from Turkey. Laser ablation is performed directly on a histological slide of the mosasaur tooth, which enables precise isotopic measurements of the various tooth tissues (Chinsamy *et al.*, 2012). Here the $^{87}Sr/^{86}Sr$ mosasaurid enamel from the Pondoland specimen will be compared to previously published calibration curves (e.g. McArthur *et al.,* 2012) to obtain an accurate age for the material collected by Rogers and Schwarz (1902).

Aside from the taxonomic assessment and dating, the current study will investigate various aspects of the palaeobiology of the SA mosasaurids. Using the material from Pondoland, particularly the isolated teeth extracted from the matrix around the muzzle unit (CGP/1/2265), this research will investigate mosasaurid dentition including the tooth attachment, tooth development and tooth replacement. These are subjects of interest in the field of mosasaur

research as they are used to assign the phylogenetic position of mosasaurs within the order Squamata. Furthermore, studying mosasaurid tooth attachment is particularly interesting as it has raised questions regarding the ancestral states of tooth attachment for high ranked taxonomic groups.

Previous studies have demonstrated that in order to properly assess tooth attachment, one needs to histologically analyse the tooth attachment tissues (Caldwell *et al.*, 2003; Caldwell, 2007; Luan *et al.,* 2009) . Therefore, it is anticipated that analysing the microstructure of an isolated fragmentary tooth using histology, will afford information regarding the tooth attachment. Histological analysis of the tooth crown tissues such as enamel and dentine could provide information about the microstructure of these tissues and time taken for tooth development. These tooth crown tissues are relatively understudied in comparison to the tooth roots and it would be beneficial to evaluate them in more detail.

The enamel architecture is of particular interest because there are contradicting reports regarding the prismatic or prismless nature of mosasaur tooth enamel (Torii, 1998; Sander, 2009; Chinsamy *et al.,* 2012). Hence, scanning electron microscopy will be used to assess and describe in detail the three-dimensional structure and organisation of the enamel by looking at the arrangement and orientation of the enamel crystallites.

Bernard *et al.* (2010) and Harrell *et al.* (2016) have used phosphate derived oxygen isotope analysis to provide information about the thermoregulatory capabilities of mosasaurs by comparing the oxygen isotope composition of mosasaurid tooth enamel to that of contemporary poikilothermic representatives. The oxygen isotope composition (δO^{18}_{PO4}) can be inputted into an equation to calculate the body temperature of extinct aquatic organisms

(Kolodny and Raab, 1988; Bernard *et al.*, 2010; Harrell *et l.,* 2016). It is fortuitous then that a fragmentary isolated shark tooth was found embedded in the matrix around the mosasaurid muzzle unit (CPG/1/2265) during preparation. Therefore, phosphate derived oxygen isotope analysis will be performed on the mosasaur tooth enamel and shark tooth enameloid following methods similar to those used by Harrell *et al.* (2016) with the aim to provide information about the thermoregulatory capability of the Pondoland mosasaur. Despite the fact that there are developmental and histological differences between shark and mosasaur teeth, the chemical signatures of the enameloid and enamel, respectively, should be comparable (Błazejowski, 2004).

1.2.1) Hypotheses of this study

I. '*Tylosaurus capensis'* is not a valid taxon.

II. There are at least 2 mosasaur taxa in SA.

III. Strontium isotope composition of the Pondoland mosasaur (CGP/1/2265) tooth enamel will indicate that the specimen is of Santonian age (86.3 ± 0.5 - 83.6 ± 0.2 mya).

IV. Tooth replacement, development, attachment and histology will be similar to those previously described.

   a. Replacement teeth and resorption pits will be positioned posterolingually to the functional teeth in the maxillae and will be orientated vertically.

   b. Histological analysis will provide information regarding tooth attachment condition. The tooth crown will be made up of a thin layer of enamel around a significantly thicker dentine layer that will provide information about tooth development time.

V. Scanning electron microscopic analysis of the mosasaurid tooth enamel will reveal prismless enamel contrary to Torii (1998) and Chinsamy *et al.* (2012).

VI. Oxygen isotope analysis of mosasaur and shark tooth enamel will provide evidence to suggest that the Pondoland mosasaur (CGP/1/2265) was capable of maintaining a body temperature higher than that of the surrounding water.

1.2.2) Aims and Objectives

1. Confirm the taxonomic identification of *Tylosaurus capensis* (Broom, 1912).
    1.1. Revise the anatomical description of the previously briefly described frontoparietal complex and dentary fragments (SAM-PK-5265).
    1.2. Provide the first anatomical descriptions of the muzzle unit and associated isolated teeth (CGP/1/2265).
    1.3. Compare the SA mosasaurid remains to other mosasaurs in order to establish whether a reassignment of SAM-PK-5265 is necessary, taxonomically identify CGP/1/2265 and in turn establish whether SAM-PK-5265 and CGP/1/2265 belong to the same individual.
2. Establish the current number of mosasaur taxa in SA.
    2.1. Provide the first anatomical description of the partial isolated vertebra recovered along the banks of the St Lucia estuary in 2016.
    2.2 Taxonomically identify the vertebra by comparing it to vertebra of other mosasaurs.
3. Compare the strontium isotope composition of the isolated tooth (CGP/1/2265) to that of the Late Cretaceous seawater in order to accurately date the material and aid in the taxonomic identification of the mosasaurid material.

3.1. Use the laser ablation method outlined by Chinsamy *et al.* (2012) to assess the $^{87}Sr/^{86}Sr$ values of several enamel samples from thin sections of the isolated fragmentary tooth in order to compare these values to the $^{87}Sr/^{86}Sr$ values of seawater during the Late Cretaceous.

4. Assess the dentition of these SA mosasaurids.

    4.1. Provide information about the tooth development and replacement patterns.

        4.1.1) Assess the patterns of tooth development and replacement using anatomical study and CT-scan analysis of the muzzle unit (CGP/1/2265).

        4.1.2) Assess the patterns of tooth development and replacement using anatomical study and micro-CT scan analysis of the dentary fragment with replacement teeth (SAM-PK-5265).

    4.2. Provide information about the microstructure of the tooth tissues and the tooth development time using the isolated teeth (CGP/1/2265).

        4.2.1) Micro-CT scan analysis of the two isolated teeth to assess the internal structure of the teeth and to help guide thin sectioning.

        4.2.2) Histological analysis of one of the isolated teeth to identify and assess the microstructure of the tissues present.

        4.2.3) Use the histological thin sections to estimate the time taken for dentine deposition using dentine thickness and lines of von Ebner.

4.2.4) Use scanning electron microscopy to analyse the enamel architecture of one of the isolated teeth.

5. Provide information about the thermoregulatory capabilities of the Pondoland mosasaur using one of the isolated teeth (CGP/1/2265).

5.1. Assess the $^{18}O/^{16}O$ ratio values of the mosasaur tooth enamel and enamel from an associated shark tooth in order to estimate and compare their average body water temperatures.

Chapter 2: Methodology

2.1) Taxonomic methods

2.1.1) Anatomical descriptions

Detailed anatomical descriptions of the muzzle unit and isolated teeth (CGP/1/2265); the frontoparietal complex and dentary fragments (SAM-PK-5265); and the isolated partial vertebra are presented. Other publications and personal observations made at the Royal Belgian Institute of Natural Sciences (RBINS) are used to compare the anatomical features of the SA mosasaur material with those of other mosasaurs for which the taxonomy is known.

Detailed photographs of the specimens were taken with a Canon Powershot sx 720 camera or a Huawei P30 mobile phone. Reconstructions and drawings were made using Microsoft 3D paint. Reconstructions were made by copying and horizontally flipping well preserved areas of the specimens and then pasting them over the poorly preserved areas. This constructed image was then traced with a dotted line, before removing the constructed image and replacing it with an image of the actual specimen. Measurements were taken using digital callipers and a measuring tape (for the larger samples). Tables and calculations were done in Microsoft Excel.

2.1.2) Strontium isotope analysis

Strontium isotope analysis was done in the multi collector inductively coupled plasma mass spectrometry (MC-ICP-MS) facility, in the Department of Geological Sciences, University of Cape Town (UCT) using a laser ablation technique. An Australian Science Instruments RESOlution-SE laser ablation unit was coupled with a NuPlasma high resolution multi collector inductively coupled plasma mass spectrometry (HR-MC-ICP-MS) instrument. The operational parameters of the laser unit and mass spectrometer are outlined in Table 2.

The ICP-MS instrument comprises 12 Faraday cups fitted with 1011 ohm resistors, 3 ETP electron multiplier ion counters and one channeltron ion counter in a fixed-position collector array (Le Roux, 2010). The ion beam was manipulated using zoom optics in order to ensure alignment and coincidence of the ion beam of interest. The data from the MC-ICP-MS presented in this study were collected using 11 of the 12 Faraday cup detectors (^{89}Y:H6 ^{88}Sr:H5, ^{87}Sr+ ^{87}Rb:H4, ^{173}Yb++:H3 ^{86}Sr+ ^{86}Kr:H2, ^{171}Yb++:H1 ^{85}Rb:Ax, ^{84}Sr+ ^{84}Kr:L2, ^{166}Er++:L3, ^{42}Ca^{40}Ar:L4). The final ^{87}Sr/^{86}Sr data presented are therefore corrected for instrumental mass fractionation using the measured ^{86}Sr/^{88}Sr ratio and a stable value of 0.1194, and for isobaric interference at 87amu by ^{87}Rb using the measured ^{85}Rb signal and the natural Rb isotope ratio. Any potential interference due to doubly-charged Yb and Er isotopes and Ca argides were monitored, and negligible corrections applied (Ramos *et al.,* 2004).

Laser ablation was performed directly on two of the thin sections of IT-1 made for histological analysis in order to precisely pinpoint the tooth enamel as was done by Chinsamy *et al.* (2012). The thin sections were mounted on a holding tray and placed inside the laser ablation sample chamber. The enamel sample sites were chosen in regions of the enamel that were appropriate i.e. had no cracks and were wide enough for the laser to ablate the enamel only and not ablate part of the dentine or glass (see Figure 5). The sites were weakly ablated prior to doing the reading in order to remove potential surface contamination (Copeland *et al.*, 2008; Chinsamy *et al.*, 2012). This initial cleaning sweep removed approximately the top 2-5µm layer of the enamel with a 100µm spot size. The data collection ablation analysis followed the pre-ablated path; however the ablation involved a narrower laser beam of 80µm with a higher energy and a slower speed (similar to Copeland *et al.,* 2008) and removed an approximately 20µm deep layer

from the enamel surface. A total of six isotopic measurements were collected from the enamel of IT-1, excluding one trial run (Figure 5).

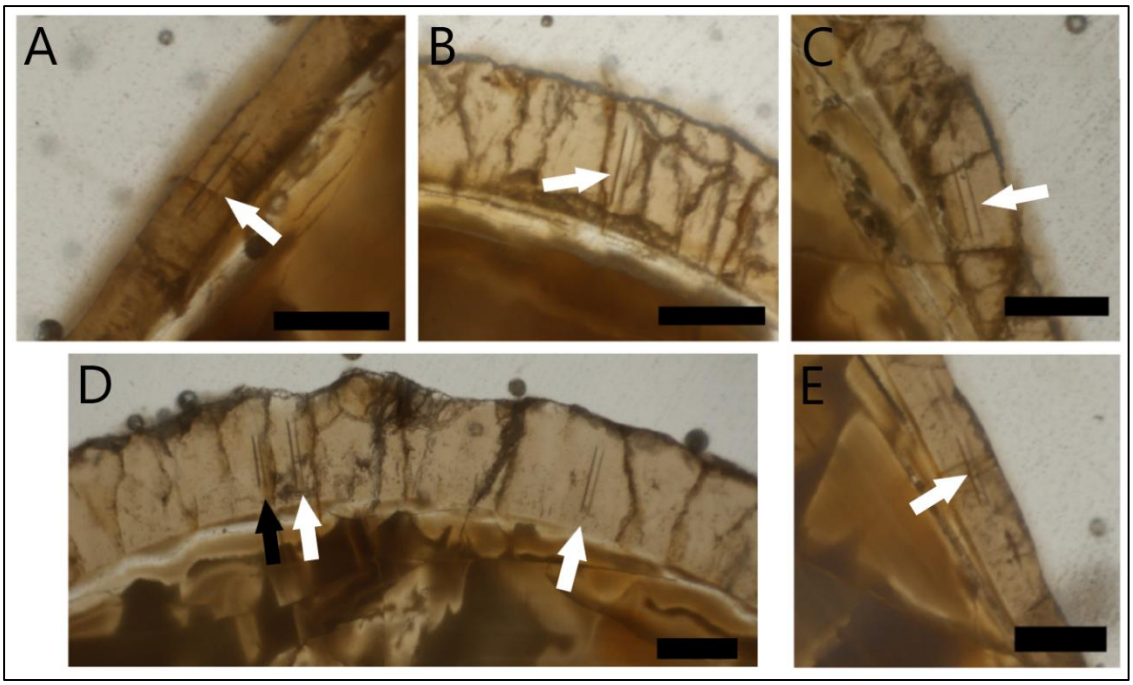

Figure 5. Ablated areas of enamel two thin sections. A-C represents a single thin section and D-E represents the other. White arrows indicate regions where the enamel was ablated for analysis. Black arrow the initial trial ablation. Scale bars: A-E = 100µm.

Table 2. Operating parameters used for $^{87}Sr/^{86}Sr$ laser ablation MC-ICP-MS analysis.

Parameter name	Parameter value
Laser ablation	
Laser	ASI RESOlution
Wave length (nm)	193nm
Line raster length	540µm
Helium flow rate	400 mL/min
Nitrogen flow rate	7 mL/min
Pre-ablation	
Frequency	30Hz
Spot overlap	75%
Beam width	100µm
Number of passes	3
Ablation	
Frequency	30Hz
Translation rate	2.5µm/s
Beam width	80µm
On sample fluence	~8 J/cm2
Data collection	

Parameter name	Parameter value
Gas background	30s
Sample	180s
Integration	0.2s

2.2) Palaeobiological methods

2.2.1) Computed tomography scanning

A computed-tomography (CT) scan was performed on the muzzle unit at the University of Cape Town Private Hospital in Cape Town, SA using a Philips Brilliance 64 slice CT Scanner. The CT scans were analysed using Mimics, a three-dimensional medical imaging software, which revealed additional details around the teeth, particularly the replacement teeth and other cranial elements that are not visible externally.

Micro-CT scans were done on the dentary fragment with replacement teeth (SAM-PK-5265) and the two isolated teeth (CGP/1/2265) at X-Sight in Somerset West, about 45km from Cape Town. The following parameters were used to scan all specimens: 190kV (voltage); 550µA (current) and 74µm (resolution). MyVGL was used to analyse the scan data and save images. These images were edited and scale bars were added using Microsoft Paint 3D.

2.2.2) Histological analysis

Isolated tooth 1 (IT-1) was removed from the matrix around the muzzle unit (CGP/1/2265) and was selected for histological analysis because it was fragmentary and of little taxonomic value. Micro-CT analysis was used to help guide the serial sectioning of the IT-1. All the thin sectioning was performed at Palaeobiology lab, in the Department of Biological Sciences at UCT, broadly following the methodology outlined in Chinsamy and Raath (1992). The specimen (IT-1) was embedded in Epoxacast resin and then cut longitudinally (labial to lingual) using an Imptech C10 abrasive cutter into three pieces. Once each piece was engraved, they were

ground straight and polished using the Imptech 30 DVT Grinder Polisher with a rotating lap-wheel and abrasive grinding discs of decreasing grit sizes (400p, 600p, 800p, 1200p grit). The polished pieces were left to dry overnight and subsequently mounted on frosted glass slides (55x75mm; 1.2-1.5mm thick) using Epoxacast resin. Struers Accutom-50 was used for cutting and grinding the slides into four longitudinal thin sections.

The thin sections were analysed and photographed using two different microscopes and cameras: A Nikon SMZ 745T dissecting microscope with a Nikon DS-Fi1 digital microscope camera attached was used with NIS-Elements ver 4 (imaging software by Nikon) to take low magnification photomicrographs. A Nikon Eclipse E200 petrographic microscope was used to assess the thin sections under polarized light. A Canon EOS 500D camera and the Canon EOS Utilities software Version 1.7 for taking high magnification images of the thin sections. Composite images were produced using NIS-Elements and Kolor Autopano Giga (APG). Microsoft Paint 3D was used to add neat scale bars, labels and annotations to the photomicrographs.

2.2.3) Oxygen isotope analyses

IT-1 and an associated fragmentary shark tooth were sampled for oxygen isotope analysis. Both were fortuitously found in the matrix around the CGP/1/2265 muzzle unit during preparation. Pre-processing and pre-treatment was performed at the Stable isotopes lab, in the Archaeology Department at UCT in August 2019. The phosphate derived oxygen composition of the shark and mosasaur enamel samples was analysed at the Laboratory of Geology at the Claude Bernard University, Lyon, France in December 2019.

Pre-processing and pre-treatment

Small amounts of enamel (~1-2mg) were removed from the shark and mosasaur teeth using a Dremel 8000 drill with a 1.2mm diamond drill tip. For the mosasaur tooth, the enamel was extracted from two different areas of the tooth where there was sufficient enamel to remove without including any underlying dentine. These areas were around the apex and around the middle of the crown. Two samples were obtained from the labial side of the shark tooth; from the apical region of the crown and enamel from the mesial and distal sides was combined to make the second sample. The extracted enamel was placed in labelled vials using filter paper and a paint brush.

The pre-treatment methods followed were outlined by Canoville *et al.* (2014) with a few changes to the timing of the pre-treatments. 1ml of 1.75% NaOCl (bleach) was pipetted into each vial containing the samples, which were left to soak for 45 minutes, whilst being shaken by hand at 15 minute intervals. They were then centrifuged using an Eppendorf Centrifuge 5415D for 90 seconds at 10000 rpm. The NaOCl was then pipetted out and replaced with distilled water; the vials were shaken and centrifuged; and this process was repeated three times to thoroughly rinse the samples.

Once rinsed the samples were soaked in 1ml of 1M CH3COOH (acetic acid) for 15 minutes and then rinsed another three times with distilled water using the centrifuge-pipette method. Most of the water was pipetted out and the openings of the vials were covered with Parafilm and small holes were poked in the tops of the vials. The samples were put in a rack and into a ScanVac Cool Safe freeze drier overnight.

Analytical protocol

The following procedures were performed at the Claude Bernard University, Lyon, France. The methods used were similar to those outlined by Rey *et al.* (2017).

The phosphate ions (PO_4^{3-}) in the apatite were isolated using acid dissolution and ion-exchange resin outlined by Lécuyer (2004). Silver phosphate (Ag_3PO_4) was precipitated in a thermostatic bath set at 70˚C, and then underwent filtration, rinsing with double deionised water and subsequent drying at 50˚C. Thereafter, a 300mg aliquot of Ag_3PO_4 was mixed with the same mass of nickelised carbon inside a silver reaction capsule. The Ag_3PO_4 was reduced to carbon monoxide (CO) by high-temperature elemental analyser (EA)-pyrolysis (Lécuyer *et al.*, 2007), from which the $^{18}O/^{16}O$ ratio could be measured (Rey *et al.*, 2017). Each sample was heated at 1450˚C by pyrolysis using a VarioPYROcube EA system (Elementar) interfaced to an IsoPrime isotope ratio mass spectrometer working in continuous flow mode at the Laboratory of Geology, Claude Bernard University, Lyon. Isotopic compositions are quoted in the standard δ notation relative to V-SMOW. Silver phosphate precipitated from standard NBS120c (a natural Miocene phosphorite from Florida) was repeatedly analysed ($\delta^{18}O = 21.71 \pm 0.20‰$; n = 30) along with the silver phosphate samples derived from the mosasaur and shark tooth enamel.

2.2.4) Scanning electron microscopy

Imaging

A piece of the enamel that had naturally fallen-off specimen IT-1 during enamel extraction for oxygen isotope analysis was used for SEM analysis. Pre-processing involved etching the enamel in 5% nitric acid for approximately 60 seconds. The enamel was air dried over night and was then gold sputter coated. SEM analysis was done using the Tescan MIRA

SEM at the Electron Microscope Unit at UCT. Terminology and descriptions of the enamel followed those outlined by Sander (2009).

EDS analysis

The same etched and sputter coated piece of enamel that was used for assessing the enamel architecture was used to perform energy-dispersive spectroscopy (EDS) on the unusual spherical structures found on the dentine (see Chapter 3, Section 3.2.1).

It was not certain which elements would be found in the sample thus a kV value of 20 was chosen in order to get sufficient x-rays in the spectrum. The detector converted the x-ray pulses for each element detected into proportions that sum to 100. If detected, Gold (Au) and palladium (Pd) were deleted from the analysis as they represent the elemental composition of the coating. Conversely, in a few cases, carbon was not detected and therefore was added to the analysis because we expect to find carbon in organic tissues such as dentine. According to M. Waldron (personal communication, March 2020), results with ratio values smaller than 1 i.e. <1% are considered inaccurate. Therefore values pertaining to sulphur (S) and sodium (Na) were ignored during data analysis.

EDS analysis was done at seven different sites around the enamel piece that had broken off of IT-1. The analysis was focused on the regions of enamel that still had underlying dentine attached. At each site 1-6 spectra were measured, the sites and positions at which the measurements were taken are shown in Figure 6.

Tables and boxplots shown in Chapter 3, Section 3.2.1 were made in Microsoft Excel 2013. The statistical calculations were also performed using Microsoft Excel 2013.

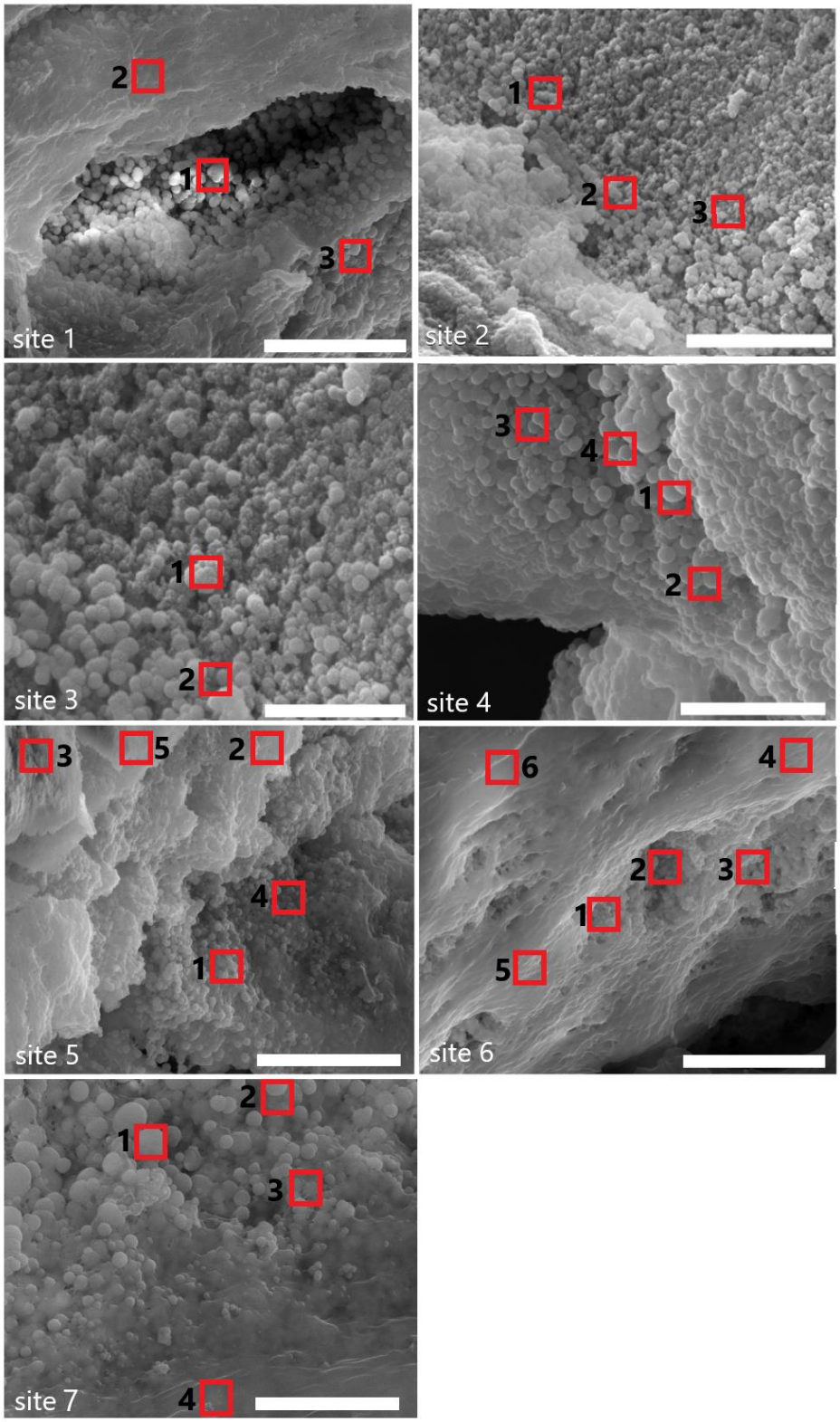

Figure 6. SEM images of the sites at which the EDS analysis was performed. The red blocks indicate the region hit by the electron beam. The spectrums measured on the spherical structures versus those measured on the flat surface of the dentine are visible here. Scale bars: sites 1, 5, 6 = 10μm; sites 2, 4 and 7 = 5μm; site 3 = 2μm.

Chapter 3: Results

3.1) Anatomical descriptions

3.1.1) SAM-PK-5265 frontoparietal complex

This specimen is comprised of four articulated cranial elements, namely an almost complete frontal, and the anterior portion of the parietal and portions of both postorbitofrontals. Additional fossil preparation in 2019 at Iziko South African Museum in Cape Town revealed some new anatomical details, which aided the following description.

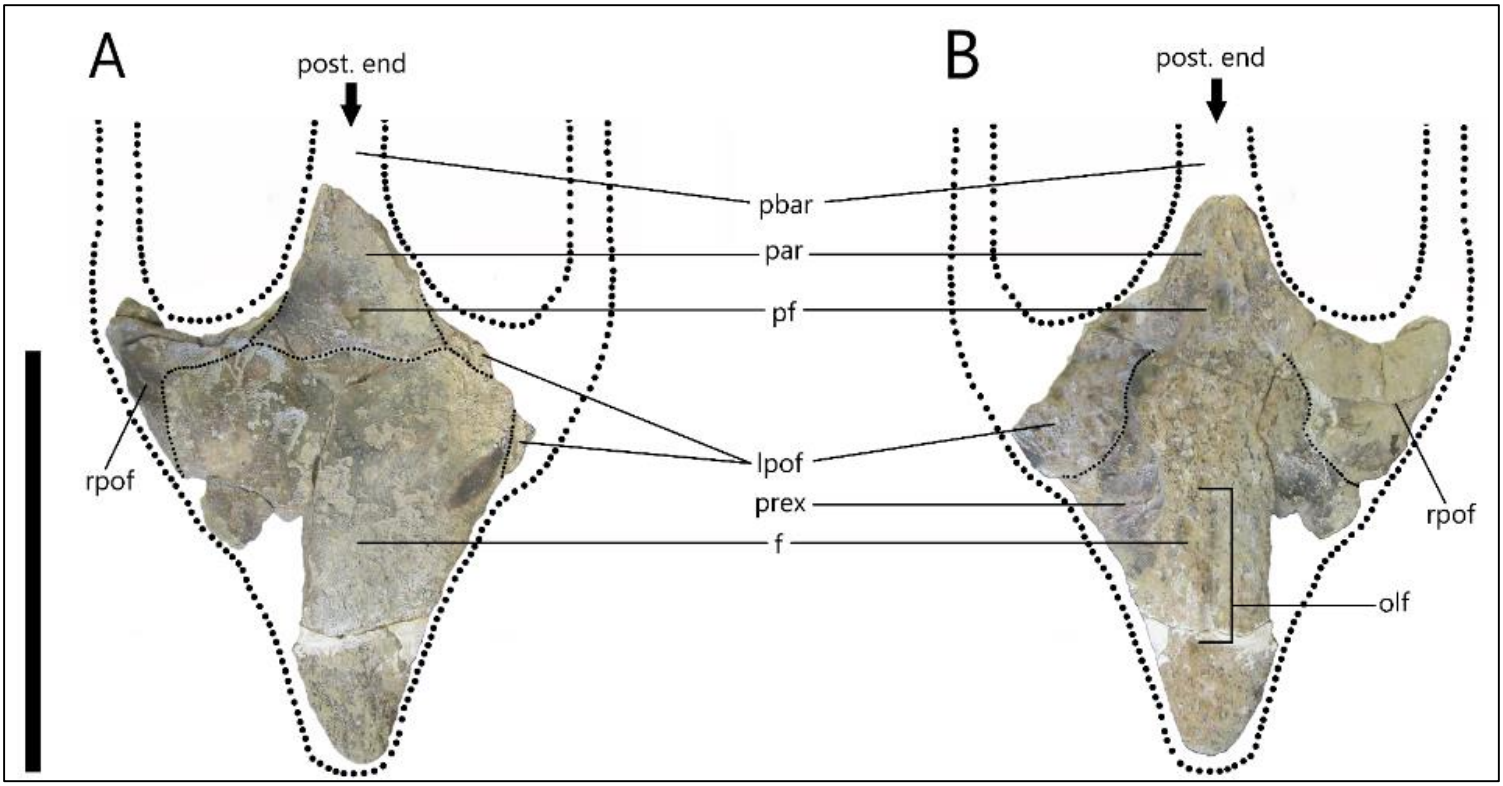

Figure 7. SAM-PK-5265 frontoparietal complex in dorsal (A) and ventral (B) views with dotted lines to reconstruct the anterior portions of the parietal bar and postorbitofrontal rami. Abbreviations: f = frontal; lpof = left postorbitofrontal; olf = olfactory tract; par = parietal; pbar = parietal bar; pf = pineal foramen; prex = prefrontal excavation; rpof = right postorbitofrontal. Scale bar = 300mm.

Frontal

The frontal is mostly complete with some fragments missing near the middle-right side of the bone, as well as the anterior-left side, which has been filled-in with plaster. There are several cracks on the bone, particularly near the postorbitofrontal and parietal sutures. The anterior tip appears to have been reattached to the frontal with plaster.

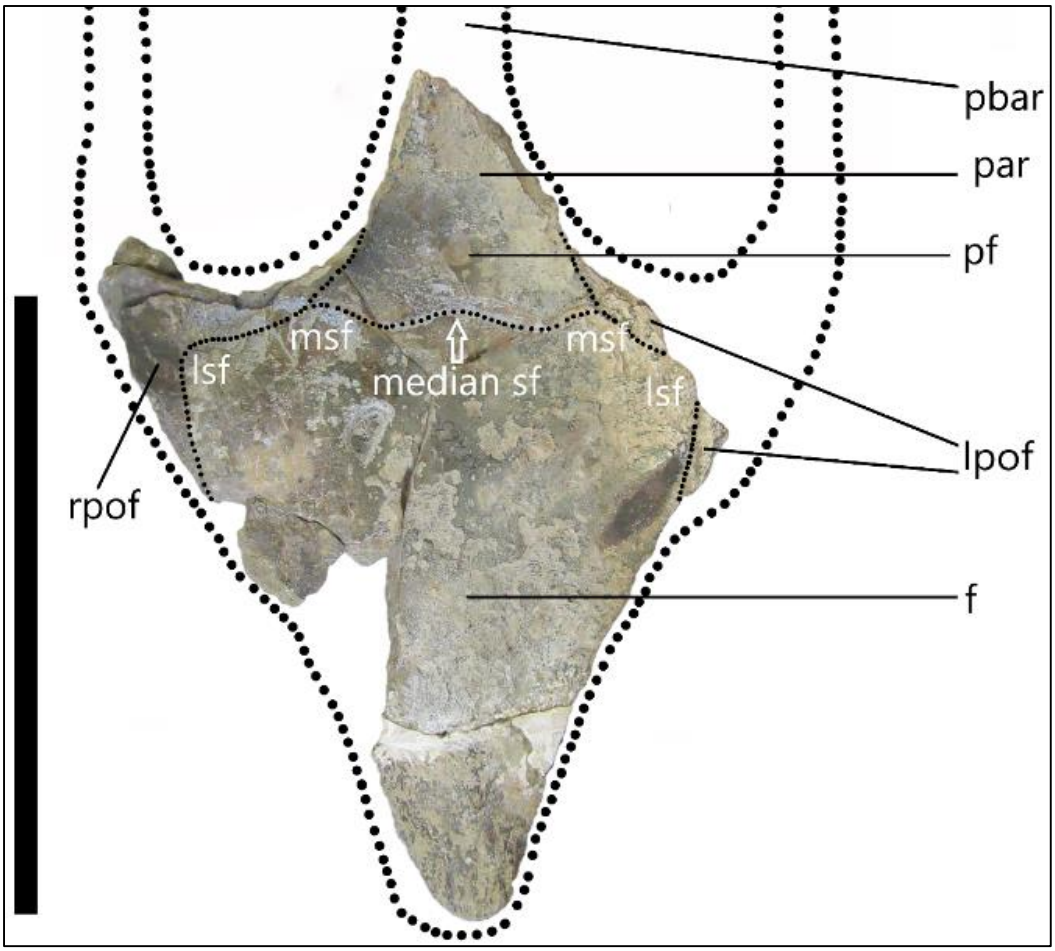

Figure 8. SAM-PK-5265 frontoparietal complex in dorsal view with dotted lines to reconstruct the anterior portions of the parietal bar and postorbitofrontal rami, as well as the sutures between the frontal, parietal and postorbitofrontals. Abbreviations: f = frontal; lsf = lateral sutural flanges; lpof = left postorbitofrontal; median sf = median sutural flange; msf = medial sutural flanges; par = parietal; pbar = parietal bar; pf = pineal foramen; rpof = right postorbitofrontal. Scale bar = 300mm.

The frontal is broad posteriorly and narrows toward the anterior end. It is dorsoventrally compressed but is robust and thick in comparison to many of the other frontals observed at the RBINS, suggesting the skull of this mosasaur was large and heavy. It is approximately 43mm thick in the centre of the bone (near the posterior end of the olfactory tract) (Figure 7B) and approximately 10mm thick where the prefrontal excavation is at the lateral edge of the bone. It also tends to decrease in thickness anteriorly with the anterior tip of the frontal being approximately 15mm thick.

Overall it is triangular with a length of 297mm from the anterior tip to the apex of the median sutural flange. It has a maximum width of 235mm from the edges of the lateral sutural flanges (Figure 8), giving it a length to width ratio of 1.3:1. The anterior tip of the frontal is rounded and broad, which was noted by Broom (1912) who suggested that this mosasaur probably had separate nasal bones, which were not preserved, as in most specimens. The lateral margins are almost straight, though reconstruction shows they do bulge slightly towards to posterior end of the frontal (Figure 7A). Anteriorly, there is no evidence to suggest that that the frontal was contributing to the shape of the posterior margins of the external nares and there are no sutures visible that could indicate the internarial bar overlapped the anterior of the frontal. However, it has been suggested that the anterior tip of the frontal is probably broken (M. Caldwell, personal communication, December 2019) and therefore the shape could be an artefact of preservation.

The dorsal surface of the frontal is smooth and relatively flat. There is a slight indentation where the median sutural flange meets the parietal. This could indicate that the anterior portion of the parietal overlaps the posterior portion of the frontal. Alternatively, it could be an artefact of fossilisation whereby the bones may have shifted slightly. The anterior half of the frontal bone

has a low, blunt midline ridge about 175mm long from the anterior tip of the frontal that extends posteriorly to form a flat surface. This is similar to the midline ridge visible on the frontals of two *T. bernardi* specimens at RBINS (R020 and R023).

On the ventral surface of the frontal, the excavation or fossa for the left prefrontal is visible (Figure 7B). The right postorbitofrontal is relatively complete compared to the left and is attached to the ventral side of the frontal. The olfactory lobe tract is a shallow excavation that is visible on the anterior half of the ventral surface and sits in line with the pineal foramen. The olfactory lobe tract terminates anteriorly before the anterior tip of the frontal and terminates posteriorly in line with the anteroventral corners of the postorbitofrontals.

The frontal bone appears to have five posterior sutural flanges/crests that form sinusoidal sutures with the parietal and postorbitofrontals (Figure 8). These crests or alae are all bluntly rounded and roughly the same width. The median sutural flange forms a crest directly beneath the pineal foramen, which is unusual. Most mosasaur frontoparietal sutures observed or figured describe one of four sutural forms: 1) a tight embayment around the pineal foramen; 2) pass through the pineal foramen; 3) are positioned beneath the pineal foramen with a gentle 'trough' that does not envelope the pineal foramen; 4) form a simple, straight suture beneath the pineal foramen (see Figure 9 for examples).

Parietal

The parietal is incomplete with roughly half of the table broken off diagonally (Figure 8). Dorsally the parietal is smooth, but the surface preservation on the ventral side is not as good (Figure 7B). Only the anterior portions of the parietal are present. Neither the suspensorial rami nor parietal alae are preserved. Both left and right postorbitofrontal processes of the parietal are preserved. The right side is more complete, but the cracks in this region make it impossible to see

the sutures between the parietal and postorbitofrontals. However, by reconstructing the line that follows the edges of the lateral parietal bar I can estimate the position of the sutures between parietal and postorbitofrontals (Figure 8).

Although the parietal is dorsoventrally compressed, it is also thick and robust like the frontal. Just posterior to the pineal foramen, the parietal table has a dorsoventral thickness of 43mm and is thicker still on the lateral edges due to the presence of lateral ridges. The pineal foramen is positioned 20.97mm posterior to the frontoparietal suture and is infilled. Dorsally the pineal foramen is almost circular in shape with a length of 13.17mm and a width of 14.12mm. Ventrally it is more oblong with a length of 26.36mm and a width of 14.12mm.

The right postorbitofrontal processes of the parietal and the right postorbitofrontal form the anterior boundary of the right supratemporal fenestra. Figure 9A-I shows a number of mosasaur taxa including SAM-PK-5265 in dorsal view with different supratemporal fenestrae shapes. Figure 9B and 9G show two *M. lemonnieri* specimens from RBINS, these supratemporal fenestrae are squarer anteriorly and form a quadrilateral shape like a trapezoid, with four distinct corners (Figure 9G). The anterior margins of the supratemporal fenestrae are flat but are angled so the anterolateral corner is positioned more anteriorly than the anteromedial corner. The angle between the parietal bar and the posterior surface of the postorbitofrontal process of the parietal is approximately 110°. The straight edged shape of the supratemporal fenestrae of *M. lemonnieri* does not resemble that of SAM-PK-5265.

The anterior margin of the supratemporal fenestrae of *Plioplatecarpus houzeaui* (R0136) (Figure 9C) is also fairly rounded and the entire fenestra has a teardrop shape; however, differences in other features of the skull, such as the frontal bone and the size of pineal foramen suggest that SAM-PK-5265 is unlike that of *P. houzeaui.* The anterior margin of the

supratemporal fenestra of SAM-PK-5265 is relatively rounded and partially resembles that of *Prognathodon solvayi* R033 (Figure 9D-E). Additionally, the parietal bar of *P. solvayi* is quite broad as it is in SAM-PK-5265; however, the position of the pineal foramen and the shape of the frontoparietal sutures are not consistent with those features in SAM-PK-5265.

Figure 9F is a drawing of the so-called immature *Tylosaurus proriger* specimen (CNM 8162) originally figured by Stewart and Mallon (2018). Similarities between SAM-PK-5265 and this specimen include the shape of the frontal and the frontoparietal suture, the position of the pineal foramen and the broadness of the anterior portion of the parietal bar. The shape of the supratemporal fenestrae in the *T. proriger* specimen is square anteriorly and is more triangular posteriorly with pointed posterolateral corners. This is consistent with the shape of the supratemporal fenestrae in the other tylosaur figured here, *Tylosaurus pembinensis* (Figure 9I). The *Taniwhasaurus antarcticus* holotype (IAA 2000-JR-FSM-1) supratemporal fenestrae has similar anterior margins as *M. lemonnieri;* however, the posterior corners are more like the tylosaurs figured, though the posterolateral corners are pointed more sharply. The anterior margins do not resemble those of SAM-PK-5265 and neither does the straight frontoparietal suture of *Ta. antarcticus* (Figure 9I).

The parietal table is relatively broad across the centre of the pineal foramen with a maximum width of approximately 105mm. Ratios of frontal width to parietal width (F:P) for a number of mosasaur taxa are highlighted in Table 3. The results from the table indicate that SAM-PK-5365 has a F:P of 2.83. This value is equally close to the values calculated for *P. solvayi* (R033) and *T. proriger* (CNM 1862), which both have a F:P of 2.95. *T. bernardi* (R0023) also did not differ widely with a F:P of 3.01, followed closely by *M. lemonnieri* at 3.06. The results suggest that the SAM-PK-5265 parietal bar is much wider relative to the frontal than that

of *Ta. antarcticus,* which has a F:P of 5.26. The parietal bar was not as wide as that of *Phosphorosaurus ortliebi* with a F:P of 0.67, although this very small ratio is due to the fact that the posterior part of frontal is missing (Konishi *et al.* 2016).

The fragmentary nature of this element makes it difficult to determine whether the lateral edges of the parietal table were curved as in *T. bernardi* (Jimenez-Huidobro and Caldwell, 2016) or were convex as in *T. proriger* (Russell, 1967; Jimenez-Huidobro and Caldwell, 2016). However, it is safe to say that the lateral edges where not straight as the right anterolateral edge of the parietal table curves medially. Contrary to Broom's (1912) interpretation, the middle section of the parietal bar, where the break occurred does not show any evidence that it may have become convex, forming a bulbous feature as in *T. proriger* (Figure 9F) or *T. pembinensis* (Figure 9I).

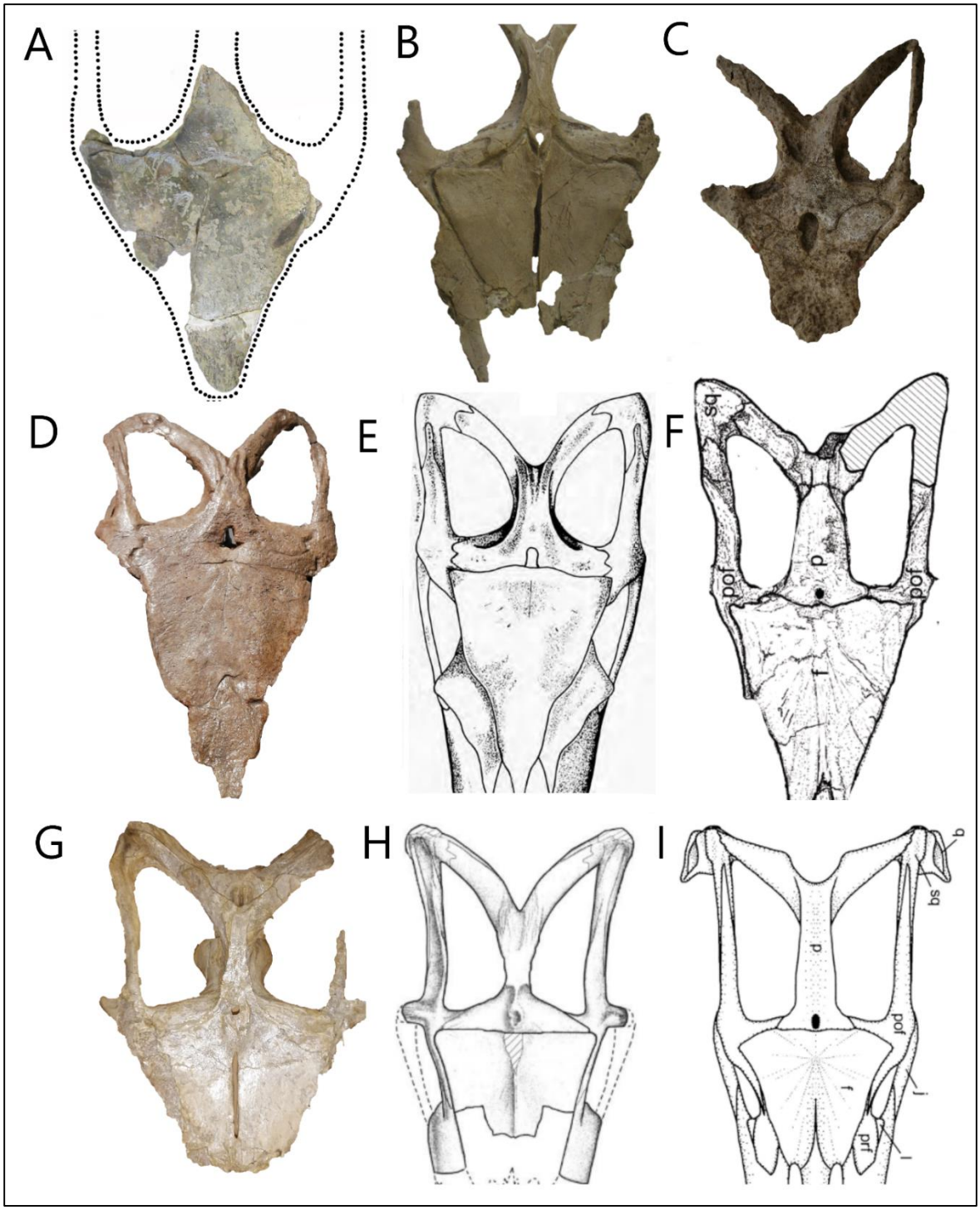

Figure 9. Different mosasaur taxa showing variations in certain skull features such as the shapes of the frontoparietal sutures, the anterior portion of the parietal bar and the shape of the anterior margin of the supratemporal fenestrae. (A) SAM-PK-5265 (B) Mosasaurus lemonnieri (RBINS R0369). (C) Plioplatecarpus houzeaui (RBINS R0136). (D) Prognathodon solvayi (RBINS R033). (E) P. solvayi (RBINS R033) drawing from Lingham-Soliar (1989). (F) Immature Tylosaurus proriger (CNM 8162) drawing from Stewart and Mallon (2018). (G) M. lemonnieri (RBINS R0366). (H) Taniwhasaurus antarcticus holotype drawing from Fernandez and Martin (2009). (I) Tylosaurus pembinensis drawing from Bullard and Caldwell (2010). Not to scale.

Table 3. The ratios of frontal (F) to parietal table (P) width of the different mosasaur taxa from Figure 9. Measurements were taken at RBINS and from other publications. The frontal width was measured between the outer edges of two lateral flanges and the parietal width was measured across the posterior most section of the parietal bar.

Species/specimen	F width (mm)	P width (mm)	F:P	Comments
SAM-PK-5265	297	105	2.83	
Mosasaurus lemonnieri (R0369)	150	49	3.06	
Phosphorosaurus ortliebi (R0034)	60	90	0.67	
Prognathodon solvayi (R0033)	168	57	2.95	
Tylosaurus proriger (CMN 8162)	~130	~44	2.95	Estimated measurement from photograph (Stewart and Mallon, 2018)
Taniwhasaurus antarcticus (holotype IAA 2000-JR-FSM-1)	~163	~31	5.26	Estimated measurement from photograph (Fernandez and Martin, 2009)
Tylosaurus pembinensis (MM V95)	~289	~71	4.07	Estimated measurements from drawings (Bullard and Caldwell, 2010)
Plioplatecarpus houzeaui (R0136)	167	43	3.88	
Tylosaurus bernardi (R0023)	~226	~75	3.01	

Postorbitofrontals

The postorbitofrontal bones should possess two short dorsal and ventral processes and two longer processes that extend anteriorly and posteriorly. The right postorbitofrontal is more complete than the left postorbitofrontal and is visibly attached to the posterior and posterolateral sides of the frontal bone (Figure 8). Only a small fragment of the anterior process and dorsal process of the left postorbitofrontal is visible in dorsal view (Figure 8).

On the ventral surface the postorbitofrontals are sutured to the frontal (Figure 7B). A small portion of the left postorbitofrontal appears to have been broken off anteriorly on the ventral surface as more of the postorbitofrontal excavation (Lingham-Soliar, 1992) is visible on

the left lateral of the ventral skull (Figure 7B). Anterior to the left postorbitofrontal excavation, the prefrontal excavation (prex) is visible but only a small part of this is visible on the right due to a large fragment of bone missing from the middle-right of the frontal.

3.1.2) SAM-PK-5265 dentary fragments

There are two dentary fragments associated with the frontoparietal complex. These were mentioned briefly in Broom's (1912) description of the frontoparietal but aside from noting that one possessed teeth, no descriptions were made.

The first fragment is from the anterior portion of the dentary, whereas the second is from the posterior portion and is comparatively less informative as it is the smaller of the two fragments and appears to have undergone some weathering.

Anterior dentary fragment

This is a partial left dentary fragment, which was determined to be from the anterior portion of the dentary due to its slenderness and the six large foramina visible on the lateral surface showing a posterodorsal entrance/exit of blood vessels and/or nerves (Figure 10C). Foramina seem to be present on the anterior half of dentaries in most mosasaurs (personal observation at RBINS). Unfortunately, bone is missing from both ends of the dentary, which means that no features of the anterior tip are visible and there is no information regarding the contact with the left splenial, angular, coronoid or surangular on the posterior end. The total length of the dentary fragment is approximately 200mm and the maximum height is approximately 43mm (from ventral surface to the bottom of the interdental spaces). However, a significant amount of bone is missing from the ventral surface as is evident from the tooth root that can be seen at the ventral surface under T.a (Figure 11, 12F). It is therefore impossible to

determine the actual height of the dentary. The maximum mediolateral width of the fragment is 39mm.

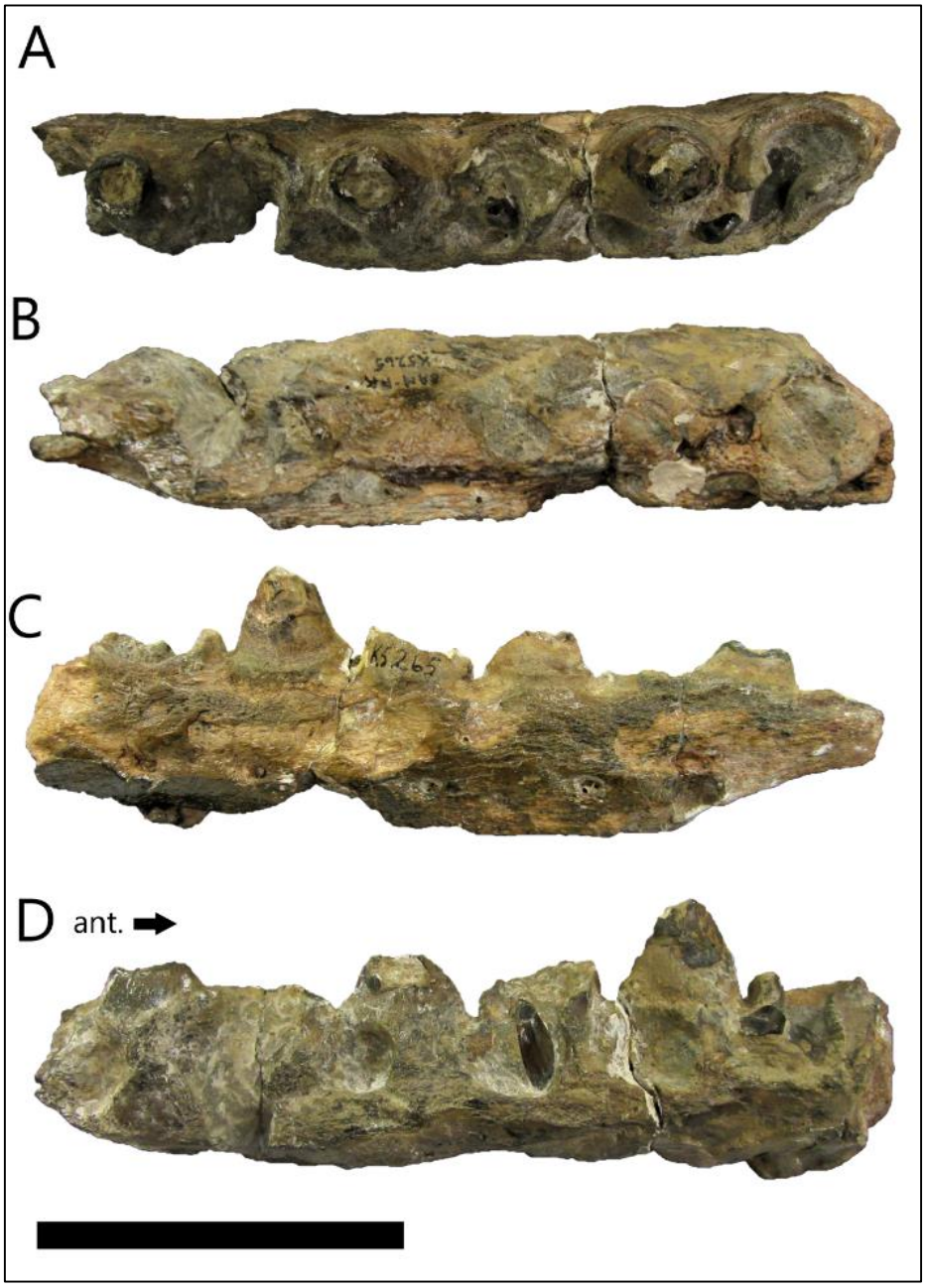

Figure 10. SAM-PK-5265 anterior dentary fragment in dorsal (A), ventral (B), lateral (C) and medial (D) view. Note directional arrow does not pertain to C. Scale bar = 100mm.

There are six functional tooth positions in the anterior dentary fragments, but no complete functional teeth in the fragment. Tooth sockets are present at tooth positions T.a, T.c and T.e; and dentine fragments are visible at tooth positions T.b, T.d and T.f. (Figure 11). The interdental spaces are small and equidistant. There are resorption pits (rp) and/or replacement teeth (RT) positioned posterolingually to the fragmentary functional teeth/tooth sockets. Resorption pits are associated with T.b, T.d and T.f (Figure 11). RT-1 is positioned posterolingually to T.a and RT2 is positioned posterolingually to T.c (Figure 11).

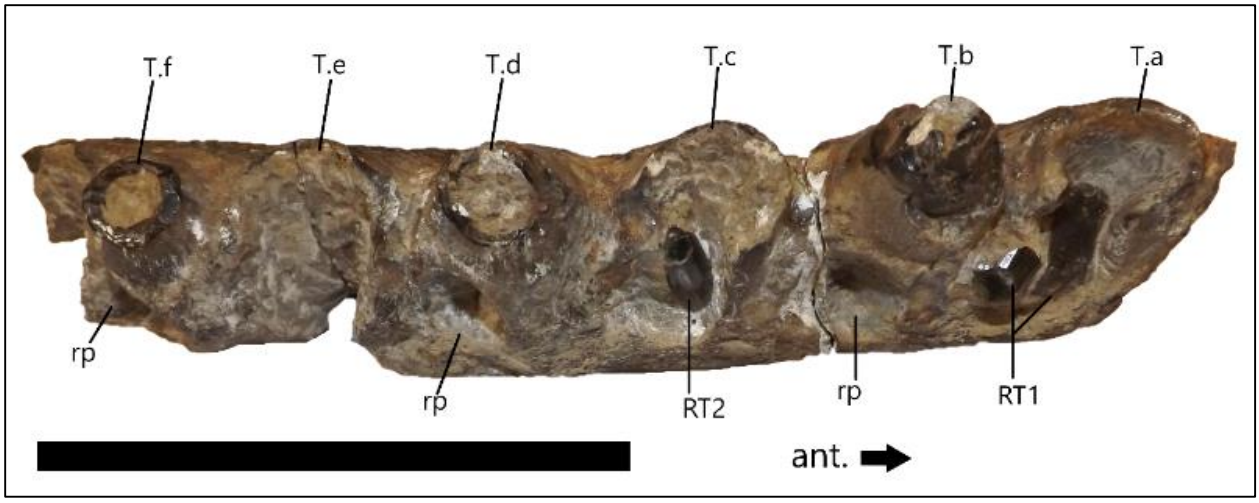

Figure 11. SAM-PK-5265 anterior dentary fragment in dorsomedial view showing the functional teeth/tooth sockets, replacement teeth and resorption pits. Abbreviations: T.a-T.f = function tooth/tooth sockets; RT1-RT2 = replacement teeth; rp = resorption pits. Scale bar = 100mm.

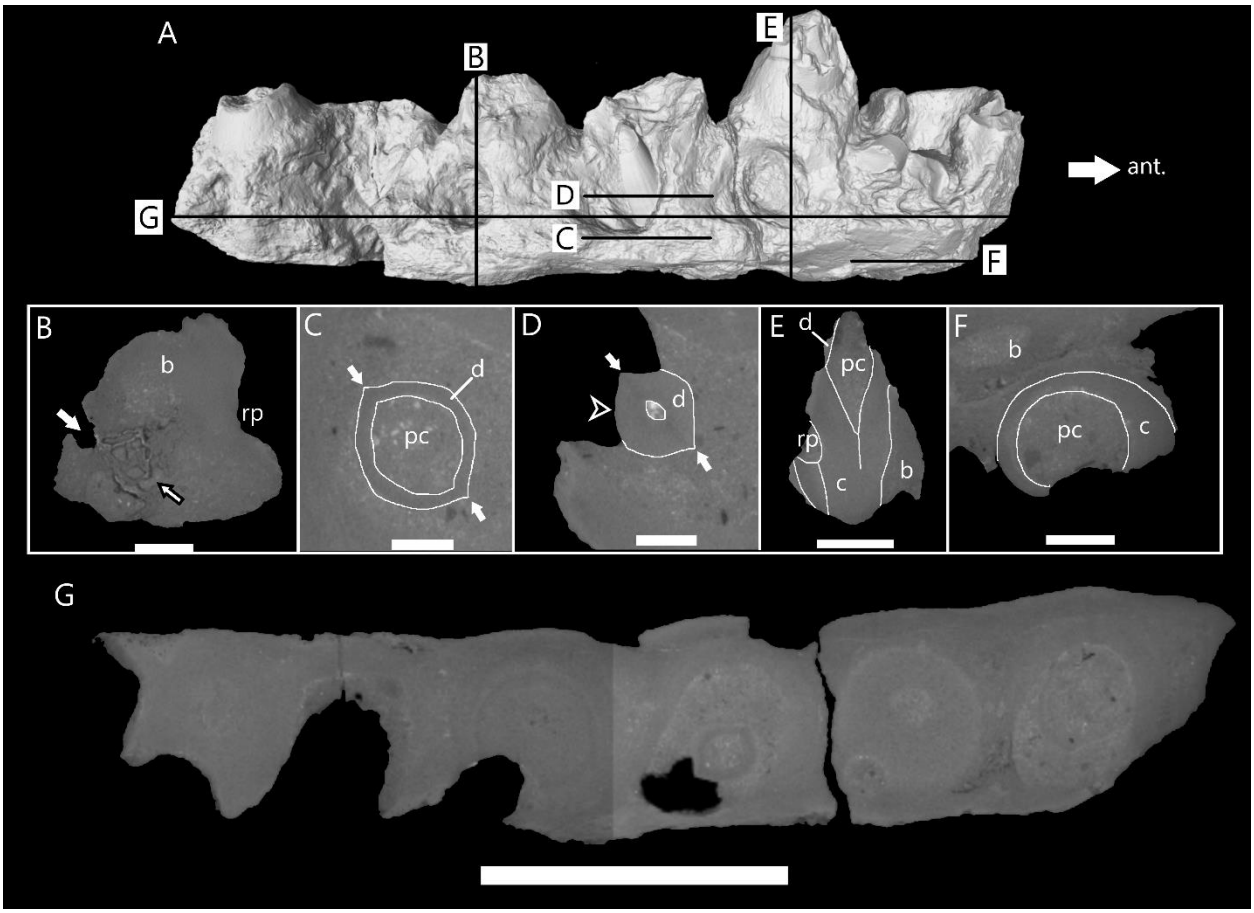

Figure 12. Micro-CT scan images of the anterior dentary fragment. (A) Three-dimensional micro-CT image of the anterior dentary fragment with lines to indicate location of the slices shown in B-G. (B) A longitudinal slice through the fragment at the position of the fourth functional tooth position (T.d) showing the resorption pit on the medial side and one of the foramina (white arrow) on the distal side. Black outlined arrow points to unusual bone tissue next to the foramen. (C) A horizontal slice through the dentary showing the base of the RT-2 crown. It has an ovate shape with two distinct carinae (white arrows) and a large pulp cavity. (D) A horizontal slice through the dentary showing the cross-sectional shape of RT-2 half way up the crown. It maintains its ovate shape with two carinae. No deep striations are visible on the surface of the tooth. (E) A longitudinal slice through T.b showing various tooth tissues, discernible by differences in their densities. The pulp cavity is infilled with sediment and most of the dentine has been lost, apart from a small amount on the medial side of the apex. (F) A cross-sectional slice taken near the ventral surface where part of T.a cementum root is visible. This suggests that there is a significant amount of bone missing from the ventral surface of the dentary. (G) A cross-sectional slice through the entire dentary fragment showing each tooth position. Abbreviations: b = bone; c = cementum; d = dentine; pc = pulp cavity; rp resorption pit. Scale bars: B = 10mm; C, D = 6mm; E = 20mm; F = 8.5mm; G = 50mm.

RT-1 is broken, which is fortuitous since it allows the observation of the sediment-infilled pulp cavity. However, it is difficult to determine the cross-sectional shape of RT-1 due to the bone and matrix surrounding it and it appears that the tooth may have been squashed slightly during fossilisation (Figure 13). The enamel surface that is visible is relatively smooth, without any deep striations.

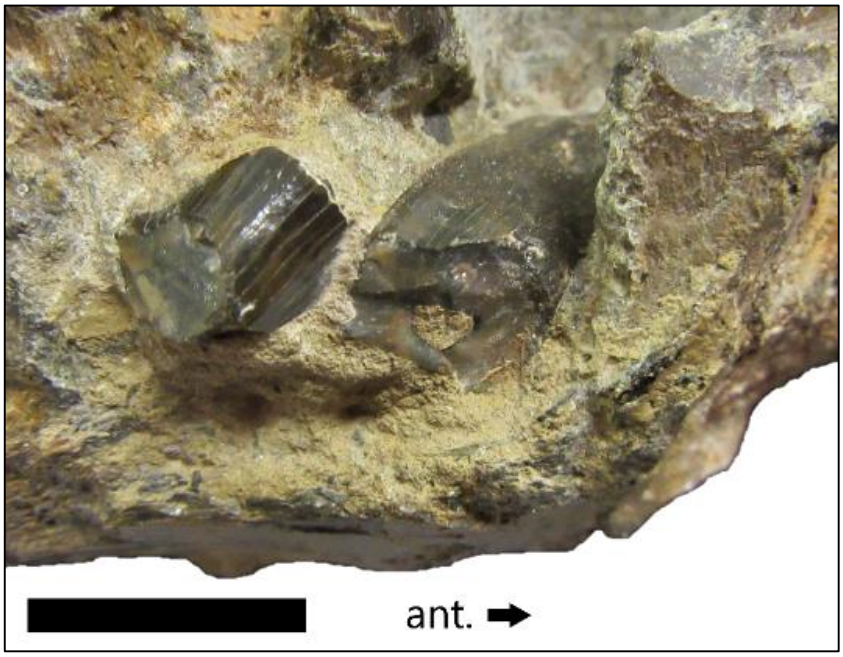

Figure 13. SAM-PK-5265 anterior dentary fragment with broken replacement tooth (RT1) at the anterior end of the fragment. The pulp cavity is visible within the tooth. Scale bar = 20mm.

RT-2 is almost complete and in its upright life-position (Figure 14). The apex of this tooth is broken off obliquely. Further preparation at the Iziko South African Museum in Cape Town allowed for the posterior carina to be observed (Figure 14B, arrow). The posterior carinae are sharp and there are no serrations visible along its length. Initially, the anterior carina was not visible as it was covered by bone. However, micro-CT scans revealed the anterior carina as well as the ovate, subconical shape of RT-2 (Figure 12C, D). The enamel layer is thin and is not visible on the micro-CT scans. There are gentle facets in the enamel surface (Figure 14A, black arrows), although these are not sharp enough to be particularly noticeable on the micro-CT scans (Figure 12D, white outlined arrowhead).

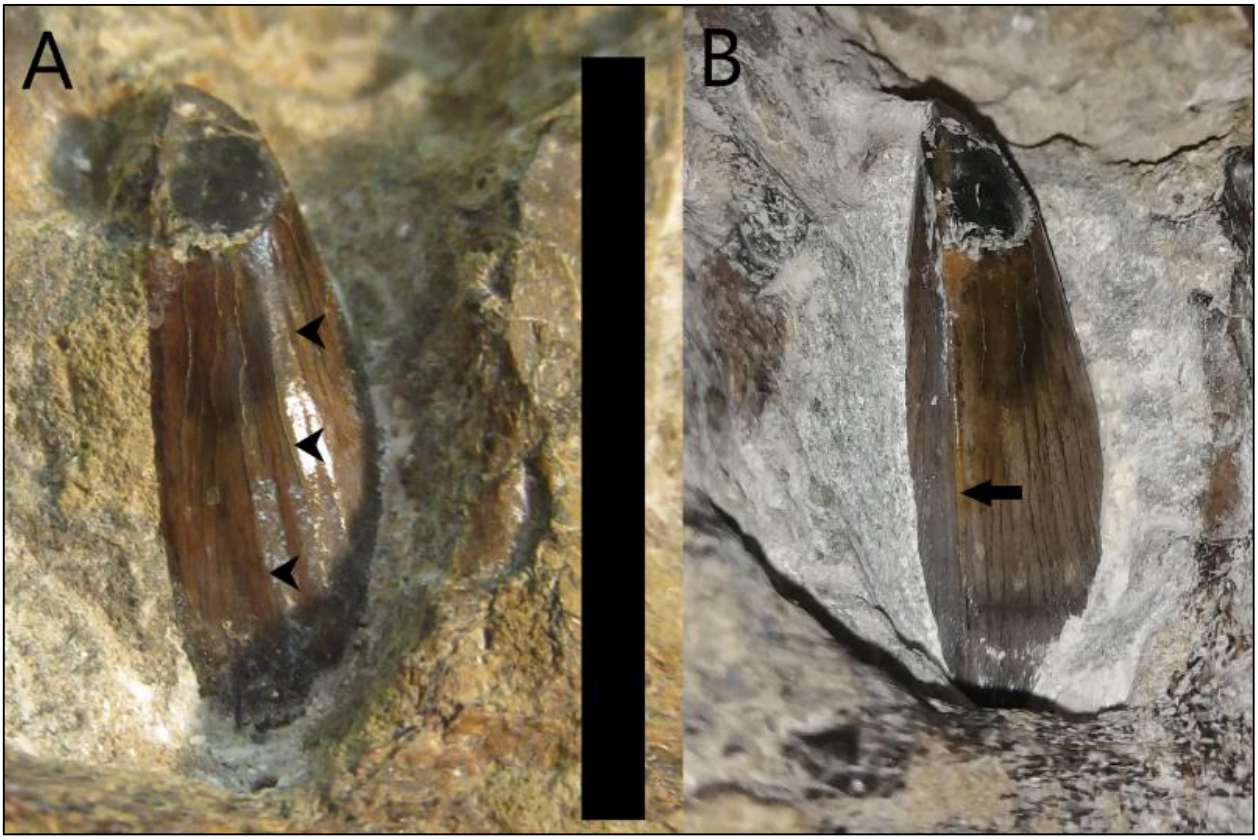

Figure 14. RT2 in the SAM-PK-5265 anterior dentary fragment. (A) Lingual view of RT2 with arrow head indicating the smooth facets. (B) Posteromedial view of RT2 after preparation to expose the posterior carina (black arrow). Scale bar = 20mm.

Posterior dentary fragment

The second left dentary fragment has a total length of 119mm and a maximum width of 44mm. It has only two and a half tooth positions preserved (T.g-T.i). There are no functional or replacement teeth present in this dentary fragment. However, T.g has a posterolingually positioned resorption pit associated with it (Figure 15), supporting its mosasaurid origin (Wiffen, 1980). Remnants of leftover dentine may be present at T.g (Figure 15). However, preservation is poor and this is uncertain.

The presence of small extant barnacles encrusted onto this dentary fragment, as well as the anterior dentary fragment, suggests that this fossil may have been exposed post-fossilisation in the intertidal zone for a period of time. The smooth appearance of the fossil also suggests that it may have been exposed to an energetic tidal environment where it experienced water-weathering.

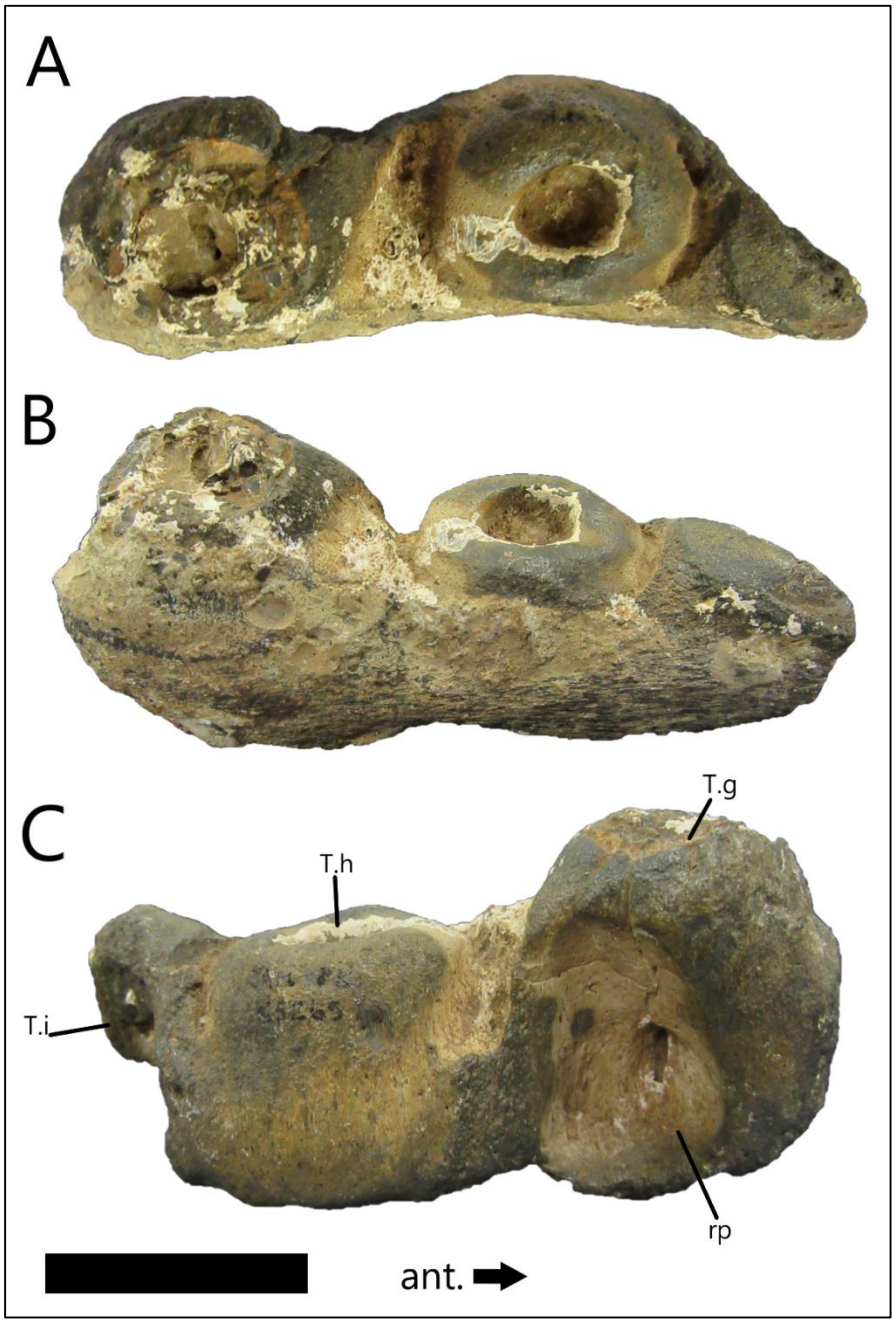

Figure 15. SAM-PK-5265 posterior dentary fragment in dorsal (A), lateral (B) and medial (C) views. The anterior (ant.) arrows pertains only to the medial view. Scale bar = 50mm.

3.1.3) CGP/1/2265 undescribed muzzle unit and associated isolated teeth

Muzzle unit

This specimen is comprised of a few attached cranial elements, which would make up most of the anterodorsal muzzle unit (Russell, 1967) including the maxillae, premaxilla, vomers, palatines, pterygoids and a few teeth (Figure 16). This cranial unit has a total length of approximately 55cm, but due to the incompleteness of the skull it is impossible to measure the actual skull length. The overall preservation is good, however, the external surfaces are not as well-preserved as the internal surfaces and internal skull elements (Figure 16B). The better preserved bones and teeth are those that were embedded in the matrix and only exposed during preparation.

Preparation of the ventral surface revealed the palate and the distortion of the skull that likely occurred during post-mortem decomposition and fossilisation (Figure 16B). It appears that it had been mediolaterally compressed during the fossilisation process and causing the left side of the skull to collapse and the skeletal elements to become displaced (Figure 16B). The left ventral side is not as well preserved as the right, nor was it prepared as fully as the right.

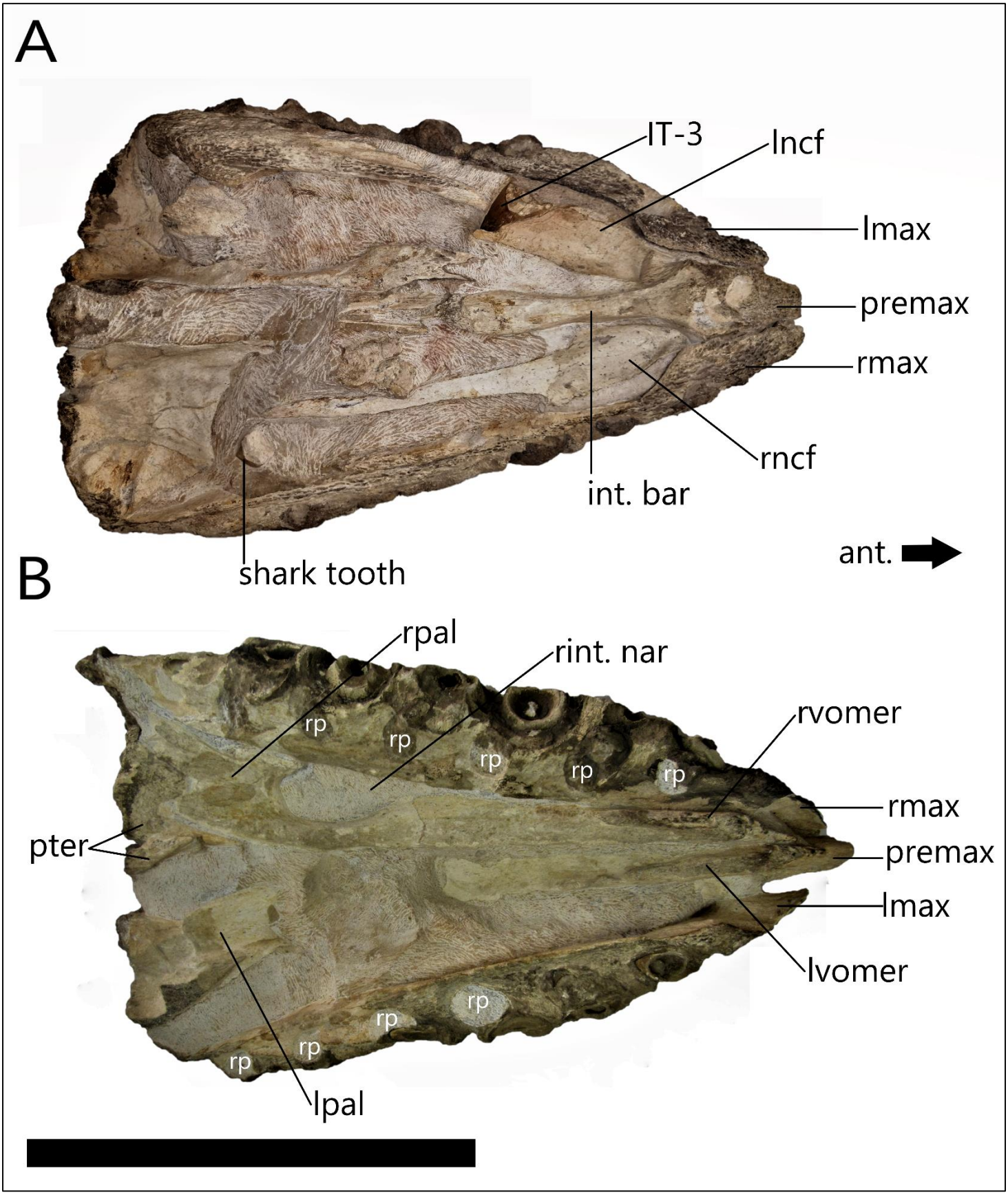
A
IT-3
lncf
lmax
premax
rmax
rncf
int. bar
ant.
shark tooth
B
rpal
rint. nar
rvomer
rp
rp
rp
rp
rp
rmax
pter
premax
lmax
lvomer
rp
rp
rp
rp
lpal

Figure 16. CGP/1/2265 muzzle unit in dorsal (A) and ventral (B) view with labels indicating the various elements discussed in the text. Abbreviations: int. bar = internarial bar; IT-3 = isolated tooth 3; lmax = left maxilla; lncf = left nasal cavity floor; lpal = left palatine; lvomer = left vomer; premax = premaxilla; pter = pterygoids; rmax = right maxilla; rncf = right nasal cavity floor; rpal = right palatine; rp = resorption pits; rvomer = right vomer; shark tooth = fragmentary shark tooth found in the matrix. Scale bar = 300mm.

Maxillae

The left maxilla is 50.5cm and the right maxilla is 55cm in length. Neither maxillae are complete. The tooth bearing regions of the maxillae are preserved, although the facial elements i.e. the thin, flat part of the maxilla that encloses the lateral sides of the face are both lost, thus exposing the left and right nasal cavity floors (Figure 16A). This is likely due to the fact that the facial elements are more delicate and therefore more likely to break off during fossilisation. In addition to this, the lateral sides of the tooth bearing elements are incomplete (Figure 17). The lateral portion of the right maxilla also appears to have undergone some surface weathering, although the replacement teeth and tooth sockets are not completely exposed, as on the left (Figure 17B), this prevented observation of any foramina that may have been present on this surface (Figure 17A).

Anteriorly, the maxillae are both mediolaterally compressed and become wider posteriorly in order to accommodate the teeth. The maxillae are not in line as the anterior tip of the left maxilla has been broken off, although the right maxilla is almost in line with the anterior tip of the premaxilla. Dorsally the anteromedial side of the right maxilla is in contact with the right lateral side of the premaxilla (Figure 16B). However, the left maxilla and premaxilla are not in contact as it appears that some of the left maxilla had broken off near this contact and the bones had shifted during taphonomic processes.

In ventral view the resorption pits are positioned posterolingual to the functional teeth/tooth sockets and are infilled (Figure 16B). Anteriorly, the right vomer is in contact with,

but not sutured to, the right maxilla with a distinct vomerine aperture; this contact is broken at the anterior margin of the right internal narial opening (Figure 16B). Posteriorly, the right palatine contacts the right maxilla. Due to the displacement of some of the cranial elements during fossilisation, there are no bones in contact with the medial surface of the left maxilla; therefore, the smooth and straight medial surface is visible (Figure 16B).

Maxillary teeth

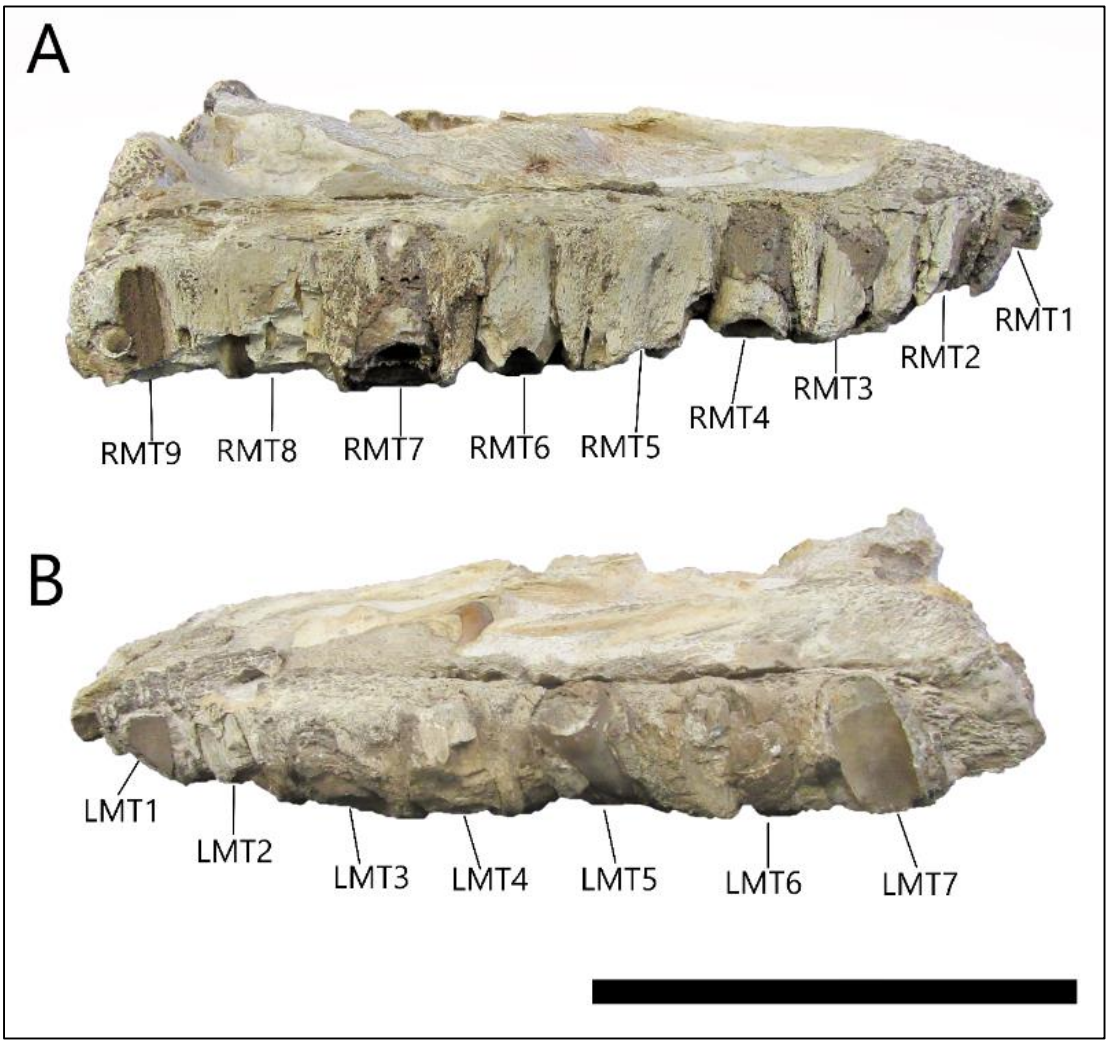

Figure 17. CGP/1/2265 muzzle unit in right (A) and left (B) views indicating the right maxillary tooth positions (RMT1-9) and left maxillary tooth positions (LMT1-7). Scale bar = 200mm.

Nine tooth positions are visible in the right maxilla and seven tooth positions are visible in the left maxilla (Figure 17). All the functional maxillary teeth are missing and had likely fallen out of the tooth sockets during decomposition. One replacement tooth is visible externally in the left maxilla, LMT5 (Figure 17B). However, CT scans of the muzzle unit revealed two replacement teeth within the right maxilla at tooth positions three and five (Figure 18A). It also revealed a replacement tooth within the left maxilla at tooth position three (Figure 18B).

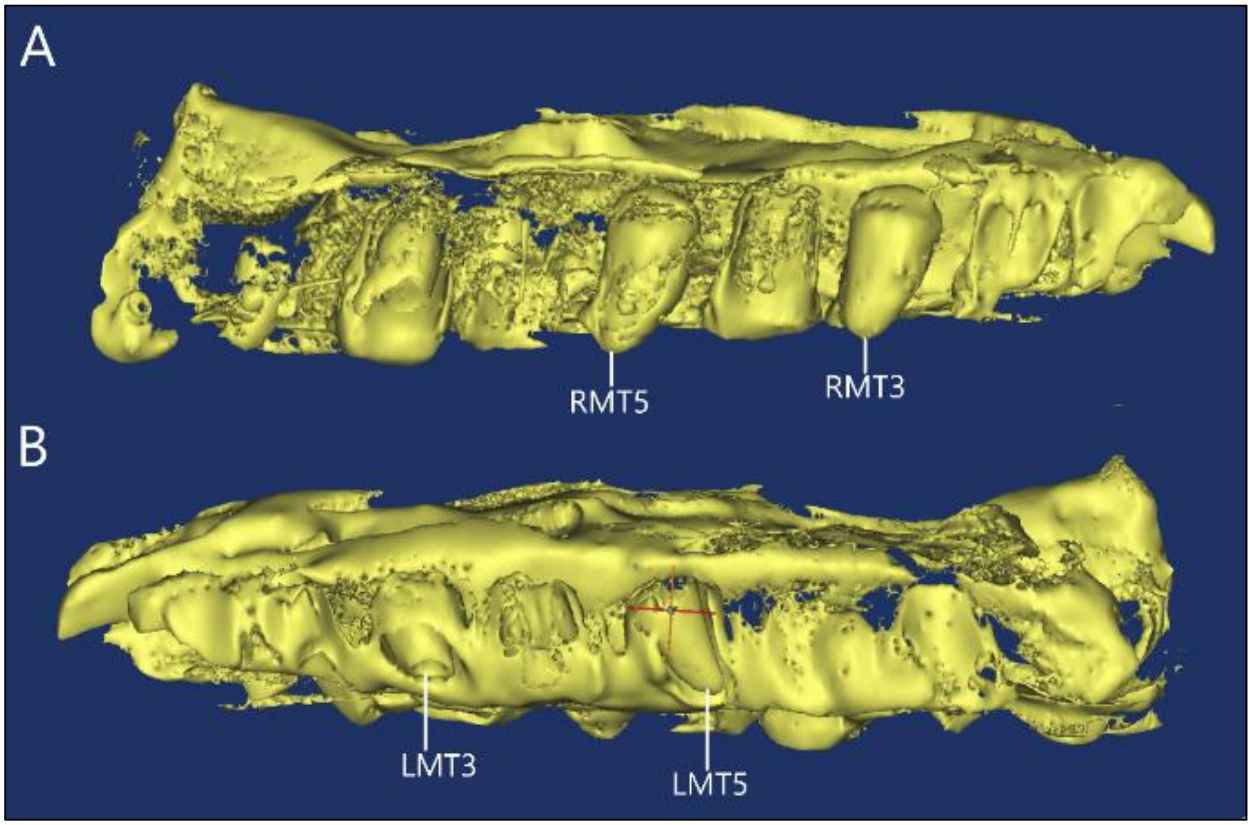

Figure 18. CT scan images of the CGP/1/2265 muzzle unit in right (A) and left (B) view showing the replacement teeth are tooth positions RMT3 and RMT5, and LMT3 and LMT5. Only LMT5 was visible externally. The replacement teeth are posteromedially recurved. Abbreviations: LMT = left maxillary tooth; RMT = right maxillary tooth.

In both the left and right maxillae there are pieces of bone broken off on the lateral sides exposing different tooth and bone tissue types. Teeth/tooth positions in the right (Figure 19) and left (Figure 20) maxillae are shown to indicate the tissue types surrounding them, which are identified based on the position of the tissue (see Figure 2) and the texture.

The right maxilla has 9 tooth positions and several fragmentary replacement teeth with remnants of the pulp cavities and, in some cases, remnants of dentine and alveolar bone is visible (Figure 19). **RMT1** is half an empty tooth socket. At **RMT2** there is no replacement tooth, but a mould of the pulp cavity is visible as well as some root cementum around it. In external ventral and lateral view **RMT3** appears to be an empty tooth socket; however, CT- scanning revealed the presence of a replacement tooth within the maxilla. **RMT4** appears to be the fragmentary cementum base on the fourth functional tooth. **RMT5** and **RMT6** both show very small pulp cavities surrounded by root cementum separated by a thin layer of alveolar bone. These are likely remnants of infilled cementum roots. **RMT7** shows a well-developed replacement tooth that has broken apically (Figure 19). The pulp cavity is open and the interior wall are lined with a crystalline sedimentary matrix surrounded by chalky dentine. At **RMT8** a small amount of root cementum is visible. **RMT9** shows a portion of the concaved surface with what appears to be alveolar bone that would have formed the medial side tooth socket.

The left maxilla has only seven tooth positions. There are no functional teeth preserved, only replacement teeth and tooth sockets. **LMT1** presents a concave surface lined with dark alveolar bone that would have formed on the medial side of the functional tooth. **LMT2** shows some root cementum in lateral view and in ventral view there is a small pulp cavity partially surrounded by chalky dentine. **LMT3** is a fragment of a replacement tooth. The pulp cavity is open and the interior walls are lined with sediment and the cavity is surrounded by chalky

dentine. There is some darker bone tissue, which is suggested to be alveolar bone (Figure 20). **LMT4** appears to be a partial cementum root for a very large functional tooth, it is at least 4cm in diameter. A small pulp cavity mould is visible. The resorption pit associated with **LMT4** is also the largest of all the resorption pits (Figure 16B). **LMT5** has a well-developed and well-preserved replacement tooth, which also consists of remnants of dentine and a thin layer of enamel surrounding a sediment infilled pulp cavity with distinct layers in the sediment (Figure 20); this tooth is slightly posteromedially curved and has a large round base, which narrows to a relatively blunt apex (Figure 20). **LMT6** shows no remnants of a functional tooth but there is a fragment of a small replacement tooth present that is directly associated with the resorption pit as seen in ventral view (Figure 16B), suggesting that this replacement tooth was in the early stages of development. **LMT7** shows a resorption pit posterolingual to a concave surface where a functional tooth was once present (Figure 20).

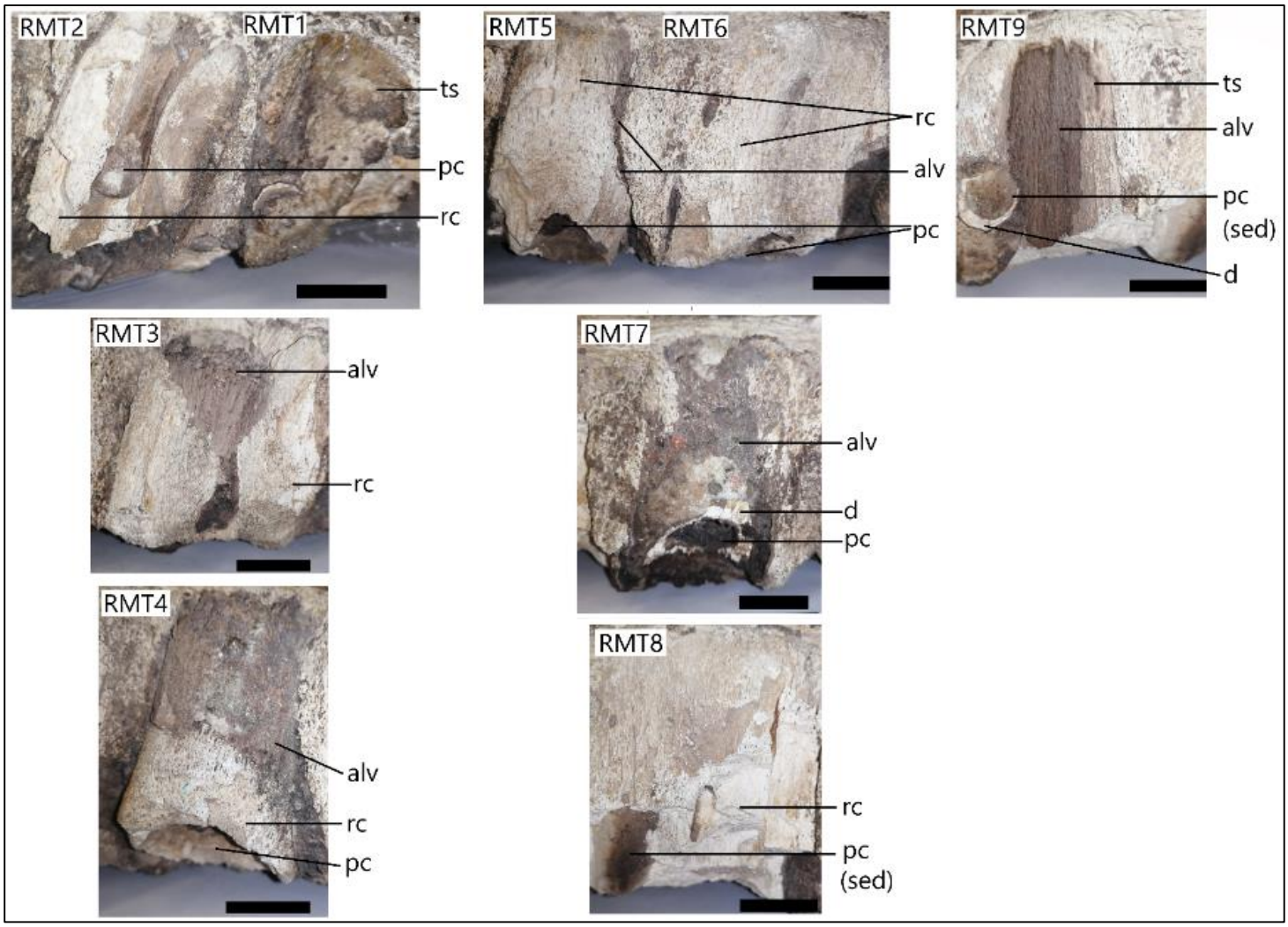

Figure 19. Lateral view of individual right maxillary teeth indicating the different tooth and bone tissue types in RMT1-RMT9.RMT1 is a partial tooth socket. RMT2 has been broken longitudinally allowing for the pulp cavity to be seen in longitudinal cross section. RMT4 and RMT7 are partial tooth crowns with the pulp cavity having been infilled in RMT4 and hollowed out in RMT7. Sediment infilled pulp cavities are partially visible in RMT8 and RMT9. The pulp cavities in RMT5 and RMT6 are much smaller than the others, suggesting that these are remnants of the cementum root or pulp canal. The root cement appears to have a very chalky texture and is light in colour, whereas the alveolar bone is darker in colour and appears to be quite resistant to flaking. Leftover dentine can be seen in RMT7 and RMT9 around the pulp cavity. This dentine has the same plaster-like texture as the dentine in the isolated teeth. alv = alveolar bone; d = dentine; pc = pulp cavity; pc (sed) = sediment infilled pulp cavity; ts = tooth socket; rc = root cementum. Scale bars = 20mm.

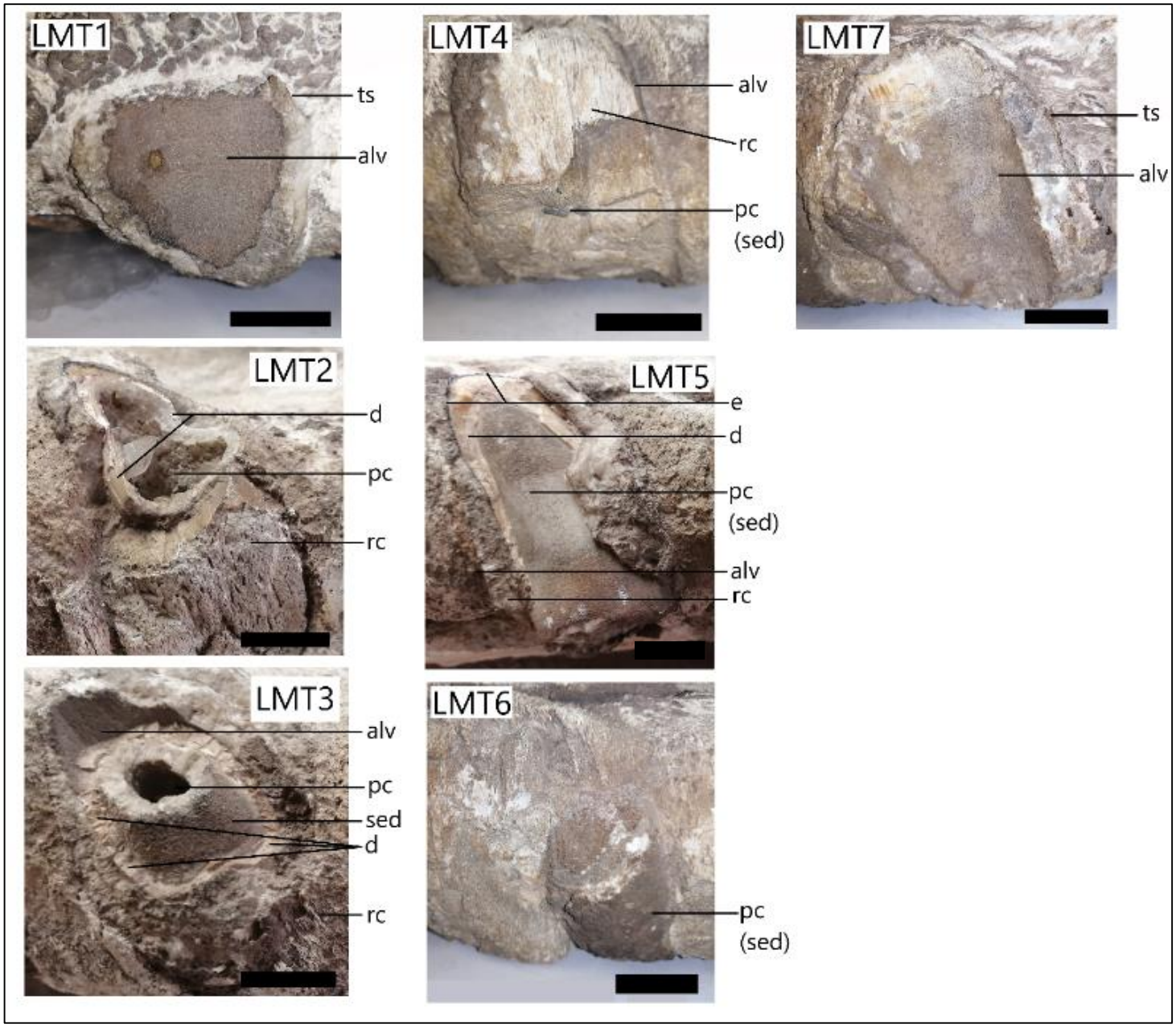

Figure 20. Lateral views of LMT1, 4, 6, 7 and ventrolateral views of LMT2, 3, 5 indicating the different tooth and bone tissue types. The alveolar bone is dark in colour and appears to be quite resistant to flaking off as seen in the right maxilla. Leftover dentine can be seen in LMT2, LMT3 and LMT5 around the sediment infilled pulp cavities. The pulp cavity in LMT3 is only partially infilled as the centre is still open, but there is a layer of sediment adjacent to the dentine layer. The dentine has the same plaster-like texture as the dentine on the isolated teeth. alv = alveolar bone; d = dentine; e = enamel; pc = pulp cavity; pc (sed) = sediment infilled pulp cavity rc = root cementum. Scale bars = 20mm

Premaxilla

Figure 21. Dorsal view of the premaxilla isolated from the rest of the muzzle unit. Scale bar = 100mm.

The premaxilla is fragmentary with the posterior and anterior most portions missing (Figure 21). This is unfortunate because many diagnostic characters of the posterior margins of the external nares and the anterior tip and premaxillary teeth are lost. The premaxilla appears to be the main contributor to the internarial bar, which is smooth and separates the two external narial openings on the top of the head. The total length of the incomplete premaxilla is 278mm.

There are no teeth or tooth sockets evident on premaxilla (Figure 22) and CT-scan imaging does not show evidence of maxillary teeth (Figure 23). In dorsal view it resembles an arrowhead with a tall trapezium shaped point between the anterior portions of the two maxillae (Figure 21). It narrows to form the internarial bar, which has a smooth surface and a minimum width of approximately 14mm, which would likely be the widest part of the external narial openings. It widens posteriorly again so that the posterior end of the internarial bar bulges both laterally and dorsally (Figure 21).

In lateral view the anterior tip of the premaxilla is rectangular and has a slight ventral curvature (Figure 22). CT-scans showed cross-sections through the anterior tip, which is

triangular in shape (Figure 23). The internarial bar is mediolaterally compressed and relatively elongated with a flat dorsal surface and a ventral point (Figure 23).

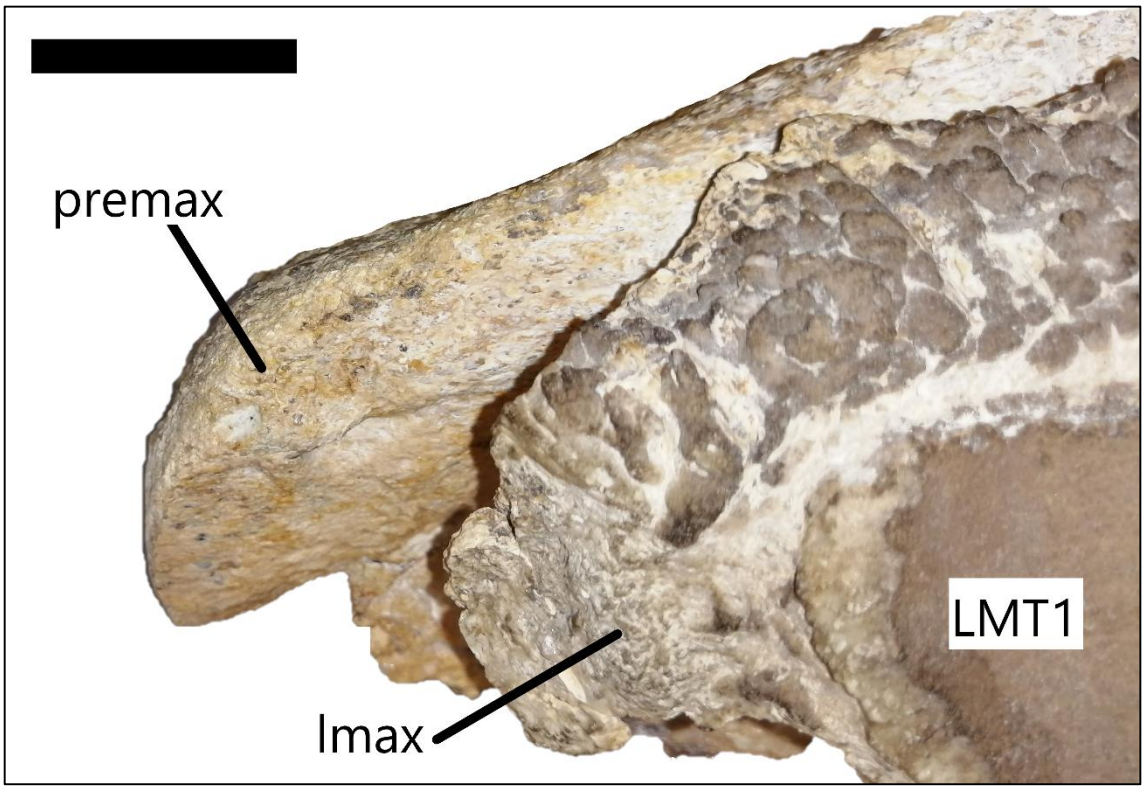

Figure 22. Anterior tip of the premaxillae in left lateral view. Abbreviations: lmax = left maxillae; premax = premaxilla; LMT1 = left maxillary tooth position 1. Scale bar = 20mm

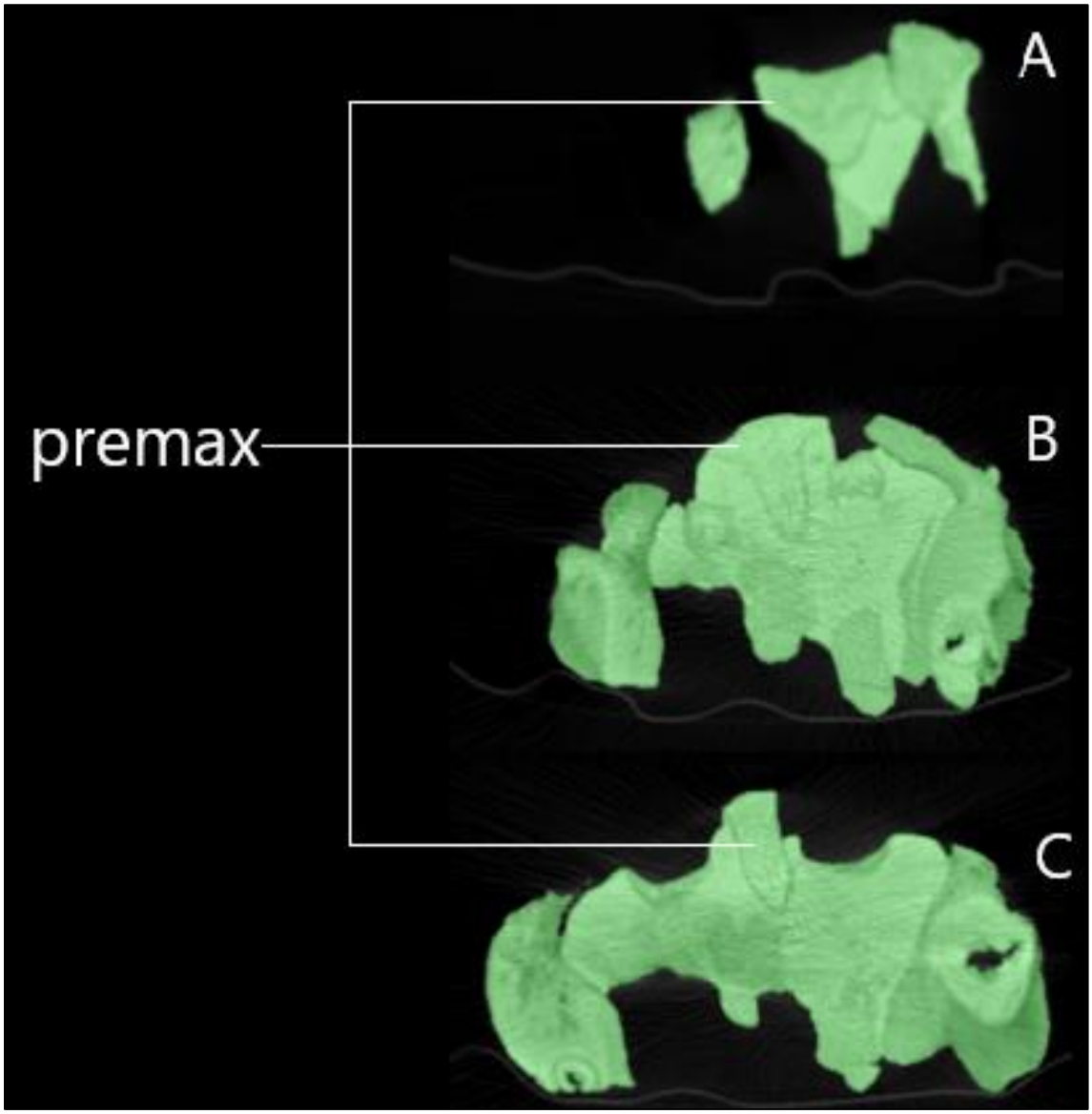

Figure 23. CT-scan images showing the cross-sectional views of the premaxilla at the anterior tip (A); behind the anterior tip (B) and in the middle of the internarial bar (C). Not to scale.

Vomer-palatine complex

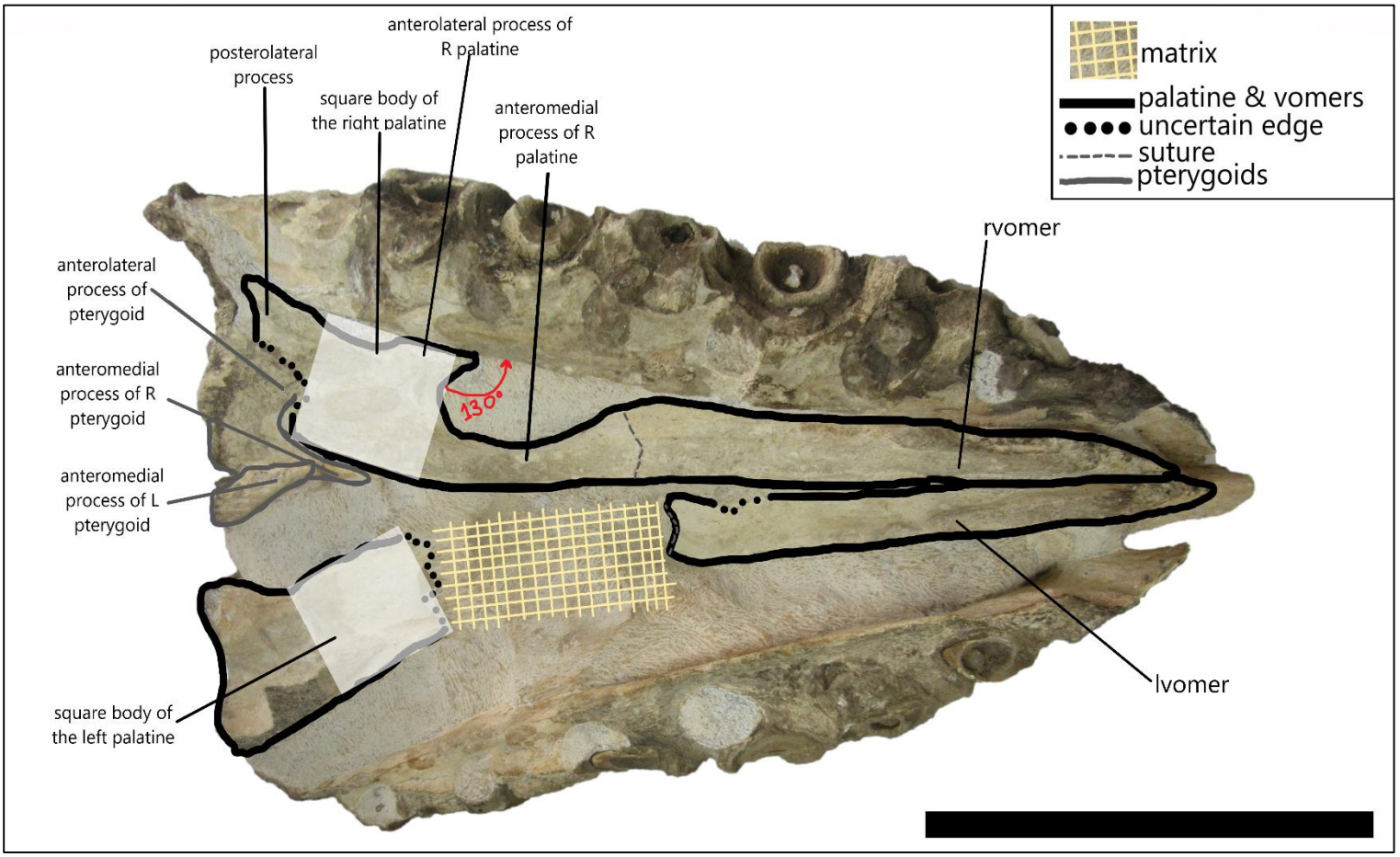

Figure 24. Ventral view of the muzzle unit with the vomer-palatines and pterygoids highlighted, as well as some of the processes referred to in the vomer-palatine complex descriptions. The opaque white squares indicate the body of the palatines – the left appears smaller due to the fact that the bone is angled slightly anteromedially whereas the right palatine is flat. Abbreviations: lvomer = left vomer; rvomer = right vomer. Scale bar = 200mm.

As noted previously, both the left and right vomeropalatines are present and relatively well-preserved. The right side is better preserved than the left with the right pterygoid in contact with the posterior region of the palatine and the posterolateral palatine buttressed against the medial maxillary wall (Figure 24). With respect to the vomers, the anterior half of the right vomer is in contact with the anterior maxillary wall enclosing the internal narial openings. The whole ventral right side was fully prepared exposing a large area between the vomer-palatine suture and the body of the left palatine (Figure 24, yellow cross-hatching); the anterior ramus of the left palatine is not visible as that portion was not prepared.

Figure 25. Ventral view of a Plioplatecarpus houzeaui (RBINS R0136) left palatine for comparison with CGP/1/2265 palatines. The notch on the posterolateral surface where the anterior process of the pterygoid fits is indicated (black arrow). Scale bar = 80mm.

The palatines in CGP/1/2265 are large with the maximum length of the right palatine from the vomer-palatine suture to the posteromedial point being approximately 187 mm, nearly one third of the length of the right maxilla. Removing the matrix around the left palatine and the internal narial opening showed the extent to which the vomers and palatines are dorsoventrally thickened. Much like the rest of the muzzle unit, these bones are large and robust.

Posterolaterally the palatine forms a large pointed process (Figure 24), which is missing in the *Plioplatecarpus houzeaui* palatine (Figure 25). The posterolateral process of the right palatine contacts the right maxilla. There is also a facet on the posterior surface of the palatine, for the anterolateral process of the pterygoid, to which it is partially fused (Figure 24). Like *Pl. houzeaui* (Figure 25, black arrow) there are no facets on the medial side of the CGP/1/2265 right palatine for the sharp anteromedial process of the pterygoid to fit into (Figure 24). That

anteromedial process sits tightly buttressed against the medial side of the palatine but does not appear to be sutured to the palatine.

The main bodies of the palatines are relatively square in shape with a scooped floor behind the internal narial openings forming the curved roof of the mouth (Figure 24, opaque white squares). The anterolateral process of the palatine belonging to CGP/1/2265 is short and therefore allows the medial maxillary wall to play a greater role in shaping the internal narial openings.

The right palatine contacts the right maxilla in line with the region between the sixth and seventh tooth position forming a wide angle of about 130° between the anterior surface of the palatine and the medial wall of the right maxilla (Figure 24). At the point where the anterolateral process of the palatine terminates posteriorly, the posterior boundary of the internal narial opening becomes smooth and round as it forms the medial side of the narial opening (Figure 24).

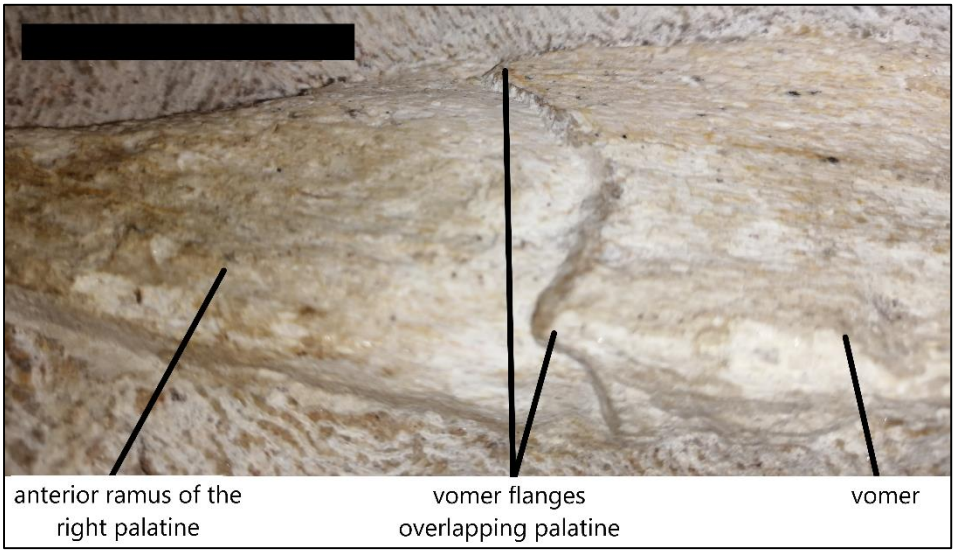

Figure 26. Dorsomedial view of the right vomer-palatine suture showing the posterior vomer overlapping the anteromedial process of the palatine. Scale bar = 30mm.

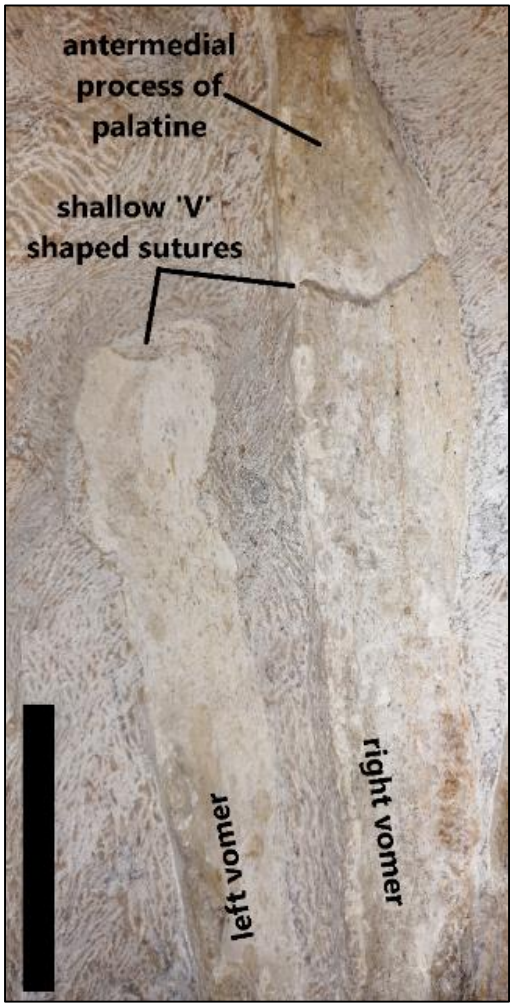

Figure 27. The left and right vomer-palatine sutures with identical 'V' shape. The right vomer is sutured with the palatine, but the left anteromedial process of palatine is not visible. Scale bar = 50mm.

The elongated anterior process of the palatine gradually narrows anteriorly to a minimum width of 19.61mm, to form a rounded medial surface of the internal narial opening and then widens slightly to meet vomer at the vomer-palatine suture (Figure 24), which is at least 33.32mm wide and is shaped like a shallow 'V' (Figure 26). Medial view of the right vomer-palatine suture clearly shows that the vomer overlaps the palatine and even has small flanges on the posterolateral corners (Figure 26). Although it is partially covered by matrix, the posterior border of the left vomer is visible, and it is identical in shape to the posterior border of the right

vomer (Figure 27). The anterior ramus of the right palatine is not visible and may be covered by matrix or is missing (Figure 27).

The vomers are elongated bones that span more than half of the anterior portion of the palate (Russell. 1967). The left vomer in CGP/1/2265 has been displaced from its original position in the skull and now lies beneath the internarial bar of the premaxilla (Figure 24). The right vomer is complete, apart from a small piece missing from the anteroventral surface but it is in its original position and is 254mm long. The vomers are both mediolaterally compressed and narrow anteriorly in ventral view (Figure 24). Both the left and right vomer have a process that runs along the lateral sides of the ventral surface. The process on the right vomer appears as though it has been broken off towards the posterior end. On the left vomer there is well-preserved crest that extends beyond the half the length of the bone and is approximately 185 mm in length.

Pterygoids

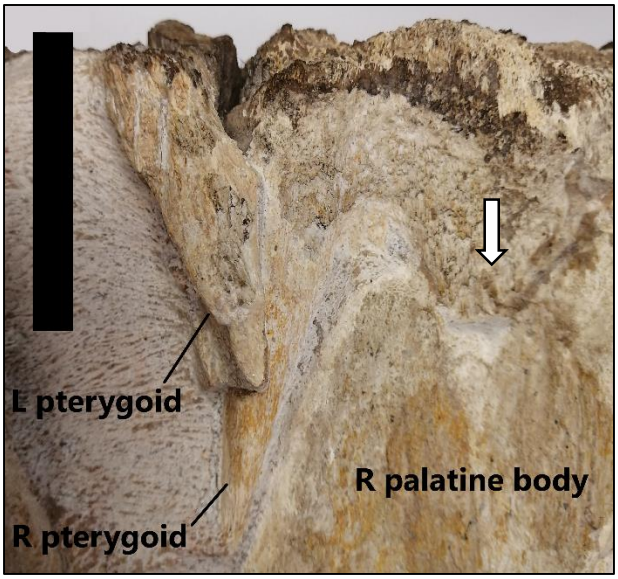

Figure 28. Anteromedial processes of the pterygoids and part of the right pterygoid that is in contact with the posterior surface of the right palatine. The left pterygoid is overlying the right pterygoid unnaturally. White arrow indicating the anterolateral process of the right pterygoid contacting the right palatine. Scale bar = 50mm.

Only the anterior parts of the pterygoids are preserved (Figure 28). Unfortunately, the tooth bearing elements and teeth, as well as the elements at the posterior end of the pterygoids such as the basisphenoid processes, ectopterygoid processes and quadratic rami are all missing. Unfortunately, there is little anatomical detail present that is taxonomically diagnostic.

The anteromedial process of the right pterygoid is in its life position and is tightly buttressed against the medial side of the palatine body. However, the anteromedial process of the left pterygoid is unnaturally overlying the right (Figure 28) due to the shifting of the left cranial bones that occurred (Figure 24). These processes are both relatively long, the right is at least 88.35mm in length and the left is 64.81mm. The left appears to be dorsoventrally deep (at least 26.12mm) although matrix is covering the dorsal most surface of the process preventing the true

depth from being measured and CT scan unfortunately did not reveal this detail. Both anterior processes are pointed at the anterior tip (Figure 28).

There is another piece of the anterior pterygoid bone attached to the lateral surface of the right pterygoid, which was referred to as the anterolateral process of the pterygoid. This bone is shorter and rounded, and anteriorly contacts, but is not fused to the posterior surface of the right palatine body (Figure 28, white arrow).

Isolated teeth

There were two isolated fragmentary teeth extracted from the matrix around the anterodorsal muzzle unit during preparation. These isolated teeth are similar to the replacement tooth LMT5 (Figure 20), thus it is safe to assumed that they belong to the same individual. The first isolated tooth, IT-1 (Figure 29) was extracted from the matrix near the middle of the palate. The second isolated tooth, IT-2 (Figure 30) was extracted from the left side of the dorsal surface near the posterior region of the internarial bar. Another isolated tooth, IT-3, was also found during preparation; however, this one is wedged beneath what appears to be the bone forming the floor of the nares (Figure 31). It was not removed due to the potential damage that its removal could cause to this region of the skull.

IT-1 (Figure 29) is the more fragmentary of the two extracted isolated teeth. It has a mostly complete enamel crown measuring approximately 46mm in length but the cementum root is absent. Much of the enamel has flaked off the tooth; however, enough remains for this tooth to be used for the oxygen isotope analysis, SEM analysis of the enamel and thereafter histological sectioning and strontium isotope analysis (see Chapter 3, section 3.2.1). CT scans of the muzzle unit show all the replacement teeth to be slightly posteromedially recurved (Figure 18). Therefore, it is assumed that the isolated teeth would have a similar orientation.

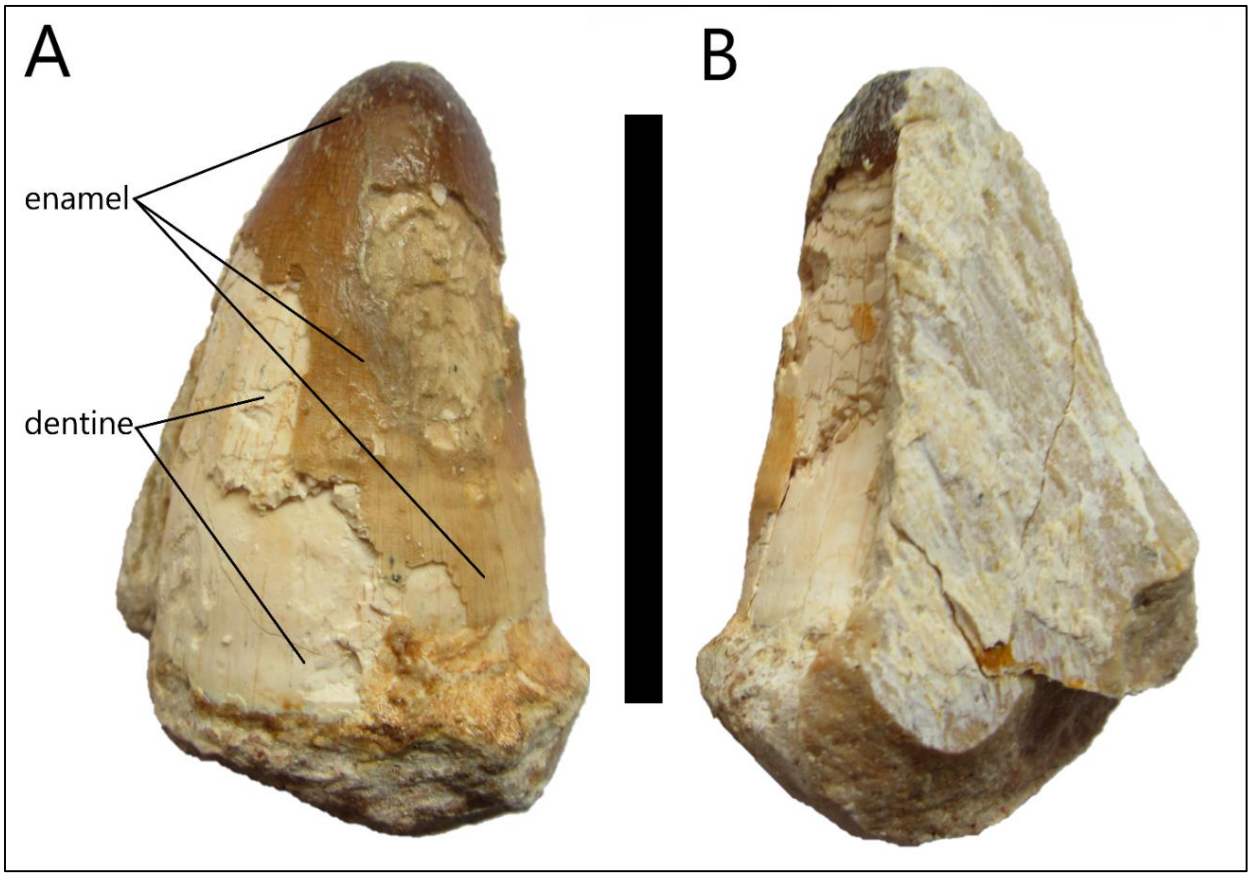

Figure 29. IT-1 in labial (A) and lingual (B) view. Only the enamel crown is present. Scale bar = 50mm.

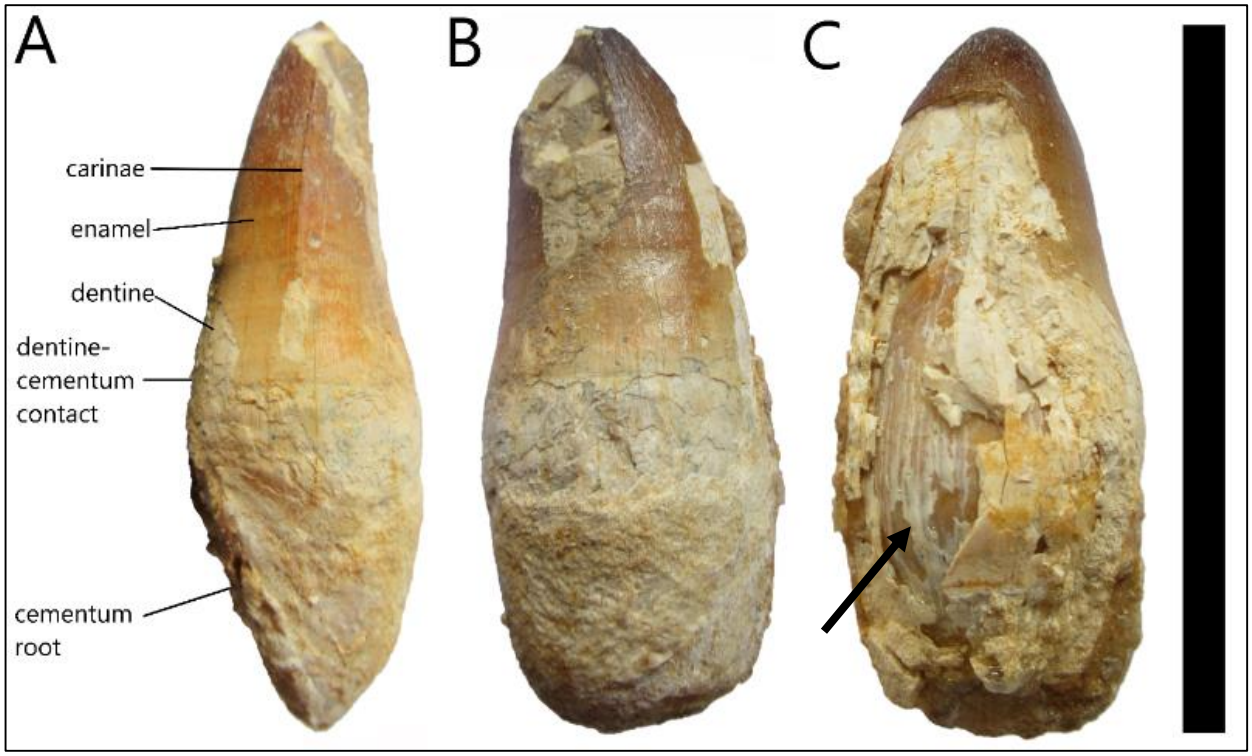

Figure 30. Posterior view of IT-2(A) with the posterior carinae, enamel, dentine, dentine-cementum contact and cementum root indicated. The tooth is slightly medially recurved. (B) Lingual view of IT-2. (C) Labial view of IT-2 with arrow pointing to the initially suspected replacement tooth. Scale bar = 90mm.

Figure 31. Part of IT-3 is visible wedged beneath the nasal cavity floor. The enamel is very similar to that seen on IT-1 and IT-2. Some of the dentine underlying the enamel is also visible.

The other isolated tooth (IT-2, Figure 30) is better preserved and more complete in the sense that it has both the enamel crown and cementum root attached, indicating that it is a functional tooth or a late-stage replacement tooth. IT-2 is anatomically and taxonomically valuable, which is why this tooth was not chosen for destructive analysis. A portion of the apex is missing from the labial side of the tooth. The enamel crown is approximately 47mm in length and the cementum root is approximately 39mm in length. Externally, there appeared to be a replacement tooth on the inside of the IT-2 (Figure 30C, black arrow). However, transverse micro-CT images through the tooth suggest that it is not a replacement tooth, but rather an infilled pulp cavity with a texture like that of the tooth (Figure 32A).

The two extracted isolated teeth have enamel crowns that are subconical in shape. The bases of the enamel crowns are bulbous and more or less circular in cross-section. They become more elliptical towards the apices as the teeth become slightly labiolingually compressed and the carinae become more pronounced (see Figures 32 and 36). The enamel on these two teeth is smooth and there is no evidence of grooves or facets (Figure 29, 30). The enamel near apical regions of the teeth does appear to be rougher and small anastomising ridges are visible (Figure 32). Both teeth possess anterior and posterior carinae. The posterior carina cannot be seen explicitly on IT-1 due to the matrix covering it but is visible in the transverse micro-CT images (Figure 36).

The carinae on IT-1 and IT-2 are finely serrated (Figure 33). This can only be seen using a hand lens or microscope. These serrations are connected, more like an ornamented enamel ridge as opposed to being individual serrations with spaces between them (Figure 33). They have a globular appearance and are approximately uniform in shape and size with each globule being around 0.25mm wide with about the same height.

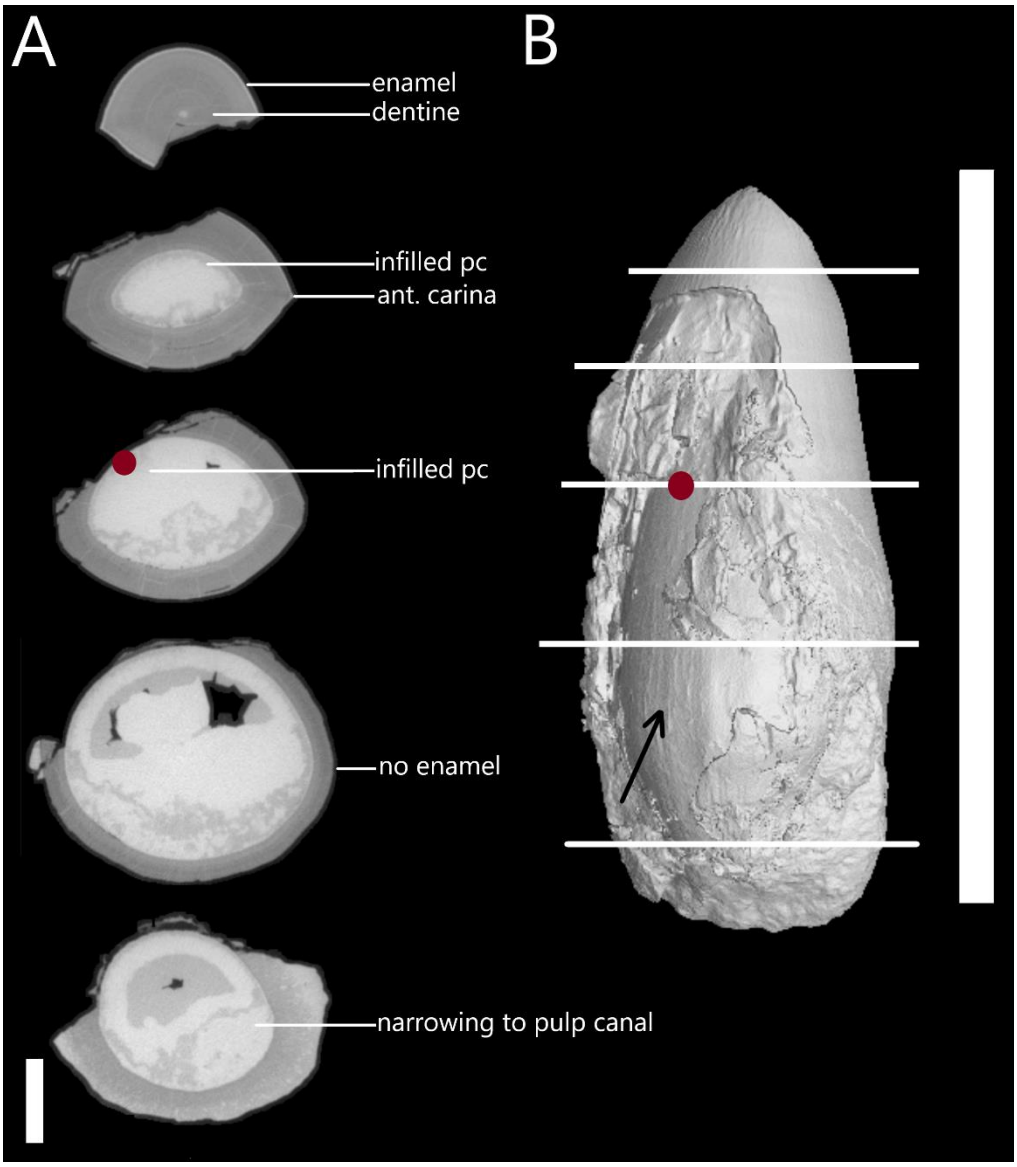

Figure 32. Transverse micro-CT images (A) of IT-2 at different points with labels indicating the tooth tissue types. The red dot shows the point at which the infilled pulp cavity (pc) [previously thought to be a replacement tooth (black arrow)] is visible on the three-dimensional image (B). The lines through the three-dimensional micro-CT image show location of the transverse sections. Scale bars: A = 9.5mm; B = 90mm.

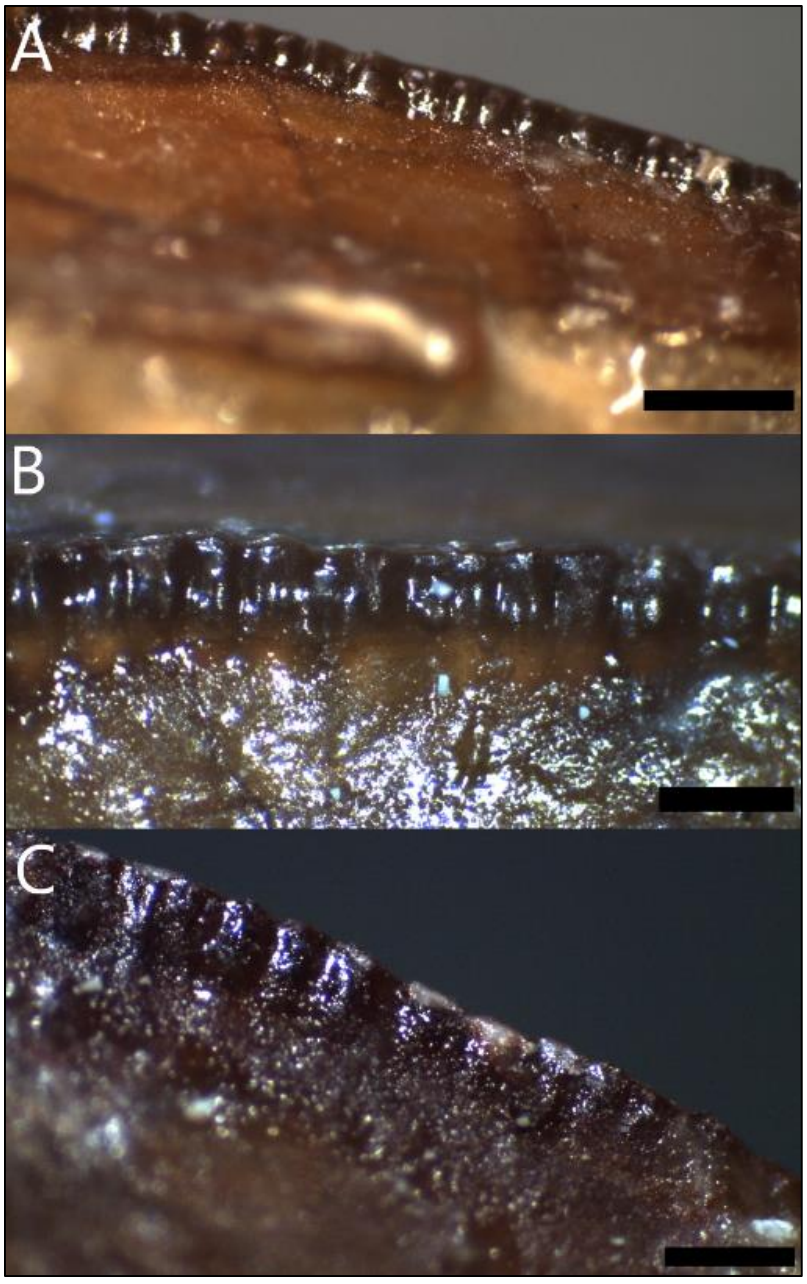

Figure 33. Fine serrations visible on the anterior and posterior carinae on IT-1. Scale bars: A = 1mm; B, C = 0.5mm.

Associated shark tooth

The shark tooth is directly associated with the CGP/1/2265 muzzle unit. It is located on the dorsal right side of the muzzle unit towards the posterior end (see Figure 16A). Only the apical region of the tooth crown is covered with a thin enamel layer; however, the shape of the entire tooth can be made out (Figure 34). It has a bilobate root. The maximum width across the root-crown boundary is approximately 25mm. The tooth is wider than it is long from the root to the apex. There is no evidence to indicate the presence of cusplets on the tooth (Figure 34). The crown has the crescentic shape with a bulbous mesial side. The distal side has a concave edge towards the apex. Along the edges of the crown are well-developed fine serrations, which are visible more clearly on the distal side (Figure 34). The serrations seem to have worn slightly on the medial side of the tooth near the apex. No fine striations or grooves are visible on the tooth surface.

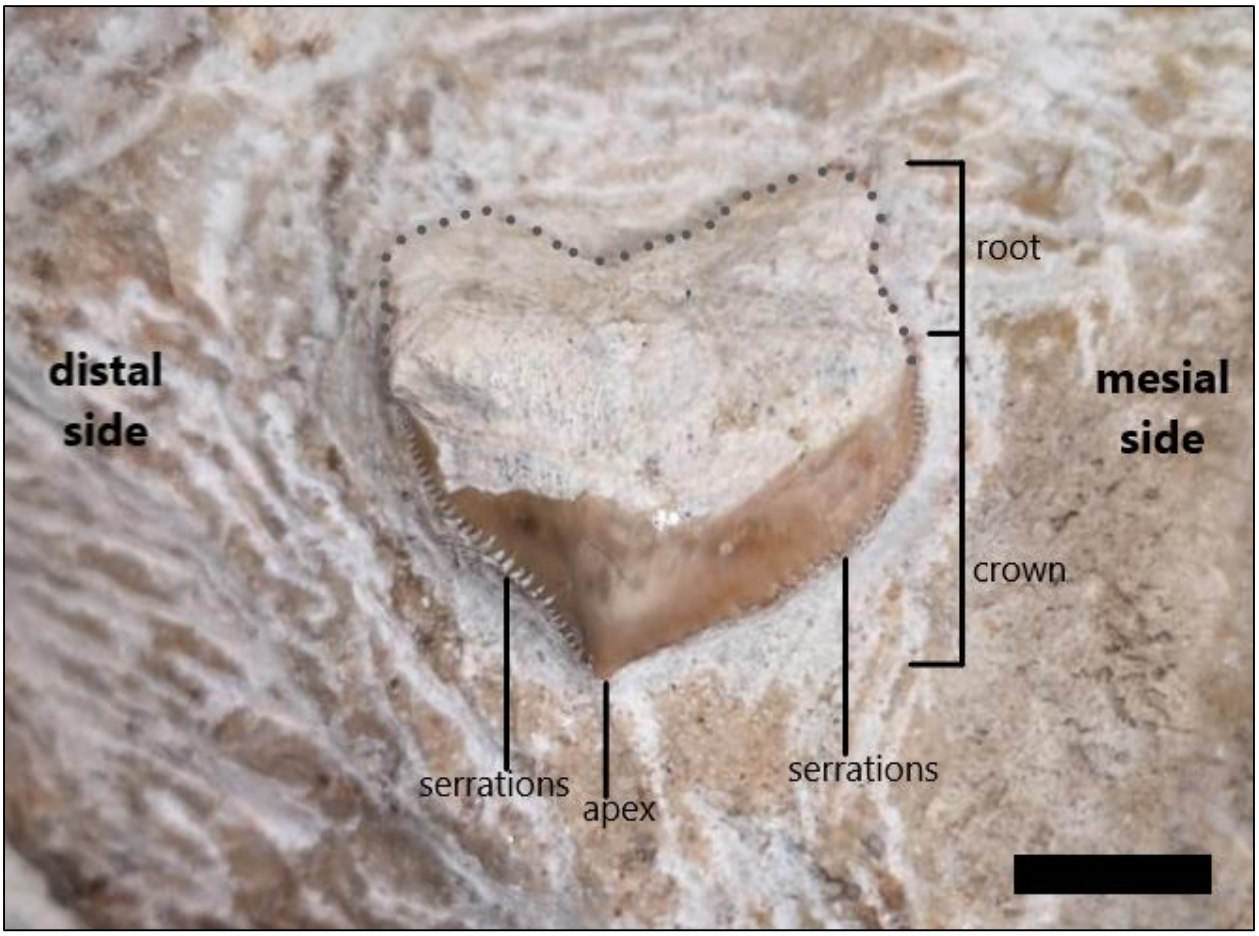

Figure 34. Shark tooth embedded in the matrix around the muzzle unit. The root and enamel-covered crown are indicated, as well as the well-developed serrations on the mesial and distal side of the tooth. The dotted line reconstructs the root base that is not as clear as the apical region. Scale bar = 10mm.

3.1.4) Isolated partial vertebra from St Lucia

This fragmentary isolated vertebra has a centrum that is longer than it is tall of wide (Figure 35). The left side of this partial vertebra is better preserved than the right as the left synapophysis is mostly complete and the posterior zygopaphysis (Figure 35A) and the left lamina of the neural arch (Figure 35F) are present. Dorsally, both prezygapophyses are absent as well as the neural spine and the poor preservation of the right side of the vertebra means that the neural arch is only preserved in part. Ventrally, the vertebra is slightly concaved between the condyle and cotyle. As with all mosasauroids, the vertebra is procoelous (Wiffen, 1990) so the concave cotyle is at the anterior face of the vertebral centrum (Figure 35C) and the convex condyle is at the posterior face (Figure 35D).

The condyle is smooth and almost complete. It has a rounded heart shape with a shallow depression dorsally, and rounded ventrally. It has a maximum width of 52.51mm and a maximum height of 51.21mm (Figure 35D). The centre of the cotyle is smooth but the edges are poorly preserved with the dorsal portions as well as the right lateral and posterior edges of the cotyle face having been broken off (Figure 35C). Despite this, it seems reasonable to suggest that the cotyle was roughly circular in shape and has a maximum height of 52.72mm and a total width of 44.96mm; however, it is impossible to measure the exact width due to its incompleteness (Figure 35C). There is no evidence of zygosphenes due to poor preservation of the region anterior to the neural spine, but a left zygantrum is visible and is a triangular indentation medial to the posterior zygapophysis (Figure 35D), which implies that zygosphenes-zygantra complexes were present.

The left synapophysis is mostly complete with some evidence of surface wear (Figure 35F). The anterior surface of the transverse process is approximately in line with the centre of the cotyle (Figure 35C) and it originates about midway between the ventral and dorsal edges of

the centrum (Figure 35F). It extends outwards and slightly dorsally (Figure 35D). The synapophysis is approximately 35.76mm long measured from the base at the outer edge of the cotyle to the extremity; approximately 25.80mm high measured near the base; and has an anteroposterior width of around 14.95mm measured at the extremity. The extremity of synapophysis is anteroposteriorly compressed and rounded at the edges (Figure 35F).

Due to the fragmentary nature of the right side of the vertebra there is no evidence of the right posterior zygapophysis, nor is there direct evidence to suggest that the neural arches were fused. However, by the position of the medial edge of the left neural arch above the neural canal (Figure 35D), it seems as though the neural arches were fused as in all mosasaur vertebra observed (personal observation of specimens at RBINS).

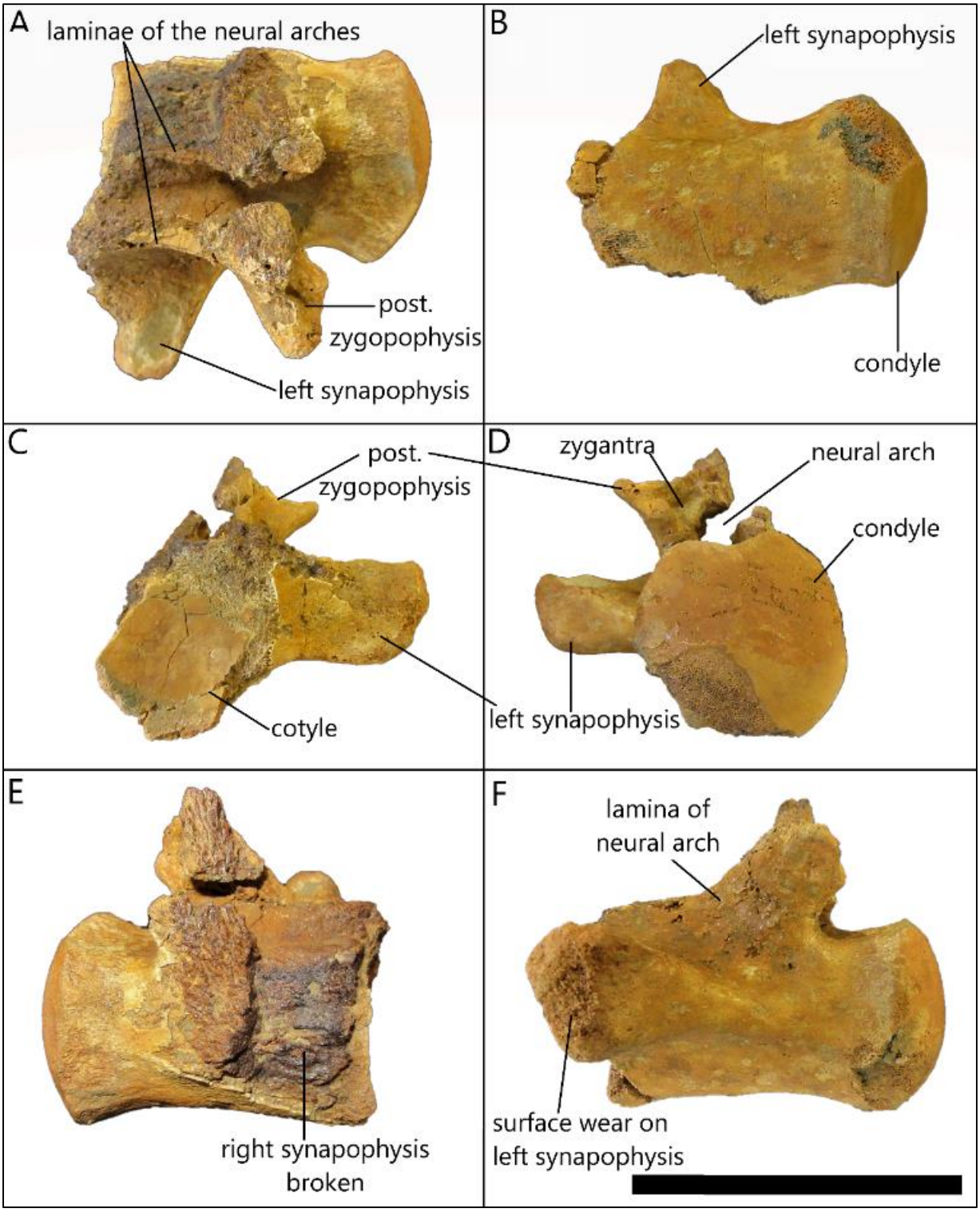

Figure 35. Indeterminate partial mosasaurid dorsal vertebra from St. Lucia in (A) dorsal; (B) ventral; (C) anterior; (D) posterior; (E) right lateral; (F) left lateral view. The main features discussed in the description are indicated. Scale bar = 80mm.

3.2) Palaeobiology and strontium dating

3.2.1) Structure of IT-1

Microanatomical and microstructural analyses of IT-1 included micro-CT analysis, histological analysis and SEM analysis of the tooth tissues.

Micro-CT

As with IT-2, IT-1 was analysed using micro-CT prior to thin sectioning. This revealed a thin, dense layer of enamel around the apex of IT-1 (Figure 36). A small central pulp cavity is visible in the transverse and longitudinal micro-CT images and this is surrounded by a thick layer of dentine. Cracks can be seen along incremental growth lines, which are suggested to be weak points in the dentine (A. Chinsamy-Turan, personal communication, January 2020). In one of the transverse micro-CT images towards the base of the enamel crown, the boundary between the pulp cavity and the surrounding dentine is indistinct. From the transverse micro-CT images, it is clear that the base of the pulp cavity is open and has most likely been infilled with sediment (Figure 36). The small pulp cavity and lack of cementum root suggests that IT-1 is a replacement tooth.

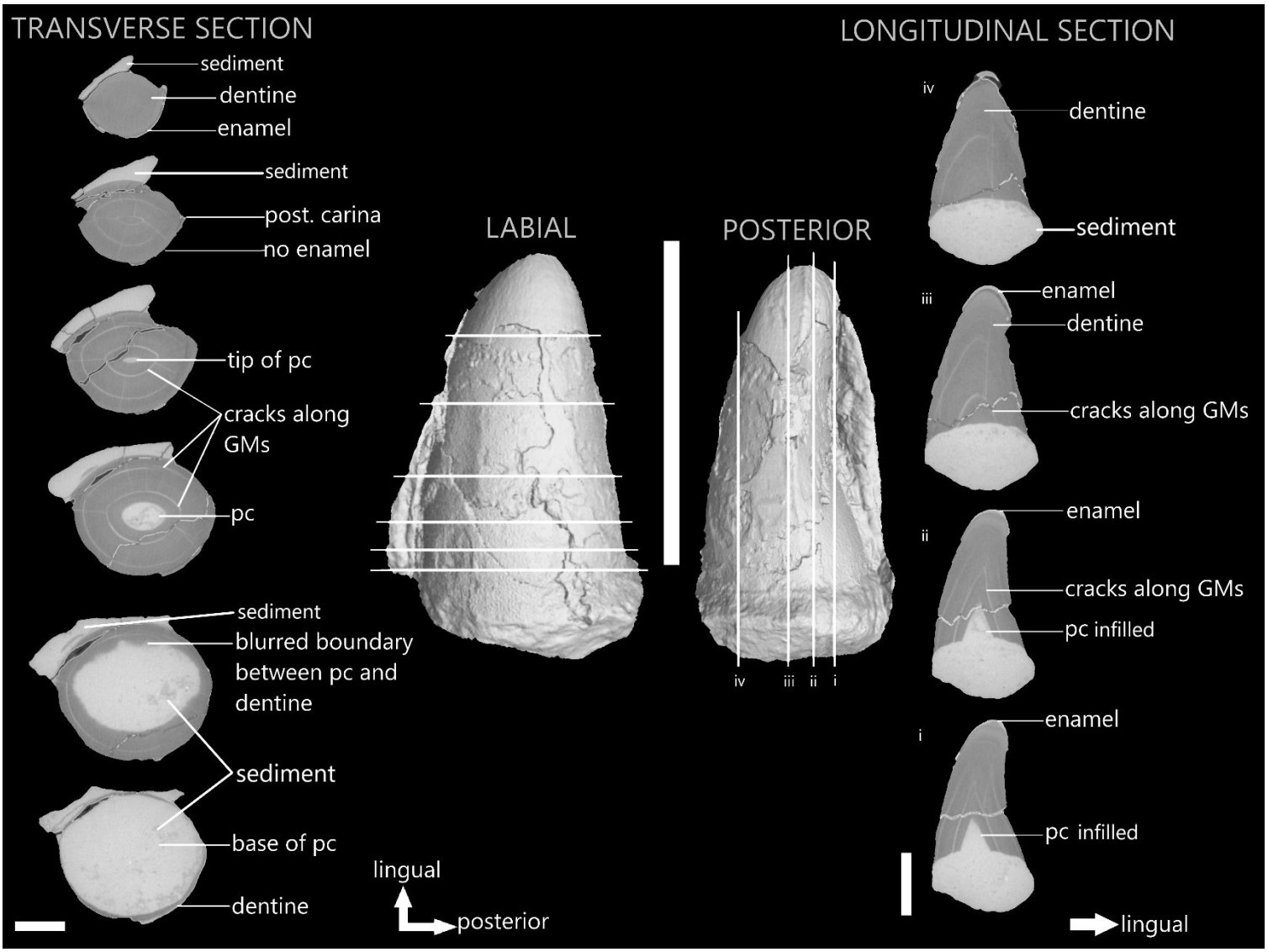

Figure 36. Transverse (left) and longitudinal (right) micro-CT images of IT-1 at different points along the enamel crown with labels indicating the tooth tissue types and features. Three-dimensional micro-CT images (centre) of IT-1 in labial view (middle left) and posterior view (middle right) showing locations of the sections. Directional arrows pertain to the transverse and longitudinal images. Abbreviations: GMs, growth marks; pc, pulp cavity. Scale bars: transverse/longitudinal sections = 10mm; 3D images = 50mm.

Histology

Histology revealed the overall preservation of IT-1 to be poor, with some tissues and areas better preserved than others. The longitudinally sectioned tooth revealed three different tissue types i.e. enamel, dentine and what was initially thought to be cementum, but was in fact sediment.

The thin layer of enamel around the apex of the tooth was well preserved and measured an average thickness of 602.95µm (Figure 37B). A decrease in the enamel thickness was noted as one measures it further from the apex (Figure 37A, black arrows). There appears to be up to five (but at least three) distinct layers between the outer enamel surface (oes) and the enamel-dentine junction (edj) (Figure 37B). The outer enamel surface is rough, possibly due to cracking during preparation. The first layer (1) is thin and is not birefringent under polarised light. It is possible that the first layer is simply glue that was put over the tooth during preparation to preserve it. The second layer (2) is the thickest layer and is birefringent under polarised light, which according to Chinsamy *et al.* (2012) is typical of prismatic enamel. Small feather-like patterns are visible within this layer (Figure 37B, white outlined arrows), as well as dark vertical striations that are irregularly spaced but generally perpendicular to the junctions between layers (Figure 37B, dotted lines).

The space between layer 2 and the edj seems to be comprised of three layers, although the junction between layers 3 and 4, and 4 and 5 is rather unclear, suggesting that the layers may not be real. Within layer 3 there are small tubule like structures that lie perpendicular to the junctions. Layer 4 is darker in colour and is featureless. Layer 5 is lighter and contains a few tiny globular structures that are randomly distributed within the layer (Figure 37B, black arrow heads).

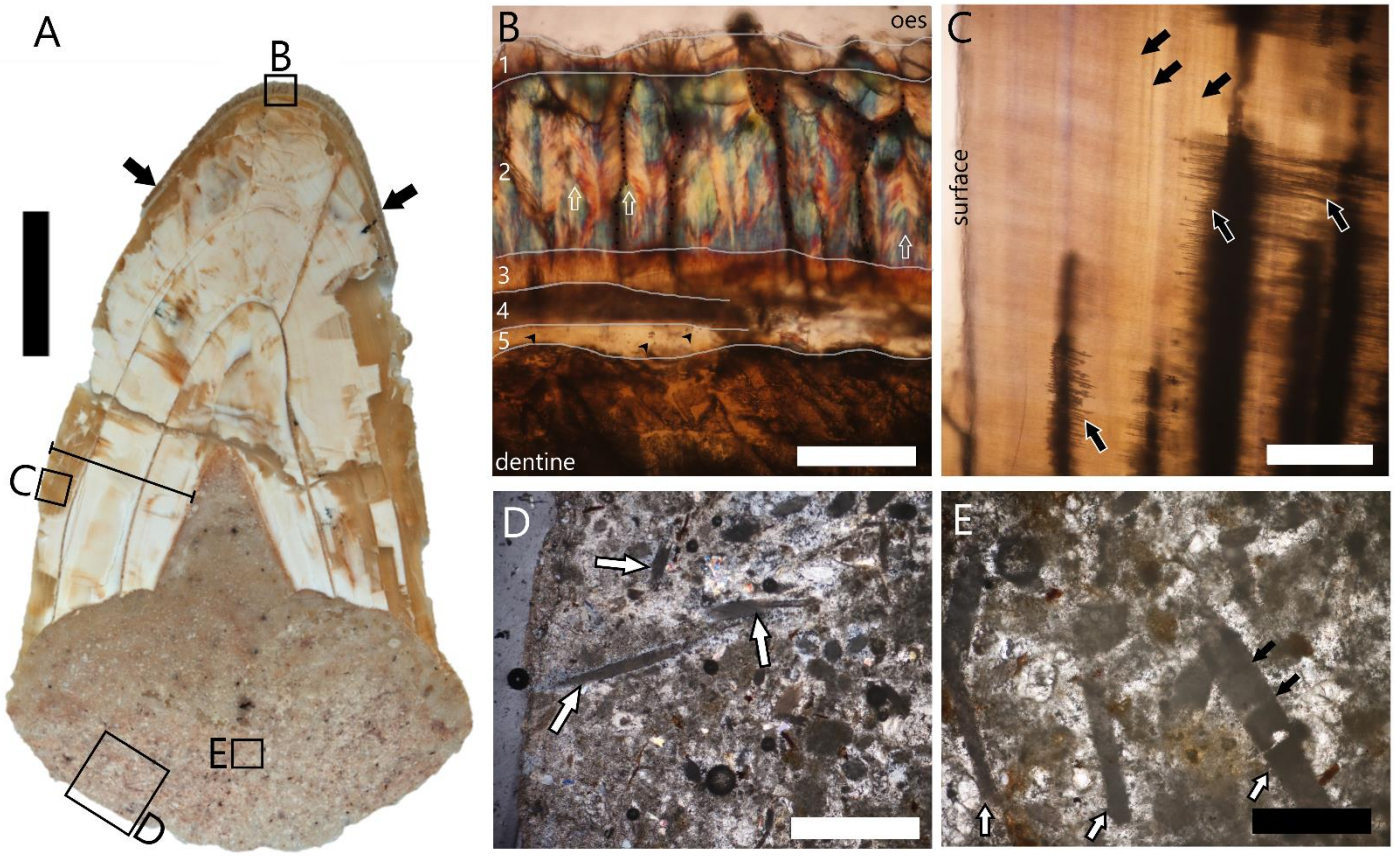

Figure 37. (A) Longitudinal thin section taken from the middle of the tooth. Black arrows indicate narrowing of the enamel layer as measured further from the apex of the tooth. Box frames indicate position of the micrographs in B-C. The line on the anterior side of the pulp cavity shows the thickness of dentine (9500µm) that was measured to estimate the number of days for formation. (B) High magnification image of the enamel at the apex of the tooth under polarised light. The outer enamel surface (oes) is shown and the discussed layers are drawn and labelled (1-5). The line between layer 5 and the dentine is referred to here as the enamel-dentine junction (edj). The white arrows point to the feather-like structures in layer 2 and the dotted lines indicate the vertical striations noted in layer 2. The black arrow heads in layer 5 point to clusters of tiny globular structures. (C) High magnification image of the dentine near the surface on the anterior side under polarised light. The dentine is not birefringent. The dentinal fibres (white outline arrow) and incremental growth lines (black arrows) are visible. (D) Low magnification image of the suspected cementum. There is nothing to suggest that this tissue is not just sediment. It shows no birefringence and consists of particles of varying shapes e.g. the rod like structures (white arrows) that are magnified in E. (E) Rod –like structures seen in the region where cementum was expected to be seen. One of the structures appears to be segmented (black arrows). Scale bars: A = 10mm; B, C = 200µm; D = 1000µm; E = 500µm.

The dentine layer is thick and consists of light and dark patches (Figure 37A) due to differences in the preservation (Maxwell *et al.*, 2011). There are cracks along the growth marks as seen in the micro-CT images, which appear histologically as narrow gaps in the dentine. Dentinal tubules are well-preserved and are seen throughout the histological sections. They run perpendicular to the surface of the tooth and the edge of the pulp cavity (Figure 37C, white outlined arrows). Incremental growth lines are visible (Figure 37C, black arrows) and are roughly parallel to the pulp cavity edge. The average distance between consecutive incremental lines is 53.93µm (n = 14; SD = 11.38µm), which is much wider than those previously measured (Chinsamy *et al.*, 2012; Owocki and Madzia, 2020). The dentine thickness near the tooth base from the edge of the pulp cavity to the surface is approximately 9500µm (see Figure 37A for dentine thickness measured).

Initially, it was assumed that the tissue seen toward the base of the tooth would be cementum. However, micro-CT scanning showed that it had infilled the pulp cavity (Figure 36), which is uncharacteristic of cementum. Furthermore, from a histological perspective, the material looks more like sediment. It is dense and particulate and consists of particles of varying sizes and shapes (Figure 37D). The most noticeable structures are rod-like with tapering ends (Figure 37D and E, white arrows), which are visible throughout the matrix. Most of the rod-like structures are fragmentary thus making it difficult to estimate the length of these rods accurately. However, Figure 37D shows a rod that looks complete and is approximately 1150µm long and ~100µm wide. Some of the structures also appears to be segmented (Figure 37E, black arrows). There are no cementeons or osteons visible to indicate that it is cementum or bone.

SEM

Enamel architecture

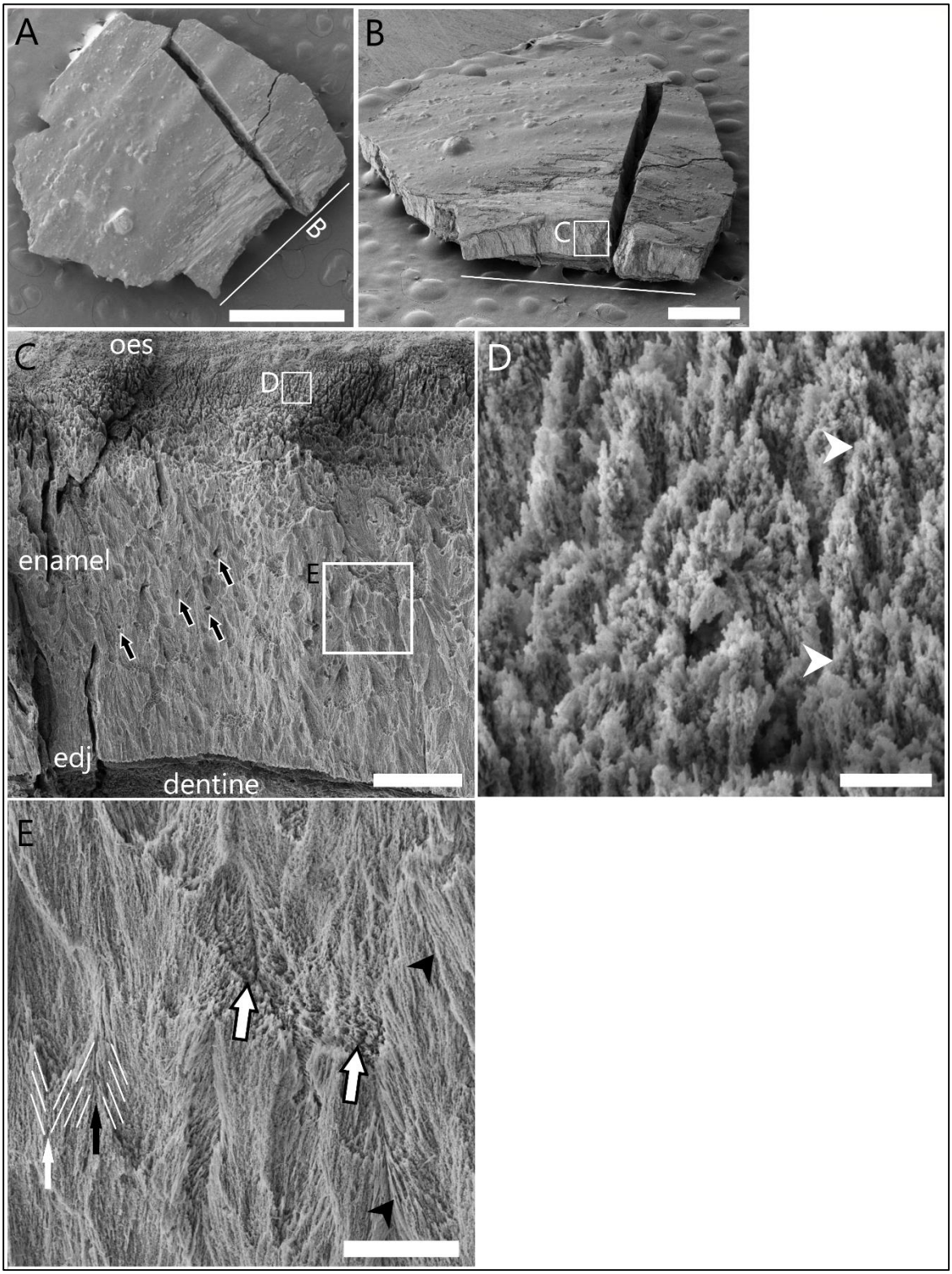

Figure 38. SEM micrographs of the piece of enamel from IT-1. The micrographs are orientated so that the outer enamel surface (oes) is towards the top of the image. (A) The piece of enamel in tangential view. The sample is cracked and there is a scratch on the surface of the enamel near the line indicating the location of B. (B) Slightly oblique view of the enamel piece. More of the detail on the enamel surface is visible in this view and a longitudinal section through the enamel is visible, which is magnified in C. (C) Discontinuities in the enamel are noted here. There is uniformity in the enamel along the horizontal layers; however, they change vertically from the enamel dentine junction (edj) to the oes. Small enamel tubules are visible in the middle of the enamel layer (black arrows). Box frames indicate the location of D and E. (D) High magnification of the upper layer of enamel near the oes. This area appears to have been scraped off slightly and is not aligned with the enamel shown in E. Small structures seen appear to be microunits, as described by Sander (2009). One microunit spans the two arrowheads. (E) Compound unit enamel from the middle enamel layer. Individual enamel crystallites are visible (black arrowheads). A columnar divergence unit (white arrow) and a columnar convergence unit (black arrow) are shown with lines to indicate the enamel crystallite orientation around them. Microunit enamel is also visible in this micrograph (white outlined arrow). Scale bars: A = 1mm; B = 500μm; C = 50μm; D = 2μm; E = 10μm.

SEM analysis of a small piece of enamel that broke off of IT-1 showed lumps, pits and scratches on the surface of the enamel (Figure 38A, B). The thickness of this piece of enamel is no greater than ~300μm, suggesting that it is from the side of IT-1 as opposed to near the apex where the enamel of the same tooth was measured to be ~600μm thick.

Longitudinal view of the enamel shows that there are varying horizontal layers between the edj and the oes, as was noted in the histological analysis. The upper portion of the enamel near the oes (Figure 38C) appears to have been scraped off, perhaps during handling or when the piece became detached. This area of the enamel is made up of microunits, which have been described and figured by Sander (2009) in nothosaur enamel. These are defined as ‘small enamel units and consist of bundles of diverging crystallites only a few crystallites across and a few crystallites long’ (Von Koenigswald and Sander, 1997). The middle portion of the enamel is made up of columnar units of diverging (Figure 38E, white arrow) and converging (Figure 38E, black arrow) enamel crystallites.

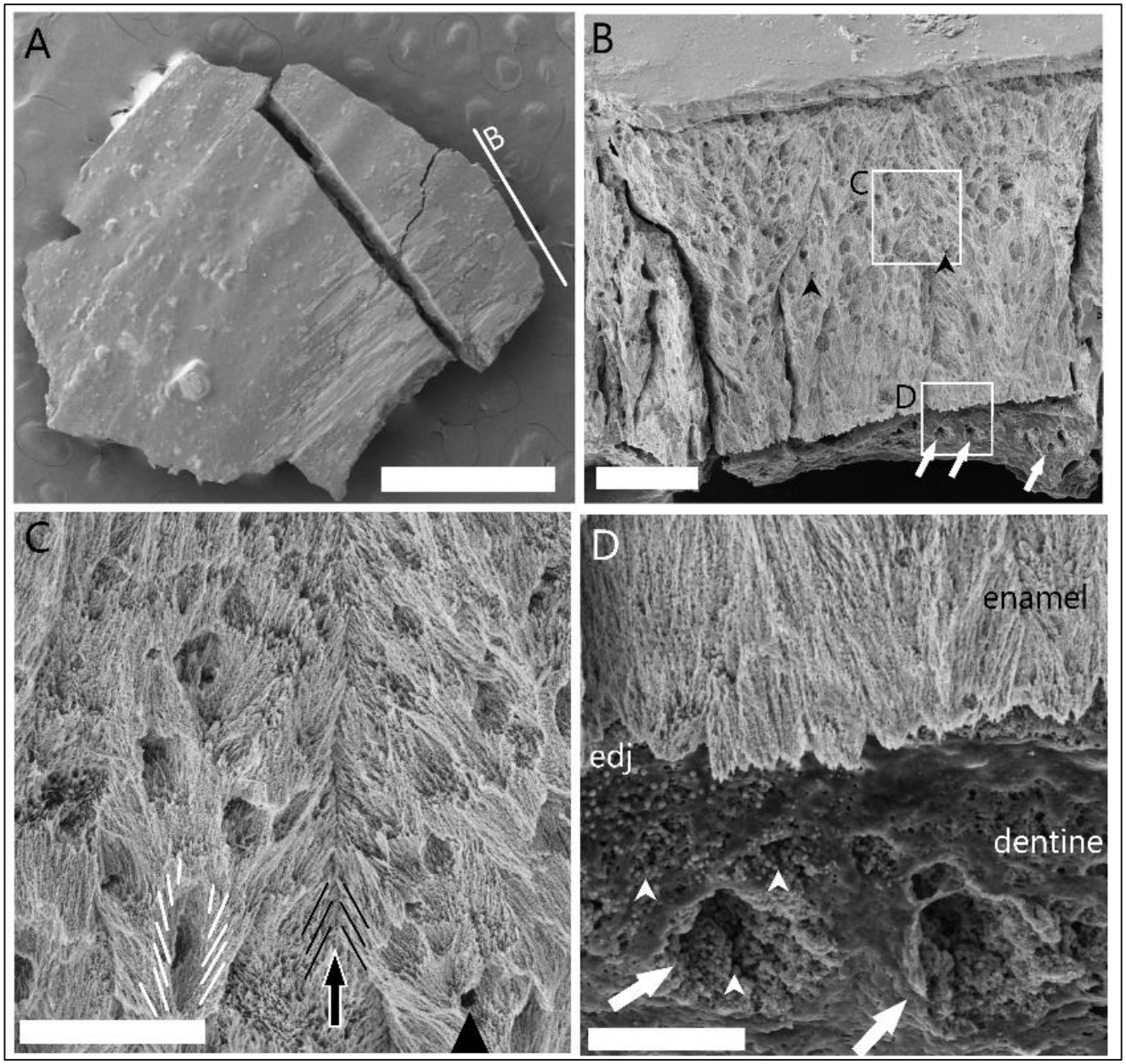

Figure 39. SEM micrographs of the piece of enamel from IT-1. The micrographs are orientated so that the outer enamel surface (oes) is towards the top of the image. (A) The piece of enamel viewed from the top. Line indicates the location of B. (B) Cross-sectional view of the enamel layer. The surface appears to have a smooth coating; however, it is suggested that this could be glue put on the surface of the tooth during preparation. The middle portion of the enamel is uniformly irregular. There are small cup-like features in the upper half of the layer and enamel tubules are visible (black arrowheads). (C) The small cup-like features are formed from the enamel crystallite divergence around them. White lines show diverging crystallites from the base of one of these 'cups' and the angle of divergence decreases towards the top. A clear convergence line is visible (black outlined arrow) and the lines around it indicate the orientation of the converging enamel crystallites. An enamel tubule is highlighted in the bottom-right corner by an arrowhead. (D) The bottom section of the enamel is fairly featureless and appears to be made up of simple parallel crystallite enamel. Dentine tubules (white arrows) are visible in this section. There appears to be small spherical structures aggregating inside the dentine tubules and also on the surface of the enamel (white arrowheads). Scale bars: A = 1mm; B = 50μm; C = 20μm; D = 10μm.

Cross-sectional view of the enamel from IT-1 reveals a slightly different texture. A smooth layer can be seen at the very top of the enamel layer; however, this is suggested to be the glue that was added to the tooth surface during preparation. There are cup-like features in the enamel, which are abundant and randomly distributed along the upper half of the enamel layer (Figure 39B). These are formed from strongly diverging crystallites at the base and the angle at which the crystallites diverge decrease towards the top of the 'cup' to meet the flat surface as shown by the fine white lines in Figure 39C. Converging enamel crystallites are visible and a clear convergent line is noted, which originated in the middle of the enamel layer and terminates only at the oes (Figure 39B, C). There are a few sparsely distributed enamel tubules throughout the enamel layer (Figure 39B, black arrowheads).

At the bottom of the enamel layer, near the enamel-dentine junction (edj), no cup-like features or enamel tubules are visible. It is relatively featureless and shows parallel crystallite enamel, which is one of the most basic forms of prismless enamel (Sander, 2009). A small layer of dentine is visible beneath the parallel crystallite enamel and dentine tubules are easily identified in the dentine layer (Figure 39B, D; white arrows). Interestingly, there are numerous small spherical structures that can be seen all over the dentine and inside the dentine tubules (Figure 39D, white arrowheads).

The spherical structures were only noted on the dentine and never on the enamel. The spherical structures are not connected to each other, but rather form large aggregations of approximately 100 isolated spheres in a two-dimensional 2μmx2μm quadrat. They have a smooth surface texture and vary in size with the largest measuring approximately 0.6μm in diameter and the smallest <0.1μm. In most cases, structures of similar size class were amassed together as seen in Figure 40B where the smaller spherical structures (black arrow) are separate

from the larger ones below the crevice (white arrow). This is also the case in Figure 40C, where hundreds of spheres of similar size are seen packed closely together. There is a greater variation in the size of the spheres visible in and around the three-dimensional mesh-like network as shown in Figure 40D.

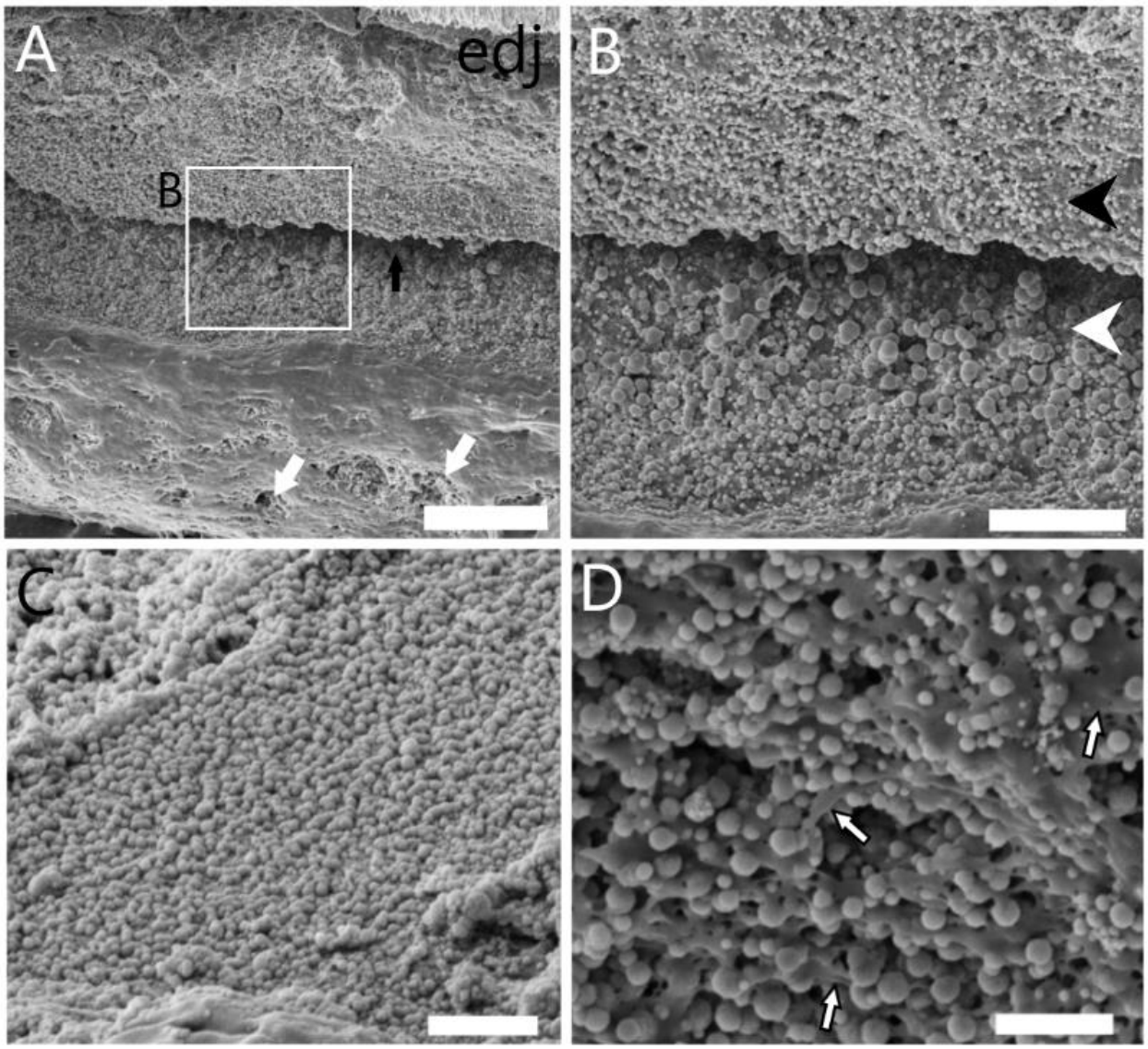

Figure 40. Micrographs of the spherical structures on the dentine from different parts of the IT-1 enamel fragment. (A) The spherical structures are numerous and can be seen here over the outer surfaces of the dentine, as well as in the crevices (black arrow) and dentinal tubules (white arrow). Box frame shows location of B. (B) High magnification micrograph of the spheres above and below the crevice. There are aggregations of smaller spheres above the crevice (black arrowhead), whereas below they are more variable in size and generally larger (white arrowheads). (C) Aggregations of similar sized spheres over a flat dentinal surface. (D) Varying sized spheres attached to and in-between struts of a mesh-like matrix (white arrows) Scale bars: A = 20μm; B = 10μm; C, D = 2μm.

EDS analysis

EDS analysis was done on the spherical structures described in the previous section and on the relatively flat surface on which the spheres sit, which was presumed to be dentine (see Table 4). The results from each measurement are shown in Table 4 respectively. Some values were removed such as gold and palladium as they represented the elemental composition of the coating; and also sodium and sulphur because those values were less than 0.1. Box plots are used to show the range of the proportions of each element and the quartile values for the elements detected on the spheres and the dentine (Figure 41). Quartiles portray the spread of the data more accurately than the means and standard deviations because there is a large amount of variation in the data.

Table 4. Values for the spectra measured at each site with the relative proportions of the detected elements carbon (C), oxygen (O), calcium (Ca), Fluorine (F) and phosphorous (P).The means and standard deviations, as well as the calculated range and median values for each element are given. The numbers in the left columns of the spheres and dentine table of values represent the site and the spectrum. E.g. 5.4 refers to site 5, spectrum 4 (see Chapter 2, Section 2.2.3). Unusual values are highlighted in grey and are suggested to be skewing the dataset for C, Ca, F and P.

Spheres	C	O	Ca	F	P	Dentine	C	O	Ca	F	P
1.1	0,23	0,26	0,51	0,00	0,00	1.2	0,23	0,26	0,51	0,00	0,00
1.3	0,56	0,27	0,17	0,00	0,00	5.2	0,31	0,15	0,24	0,27	0,03
2.1	0,12	0,27	0,31	0,15	0,15	5.3	0,18	0,31	0,33	0,02	0,16
2.2	0,10	0,28	0,31	0,17	0,14	5.5	0,30	0,27	0,24	0,11	0,07
2.3	0,07	0,21	0,45	0,05	0,21	6.4	0,39	0,13	0,32	0,11	0,05
3.1	0,09	0,26	0,35	0,15	0,15	6.5	0,45	0,15	0,31	0,05	0,04
3.2	0,14	0,26	0,30	0,17	0,13	6.6	0,38	0,15	0,22	0,21	0,04
4.1	0,65	0,35	0,00	0,00	0,00	7.4	0,35	0,14	0,24	0,22	0,05
4.2	0,67	0,33	0,00	0,00	0,00						
4.3	0,68	0,32	0,00	0,00	0,00						
4.4	0,64	0,36	0,00	0,00	0,00						
5.1	0,23	0,14	0,26	0,33	0,03						
5.4	0,20	0,13	0,29	0,34	0,03						
6.1	0,24	0,13	0,35	0,23	0,06						
6.2	0,25	0,10	0,53	0,05	0,07						
6.3	0,26	0,11	0,57	0,00	0,06						
7.1	0,15	0,17	0,28	0,33	0,07						
7.2	0,16	0,16	0,27	0,33	0,07						
7.3	0,18	0,13	0,30	0,31	0,07						
Mean	0,29	0,21	0,31	0,13	0,06	Mean	0,35	0,18	0,30	0,12	0,05
SD	0,20	0,09	0,18	0,13	0,06	SD	0,08	0,06	0,08	0,09	0,04
Range	0,61	0,26	0,57	0,34	0,21	Range	0,27	0,18	0,29	0,27	0,16
Median	0,23	0,26	0,30	0,15	0,06	Median	0,33	0,15	0,27	0,11	0,04

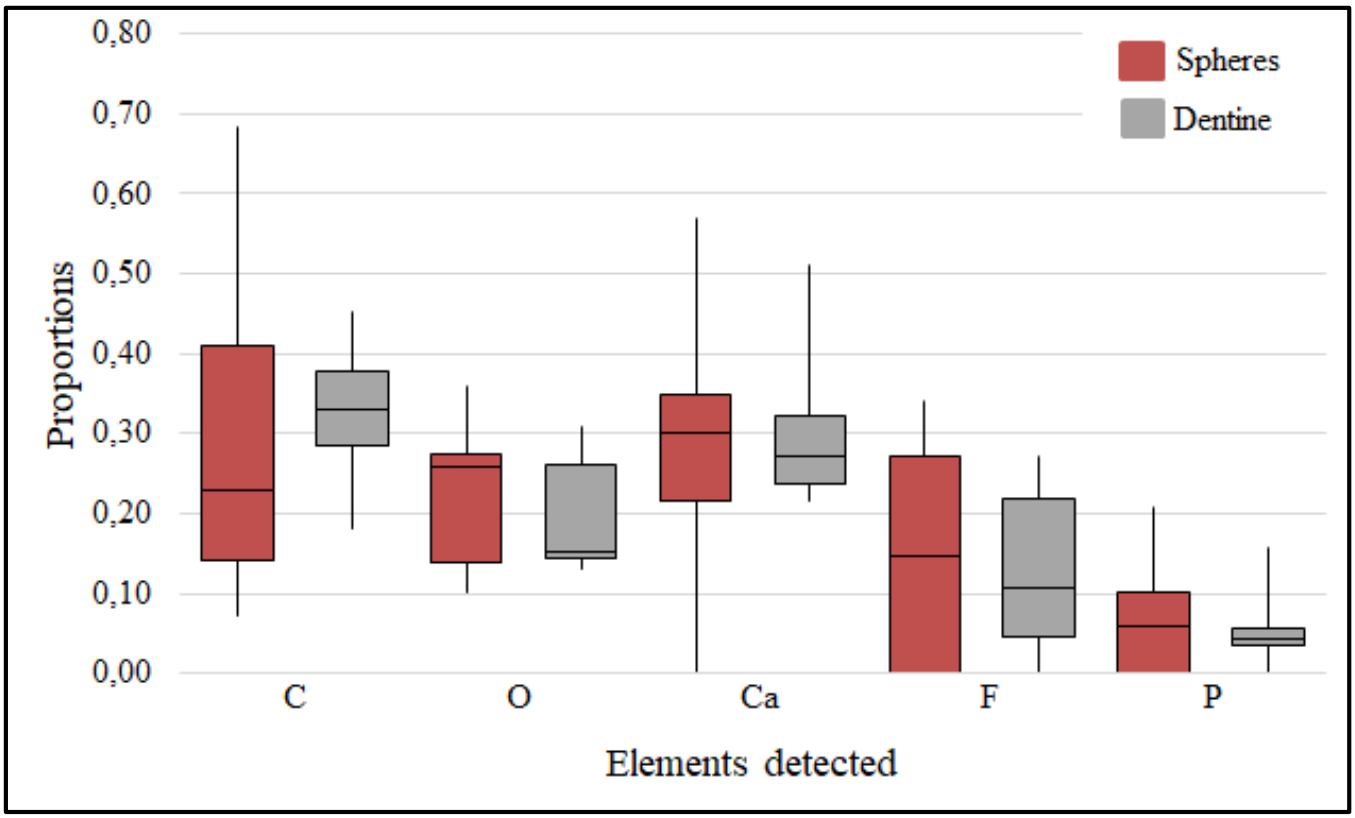

Figure 41. Box plot summarising the EDS analysis of the spheres (in red) and dentine (in grey). In the case of all the elements detected, the spheres have a greater range than the dentine.

Carbon (C)

The boxplot showing results for the proportion of carbon of the spheres has a slight positive skew. The median value is 0.23. The minimum value equates to 0.07 and the maximum value is 0.68, which is a large range and suggests that the proportion of carbon in the spheres was highly variable. The measured proportions of carbon in the dentine had a much smaller spread and a normal distribution. The median and minimum values were higher than for the spheres (median C dentine=0.33; minimum C dentine=0.18). The maximum value for the dentine (maximum C dentine=0.45); however, the site 4 of the spheres show unusually high values in comparison to the rest of the data set (Table 4, highlighted in grey) when these values are

removed the maximum value for carbon in the spheres is lowered to 0.57, and the data has a more normal distribution.

Oxygen (O)

The boxplot showing results for the proportion of oxygen of the spheres has a negative skew, but the proportion of oxygen of the dentine has a positive skew. The median values of the spheres and the dentine differ quite strongly (median O spheres = 0.26; median O dentine = 0.15). Spread of the data is not too dissimilar as the minimum (minimum O spheres = 0.1; minimum O dentine = 0.13) and maximum (maximum O spheres = 0.36; maximum O dentine = 0.31) values are similar.

Calcium (Ca)

The boxplot showing results for the proportion of calcium of the spheres has a slight negative skew, whereas the dentine has a slight positive skew. However, the median values for the spheres and dentine are very similar (median Ca spheres = 0.30; median Ca dentine = 0.27). The spheres have a much greater range than the dentine because the maximum and minimum values for Ca of the spheres are quite extreme (minimum Ca spheres = 0.00; maximum Ca spheres = 0.57). The data limits of the dentine are much closer (minimum Ca dentine = 0.22; maximum Ca dentine = 0.51). However, Table 4 shows that site 4 yielded unusual data for the calcium. Whereas all the other sites showed values greater than 0.17, no calcium was detected from any of the spectra measured in site 4. When these values are removed the boxplots for calcium of the dentine and spheres become similar.

Fluorine (F)

The boxplots showing results for the proportions of fluorine of the spheres and dentine suggest that the spheres consist of a larger amount of fluorine than the dentine. The median

values between the spheres and dentine differ slightly (median F spheres = 0.15; median F dentine = 0.11). The boxplot with the results for the fluorine in spheres shows the minimum and the first quartile values both equal to 0.00. There was no fluorine detected at site 1 or 4 and site 6 spectrum 1 (6.1). For the dentine, only site 1 spectrum 2 retrieved a value of 0.00 for fluorine a; however, this is likely due to the relatively smaller sample size. The maximum value measured on the spheres was slightly larger than that on the dentine (maximum F spheres = 0.34; maximum F dentine = 0.27).

Phosphorous (P)

Small amounts of phosphorous were detected in both the spheres and the dentine. The minimum values for the spheres and dentine were both equal to 0.00 and the maximum values were similar (maximum P spheres = 0.21; maximum P dentine = 0.16). The median value for the proportion of phosphorous in the spheres was slightly lower than that of the dentine (median P spheres = 0.06; median P dentine = 0.11). The data for the dentine has a much smaller interquartile range than for the spheres. This is likely due to the fact that it has fewer values equal to 0.00 than the spheres. Similar to fluorine (and calcium for site 4), there was no phosphorous detected in site 1 nor 4.

3.2.2) Oxygen isotope analysis

Oxygen isotope composition (δO^{18}_{PO4}) was obtained from two enamel samples from the CGP/1/2265 mosasaur tooth and two from the associated shark tooth (Table 5). From the results, values for the body temperature (°C) were calculated using Lécuyer *et al.* (2013) phosphate-water oxygen isotope fractionation equation (equation 4).

$$T(°C) = 117.4(\pm 9.5) - 4.50(\pm 0.43)\ [(\delta^{18}O_{phosphate} - \delta^{18}O_{H20}] \qquad (4)$$

(Lécuyer *et al.*, 2013)

Mean δO^{18}_{PO4} ranged from 18.94‰ for the first mosasaur sample to 21.28‰ for the first shark sample. Both mosasaur δO^{18}_{PO4} values were lower than the shark values, which equates to higher body temperatures. Body temperatures for the two mosasaur tooth samples were 35.94°C and 30.47°C with a mean of 33.21°C (SD = 3.87°C). Estimated body temperature values for the shark samples were 25.88°C and 29.13°C with a mean value of 27.51°C (SD = 2.3°C). A two-sample t-test assuming unequal variance between the calculated body temperatures of the mosasaur and shark was conducted. It was found that there was not a significant difference between the mosasaur (mean = 33.21°C; SD = 3.87°C) and shark (mean = 27.51°C; SD = 2.3°C) estimated body temperatures (t = 1.79; p = 0.24).

Table 5. δO^{18}_{PO4} mean and standard deviation (SD) of the mosasaur and shark samples with body temperature values calculated using the phosphate-water oxygen isotope fractionation equation presented by Lécuyer et al. (2013).

Sample	δO^{18}_{PO4} mean (‰)	δO^{18}_{PO4} SD (‰)	Temperature mean (°C)
Mosasaur 1	18.94	0.25	35.94
Mosasaur 2	20.22	0.17	30.47
Shark 1	21.28	0.19	25.88
Shark 2	20.53	0.23	29.13

3.2.3) Strontium isotope analysis

Six readings produced the following mean $^{87}Sr/^{86}Sr$ values: (1) 0.707828 (2) 0.707817 (3) 0.707826 (4) 0.707807 (5) 0.707820 (6) 0.707806. All readings yielded 2-sigma error values of 0.00030. The mean $^{87}Sr/^{86}Sr$ was calculated to be 0.707817 with a standard deviation of 0.000019. Using the look-up table Version 4 from McArthur *et al.* (2012) the numerical ages for each $^{87}Sr/^{86}Sr$ value could be calculated (see Table 6). From the calibration curve adapted from McArthur *et al.* (2012) it appears that IT-1 from the CGP/1/2265 muzzle unit dates to the End Maastrichtian. The mean age was calculated to be 66.85Ma (standard deviation = 0.46Ma),

which is relatively close to the Cretaceous/Palaeogene (K/Pg) extinction event that led to the extinction of the mosasaurids (amongst other organisms) (Figure 42).

Table 6. Mean strontium isotopic composition measured from six enamel samples of IT-1 with the 2-sigma error and corresponding lower, mean and upper limits of numerical age (in millions of years) calculated using the look-up table Version 4 from McArthur et al.(2012). K/Pg Sr isotope ratio and ages were taken from McArthur et al. (2012). Only mean ages greater than 66Ma were included as mosasaurs became extinct at the end of the Cretaceous. Limiting ages at 95% confidence limits.

Sample	$^{87}Sr/^{86}Sr$ mean	σ2 error	Upper Cretaceous Age (Ma)		
			Lower limit	Mean	Upper limit
1	0,707828	0.00030	>63,54	66,30	<66,62
2	0,707817	0.00030	>66.62	66,87	<67,14
3	0,707826	0.00030	>65,82	66,43	<66,71
4	0,707807	0.00030	>67,08	67,36	<67,68
5	0,707820	0.00030	>66,45	66,74	<66,99
6	0,707806	0.00030	>67,12	67,41	<67,74
K/Pg	0.707831	-	>64,38	66,00	<66,45

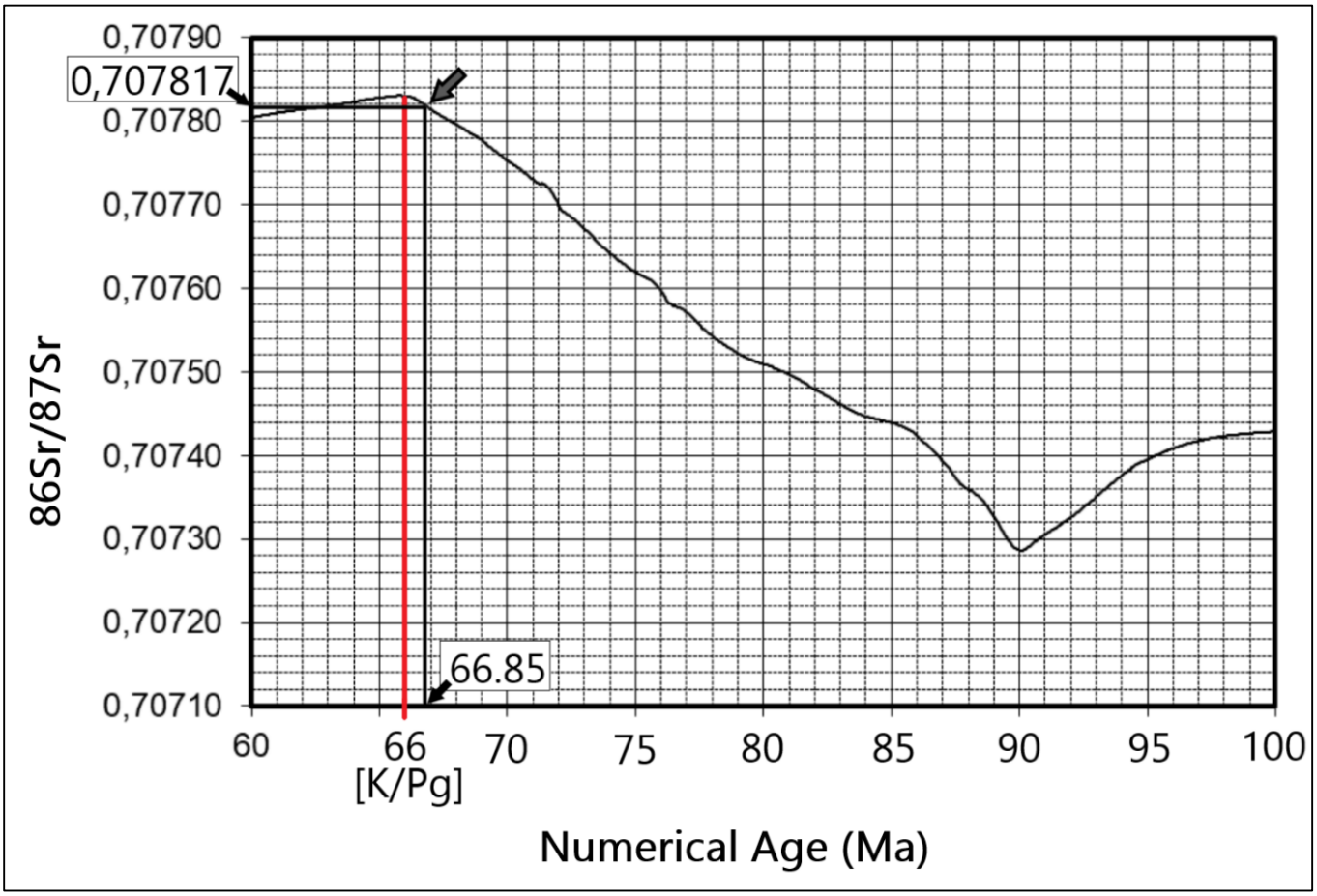

Figure 42. LOWESS curve of strontium isotope ratios to numerical ages for the Late Cretaceous [100.5-66Ma]. A horizontal line is drawn from the mean Sr ratio value (~0.707817) calculated from the six samples taken from IT-1to where it intercepts with the curve (dark grey arrow). A vertical line from the curve intercept to the x-axis gives the corresponding mean age at the time of tooth development (~66.85Ma). The Cretaceous/Palaeogene boundary (K/Pg) is indicated by the red vertical line. Figure adapted from McArthur et al. (2012)

Chapter 4: Discussion

4.1) Taxonomy of the South African mosasaurids

Much of the uncertainty surrounding the taxonomy of the SA mosasaurid material stems from not knowing exactly how many individuals are represented by the material. According to Rogers and Schwarz (1902) it appears that the muzzle unit (CGP/1/2265) and the frontoparietal complex and dentary fragments (SAM-PK-5265) were found together, thus it is plausible that these two specimens belong to the same individual. It is puzzling nonetheless that Broom (1912) only described the frontoparietal complex (SAM-PK-5265) and made no mention of the muzzle unit (CGP/1/2265), which is an important component of the material. It seems as though Broom (1912) interpreted the 'lower jaw belonging to the reptilian genus *Mosasaurus*' in Rogers and Schwarz (1902, p. 41) as being the two dentary fragments associated with the frontoparietal complex (SAM-PK-5265). The fact the two specimens were given completely different specimen numbers and were housed in different parts of the country suggests that they may have been separated quite soon after discovery. It may be that Broom was unaware of the muzzle unit when he described the SAM-PK-5265 material. Once the muzzle unit (CGP/1/2265) was 'rediscovered' in the Council for Geosciences collections in Pretoria, on the basis of Rogers and Schwarz (1902), it was speculated that SAM-PK-5265 and CGP/1/2265 may belong to the same individual (Chinsamy-Turan *et al.,* 2018).

Independent descriptions of each of the mosasaur specimens (see Chapter 3 section 3.1) are used to assist in the taxonomic identifications of the fossils. The following sections discuss the taxonomies and relationships of the muzzle unit and isolated teeth (CPG/1/2265); the frontoparietal complex and dentary fragments (SAM-PK-5265) and the taxonomy of the isolated fragmentary vertebra from St Lucia. There are two possible scenarios herein discussed for the

relationship between the muzzle unit (CGP/1/2265) and the frontoparietal complex (SAM-PK-5265). In the first scenario the two specimens belong to the same individual, whereas the second scenario highlights reasons why they could be different species.

4.1.1) Taxonomy of CGP/1/2265 and SAM-PK-5265 and their relationships

Taxonomy of CPG/1/2265 muzzle unit and isolated teeth

The size and robustness of the muzzle unit indicates an overall massive skull. The maxillae are large with mediolaterally thick tooth bearing parts to accommodate the heavy dentition. The massive nature of the skull elements of this specimen agrees with the mosasaurine genus *Prognathodon* (see Appendix B for generic diagnosis of *Prognathodon* modified from Russell, 1967; Bell, 1997 and Konishi *et al.,* 2011). A maximum of 9 teeth were counted in the right maxilla, but anterior and posterior portions of both maxillary bones are missing. It is likely that the complete maxillae could have held 3-4 more teeth, therefore meeting the 12-13 maxillary teeth criterion for *Prognathodon.*

The isolated teeth (IT-1 and IT-2) also seem similar to *Prognathodon.* They are unlike the teeth of *P. solvayi* (R033)*,* which are sharper, more medially recurved and quite strongly facetted (personal observation of specimens at RBINS). They are more similar to the teeth of *P. giganteus* (R106), which have smooth enamel surfaces; anterior and posterior carinae, and fine serrations on the carinae of two replacement teeth (personal observation at RBINS), which is considered a significant feature of *Prognathodon* (Konishi *et al.*, 2011). At the same time, *P. giganteus* teeth are labiolingually flattened, anteroposteriorly wide, less globular and slightly sharper than IT-1 and IT-2 (personal observation at RBINS). Grigoriev (2013) figured teeth belonging to *P. lutugini* (previously *Dollosaurus lutugini)* from Campanian deposits of Eastern Ukraine, which also resemble those of CGP/1/2265 in that they are bicarinate with fine serrations and have the

same wrinkled enamel texture towards the apical regions of the teeth (Figure 43B', C'). However, similar to those of *P. solvayi*, *P. lutugini* teeth appear to be more recurved and sharper than IT-1 and IT-2 (Figure 43C).

The isolated teeth of CGP/1/2265 appear most similar to two tooth crowns (OCP.DEK/GE 349 and OCP.DEK/GE 350) from the Maastrichtian of Morocco, which were assigned to *P. currii* (Bardet *et al.* (2005) (Figure 43D-E). The similarities include a subconical shape; a slightly swollen basal crown that is elliptical in cross-section; well-developed anterior and posterior carinae that are serrated; lingual and labial surfaces are subequal in size (compare Figure 43A' and E'); enamel approximately 0.5mm thick (see Chapter 3 section 3.2.1), particularly at the apex of the tooth giving it a darker colour (see Figure 43A, B); unfaceted and smooth enamel except for the upper two thirds of the crown that have crude anastomising ridges (Figure 43A', B'). Differences include the fact that *P. currii* have straight tooth crowns (Bardet *et al.*, 2005), whereas IT-1 and IT-2 have a slight posteromedial recurvature. There is also a small sharp point at the apex of OCP.DEK/GE 350 tooth crown (Figure 43E, E') that is not visible on OCP.DEK/GE 349 probably due to wear (Figure 43D'). The apex of IT-2 is missing, but Figure 43A' shows IT-1 in occlusal view and there seems to be a similar tooth wear pattern at the apex. IT-1 has been identified as a replacement tooth thus one would not expect to find evidence of wear. However, it is possible that the sharp point on the apex of IT-1 was worn down if it was exposed in the mouth.

There are concerns regarding the assignment of the CGP/1/2265 to *P. currii* based on the isolated teeth (M. Caldwell, personal communication, July 2020). The *P. currii* type specimen has no complete or well-preserved tooth crowns and the dentition has been largely described from reconstructions (Christiansen and Bonde, 2002). Therefore, despite the similarities shared

between the isolated teeth of CGP/1/2265 and the teeth figured by Bardet *et al.* (2005), the assignment of the two tooth crowns from Morocco (OCP.DEK/GE 349 and OCP.DEK/GE 350) to *P. currii* is equivocal and needs to be treated with caution. Despite the similarities shared between the isolated teeth of CGP/1/2265 and the teeth figured by Bardet *et al.* (2005) the assignment to *P. currii* is uncertain and the CGP/1/2265 isolated teeth are thus assigned to *Prognathodon* sp.

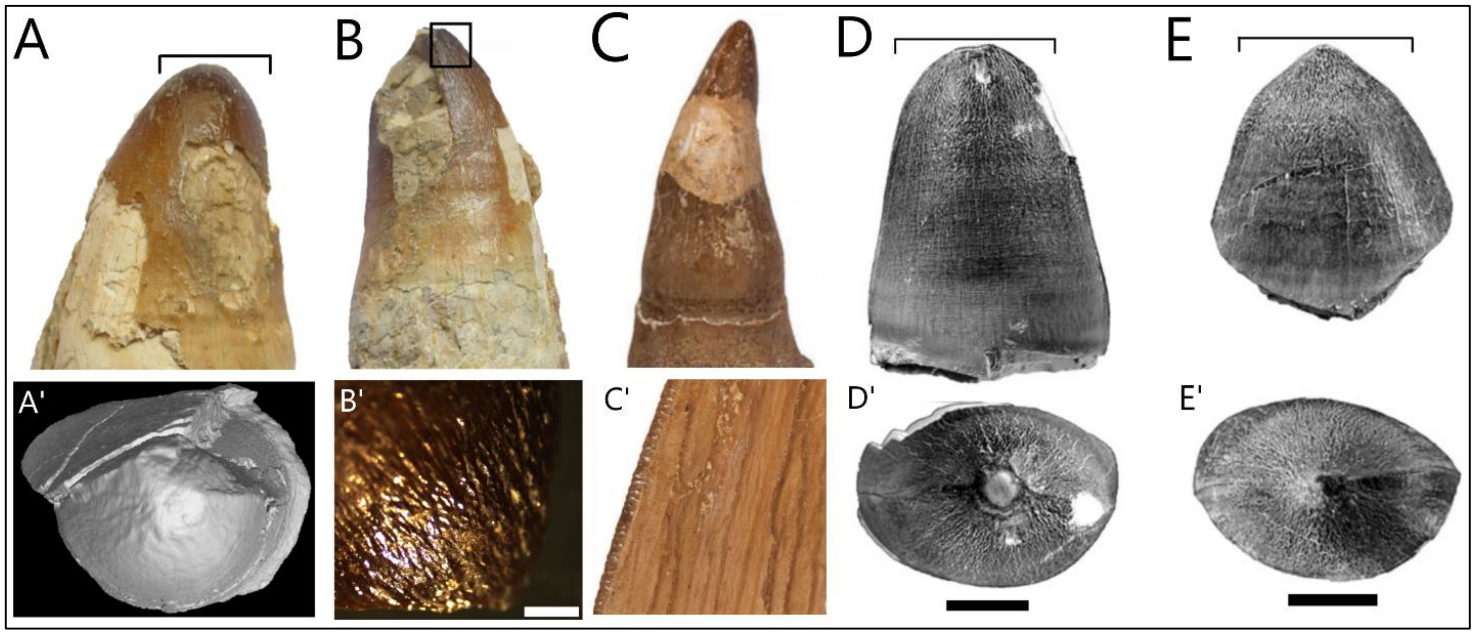

Figure 43. (A) IT-1 in labial view. (A') Three-dimensional micro-CT scan image of IT-1 in occlusal view with the blunt apex and anastomising ridges visible. (B) IT-2 in lingual view with box frame giving locational information for B'. (B') High magnification image of anatomising ridges at the apical region of IT-2 taken using a dissecting microscope. (C) Photograph of CCMGE 818 P. lutugini tooth crown in lingual view adapted from Gregoriev (2013). (C') High magnification image of the fine serrations on the carinae of P. lutugini adapted from Gregoriev (2013). (D) Photograph of OCP.DEK/GE 349 P. currii tooth crown in labial or lingual view adapted from Bardet et al. (2005). (D') Photograph of OCP.DEK/GE 349 P. currii tooth crown in occlusal view adapted from Bardet et al. (2005). (E) Photographs of OCP.DEK/GE 350 P. currii tooth in labial or lingual view adapted from Bardet et al. (2005). (E') Photographs of OCP.DEK/GE 350 P. currii tooth in occlusal view adapted from Bardet et al. (2005). Scale bars: A, A', B, C, C' = not to scale; B' = 2mm; D, D', E, E' = 10mm.

Taxonomy of dentary fragments (SAM-PK-5265)

Unfortunately, the dentary fragments themselves are of little diagnostic value because there is a lot of bone missing from the anterior and posterior ends of the fragments as well as from the ventral surfaces. Furthermore, the posterior dentary fragment contains no teeth and appears to be water-worn, which Broom (1912) similarly noted. This caused the loss of most of the surface detail on this fragment. However, the size and shape of the tooth sockets can be determined (Figure 15A). These are large (~430mm) and rounded and are like those visible in the maxillae of the muzzle unit as well as the tooth bases of IT-1 and IT-2, which are best seen in the micro-CT scan cross-sections (Figure 32 and 36).

The anterior dentary fragment possesses some remnants of functional teeth and replacement teeth and provides more diagnostic information. Micro-CT analysis of SAM-PK-5265 anterior dentary fragment revealed that the replacement tooth shared some similarities with IT-1 and IT-2 from the muzzle unit (CGP/1/2265). It is subconical in shape, elliptical in cross-section around the midsection (Figure 12C) and it has both anterior and posterior carinae (Figure 12D). The replacement tooth is relatively small in comparison to the functional tooth that preceded it (Figure 11), suggesting it had not yet reached stage 4 of Caldwell's (2007) eight-stage ontogenetic pattern for mosasaur tooth development.

However, there is still uncertainty about whether the dentary fragments (SAM-PK-5265) belong to the same individual as the muzzle unit and isolated teeth (CGP/1/2265). It is expected that the replacement teeth will have the same characteristics of the functional teeth they precede, and there are approximately four smooth facets visible along the exposed length of the replacement tooth in the anterior dentary fragment, which are not present on the isolated teeth from the muzzle unit (CGP/1/2265). Furthermore, the apical region of the replacement tooth is

missing and therefore it is impossible to assess the shape of the tooth apex, or to detect any anastomising ridges that may have been present.

Jiménez-Huidobro and Caldwell (2019) suggested that the SAM-PK-5265 dentary fragments and frontoparietal complex be reassigned to *Taniwhasaurus* based on the facetted enamel of the replacement teeth in the anterior dentary fragment. Through further preparation and micro-CT analysis, this study revealed the presence of unserrated anterior and posterior carinae on the replacement teeth, which is another feature of *Taniwhasaurus.* However, the enamel ornamentation on the replacement teeth in the anterior dentary fragment does not resemble that of the teeth of *Ta. antarcticus* (Martin and Fernandez, 2007; Fernandez and Martin, 2009) or *Ta. oweni* (Caldwell *et al.*, 2005)*,* which show strong and deep vertical striations. The facets on the SAM-PK-5265 replacement tooth are smooth, gentle and not as numerous, making them more similar to those of *Ta. mikasaensis* from the upper Santonian-lower Campanian of Island of Hokkaido, Japan (Caldwell *et al.*, 2008).

Taxonomy of the frontoparietal complex (SAM-PK-5265)

Scenario 1: The frontoparietal complex (SAM-PK-5265) belongs to the same individual as the muzzle unit (CGP/1/2265) and is a Prognathodon.

SAM-PK-5265 frontoparietal complex possesses some of the key diagnostic characters of the genus *Prognathodon* (see Appendix B for generic diagnosis of *Prognathodon* modified from Russell, 1967; Lingham-Soliar and Nolf, 1990 and Konishi *et al.*, 2011)*.* SAM-PK-5265 frontoparietal complex has a short, triangular frontal that is only slightly longer than wide. The lateral edges of the frontals are almost straight, with a slight outward bulge posteriorly, which is also evident in the diagram of the *P. overtoni* specimen (TMP 2007.034.0001) from the lower

Bearpaw Formation, southern Alberta, Canada (Konishi *et al.,* 2011, p.1030). Portions of the postorbitofrontals are visible lateral to the frontal as in *P. overtoni* (Konishi *et al.*, 2011).

Konishi *et al.* (2011) explained how the medial expansion of the anterior prefrontals of *P. overtoni* specimen, TMP 2007.034.0001 caused the anterior tip of the frontal to be narrow and prevented the external narial openings from invading of the anterior of the frontal. Similarly with the SAM-PK-5265 frontoparietal complex, there is no evidence to suggest that the internarial bar overlapped the frontal or that the frontal contributed to the shape of the posterior external narial openings, which is diagnostic of *Prognathodon* (except for in *P. saturator* and in *P. currii)*. Therefore, it is suggested that the anterior tip of the frontal bone in SAM-PK-5265 is broken and thus was probably not as broad as was previously interpreted. Its smooth and rounded appearance may be an artefact of water-wear.

The frontoparietal suture is sinusoidal and the medial sutural flanges of the frontal broadly enclose the anteromedial portion of the parietal surface (see Figure 8), which is diagnostic for *Prognathodon* (except *P. saturator*). The median sutural flange forms a crest directly anterior to the pineal foramen (Figure 8), which is unusual in mosasaurids (see Chapter 3, section 3.1.1), but could be an artefact of shifting bones during fossilisation. The parietal foramen is completely enclosed by the parietal, far from the frontoparietal suture and is small, which Russell (1967) suggested to be diagnostic for *Prognathodon*. The parietal bar is broad and does not appear to bulge anteriorly.

Scenario 2: The frontoparietal complex (SAM-PK-5265) belongs to a different individual and a different taxon to the muzzle unit (CGP/1/2265).

The frontoparietal complex (SAM-PK-5265) possesses a number of characteristics that do not support assignment to *Prognathodon.* For instance, it does not possess a dorsal midline

keel or the grooves in the surface behind the keel, like in *P. overtoni* specimen TMP 2007.034.0001 (Konishi *et al.*, 2011). The posterolateral edges of the frontal bone are rounded and blunt and are not wing-like as they are in *Prognathodon* (see Appendix B). The parietal postorbital processes are short, they do not reach the posterolateral corner of frontal as the generic diagnosis for *Prognathodon* suggests (see Appendix B).However, the bone is not particularly well-preserved and is suggested to be water-worn, thus some of the finer surface detail may have been lost. These delicate features are relatively prone to post-mortem obliteration, thus we cannot say unequivocally that it is not a *Prognathodon*.

The posterior half of the frontal and the frontoparietal suture closely resembles that of an immature *T. proriger* from the Canadian Museum of Nature (CMN 8162) figured by Stewart and Mallon (2018). However, the large size of the frontoparietal complex (SAM-PK-5265) does not indicate that it belonged to a young individual. Jimenez-Huidobro and Caldwell (2016) also suggested that the frontoparietal suture shape can vary through ontogeny and has been shown to vary within adult individual species of tylosaurines. The parietal table in SAM-PK-5265 more readily converges posteriorly, while the parietal table in *T. proriger* (plus *'T. kansasensis'* specimens) bulges laterally in the mid-length. The table is rectangular with parallel sides in other Tylosaurus species (Bullard and Caldwell, 2010).

There are a few ways in which the SAM-PK-5265 frontoparietal complex is similar to that of *Ta. antarcticus,* which is interesting because phylogenetic analysis of the tylosaurine mosasaurs placed *'T. capensis'* as a sister taxon to *Ta. antarcticus* (Jiménez-Huidobro and Caldwell, 2019). The posterolateral corners of the frontal bone, as well as the nearly straight posterolateral sides of the frontal are similar to those of *Ta. antarcticus,* although the frontoparietal sutures differ (Fernandez and Martin, 2009).

Given the fact that the SAM-PK-5265 dentary fragments are also suggested to belong to *Taniwhasaurus* (Jiménez-Huidobro, 2016; Jiménez-Huidobro and Caldwell, 2019) and the remains belong to the same specimen, it seems okay to suggest the associated frontoparietal complex also belongs to *Taniwhasaurus.* This would also make palaeobiogeographical sense given the prominence of the genus in the Southern Hemisphere - Antarctica (Novas *et al.*, 2002; Fernandez and Martin, 2009) and New Zealand (Caldwell *et al.*, 2005).

4.1.2) Strontium dating

According to Rogers and Schwarz (1902) the Pondoland mosasaurid remains were found in a Santonian-aged deposit. However, in this study the use of strontium isotope dating has enabled more accurate dating of the material from Pondoland (CGP/1/2265): the results of the strontium isotope analysis of the enamel of IT-1 suggests that specimen CGP/1/2265 is Maastrichtian-aged with a mean $^{87}Sr/^{86}Sr$ of 0.707817, which equates to 66.84Ma (using McArthur *et al.*, 2012) (Figure 42).

Unfortunately, dating this material does not provide further concrete information about the relationship between the two specimens. It is still possible for SAM-PK-5265 to be a different individual and age to CGP/1/2265. Strontium isotope analysis of enamel from one of the replacement teeth in the anterior dentary fragment (SAM-PK-5265) could resolve this issue and, if both specimens are found to be the same age, could provide strong evidence for them belonging to the same individual. However, it was not possible to obtain permission for this due to the rarity of the specimen and the destructive nature of the strontium dating methods (thin sectioning + laser ablation/solution method). However, developments of less destructive dating methods in the future could allow for the age of the SAM-PK-5265 anterior dentary fragment to

be determined, which would provide sturdy evidence of the specimens' relationship or lack thereof.

4.1.3) Taxonomy of the shark tooth associated with CGP/1/2265

There is morphological, geographical and temporal evidence to suggest that the isolated shark tooth found associated with the CPG/1/2265 muzzle unit belonged to the extinct shark species, *Squalicorax pristodontus* (Agassiz, 1843). *Squalicorax* is an extinct genus of the Anacoracidae family (Order: Lamniformes) and are common in Cretaceous deposits all around the world (Compagno, 1990; Shimada and Cicimurri, 2005). Remains have been found in North and South America, Australia, Asia, Europe and Africa (Shimada and Cicimurri, 2005). Furthermore, remains of mosasaurs and *Squalicorax* sharks have been found together previously (Dortangs *et al.,* 2002; Konishi *et al*., 2011; Konishi *et al.*, 2014)

Gottfried and Rabarison (2001) figured and described *S. pristodontus* teeth from the Late Cretaceous and Paleocene deposits of the Mahajanga Basin in north-western Madagascar, which is relatively geographically near to the Pondoland. This indicates that these sharks were present in the region around the same time. Gottfried and Rabarison (2001) described the same fine serrations, bulbous mesial side and a crescentic shape that is noted in the CGP/1/2265 isolated shark tooth.

S. pristodontus teeth and mosasaurid remains have been recovered together from Late Cretaceous deposits of Devon Island, Canada (Chin *et al.*, 2008). The isolated *S. pristodontus* tooth figured by Chin *et al.* (2008, Figure 5C, p.2680) is very similar to that which was found in the matrix around the muzzle unit. Shimada and Cicimurri (2005) also figured a number of teeth belonging to various species of the *Squalicorax* genus and the drawing of the *S. pristodontus* tooth, as well as the temporal range of the species from Early Campanian to the Upper

Maastrichtian (Shimada and Cicimurri, 2005, Figure 1, p.242) further supports the identification the CGP/1/2265 isolated shark tooth as *S. pristodontus.*

4.1.4) Taxonomy of the isolated vertebra from St Lucia

The presence of left synapophysis, which articulates with the ribs, as well as the long length of the centrum (74.94mm) suggests that this is a dorsal vertebra. In posterior view (Figure 35D) the isolated vertebra from St Lucia looks like the dorsal vertebra of specimen NHMM 006696, belonging to *M. hoffmannii* (Street and Caldwell, 2017, Figure 18a-e, p545).

Similarities between the isolated vertebra from St Lucia and *M. hoffmannii* dorsal vertebra (NHMM 006696) include: a cylindrical centrum that is longer than it is tall or wide; a rounded heart-shaped condyle (Figure 35D); an almost circular cotyle (Figure 35C); a slight concavity between the articular faces on the ventral side (Figure 35F) (Street and Caldwell, 2017) and dorsoventrally thick and slightly dorsoanteriorly orientated synapophyses.

Zygosphenes and zygantra are features that are present and well-developed in *Clidastes, Prognathodon* (Lingham-Soliar and Nolf, 1990; personal observation at RBINS) and *Globidens* (Polcyn *et al.,* 2010; Konishi *et al.*, 2011) and are present but not as well-developed in *Mosasaurus, Plotosaurus* and *Platecarpus* (except in cervical vertebrae) (Russell, 1967).

The relatively well-developed triangular zygantra in the St Lucia vertebra (Figure 35D) is different to those noted in (NHMM 006696). The zygantra in NHMM 006696 dorsal vertebra are described as being reduced (Street and Caldwell, 2017) as indicated for *Mosasaurus* (Russell. 1967). However, the shape of the zygosphenes and zygantra differ depending on the vertebral position, which is unknown in the NHMM 006696 specimen.

Unfortunately, due to the fragmentary nature of the specimen nothing can be inferred about the dorsally depressed cotyle; the orientation of the neural arches or spines, or keel on the

ventral surface, which may have been lost due to wear as seen on the left synapophysis (Figure 35F). Thus, it is suggested that the isolated fragmentary vertebra from St Lucia belonged to a member of the genus *Mosasaurus* sp., cf. *M. hoffmannii.* However, the fragmentary nature of the specimen makes it difficult to identify to species level with certainty.

4.2) Palaeobiology

4.2.1) SA mosasaur dentition and structure of IT-1

IT-1 was assessed using combination of methods including gross morphology, micro-CT scanning, histology and SEM analysis in order to extract palaeobiological information about the mosasaur from Pondoland (CGP/1/2265), more specifically to see whether the tooth development, replacement, histology and enamel architecture was similar to that of other mosasaurids.

Tooth development and replacement

Due to IT-1 and IT-2 having been isolated in the matrix around the CGP/1/2265 muzzle unit it is not possible to know for sure where the teeth were positioned in the jaws during life. However, resorption pits and tooth sockets visible in the maxilla of CGP/1/2265 show a typical mosasaurid pattern with the resorption pits positioned posterolingually to the functional tooth sockets (see Figure 16B).

Gross morphology of IT-1 compared with IT-2, suggested that the main portion of its cementum root had broken off. However, the under-developed pulp cavity seen on the micro-CT scans indicated that IT-1 was in fact a replacement tooth. The presence of a pulp cavity implies that IT-1 was a rather mature replacement tooth because the replacement tooth examined by Chinsamy *et al.* (2012) had no pulp cavity and appears to still be within the resorption pit at the point of sectioning. Conversely, the pulp cavity in IT-2 is much larger at the tooth base (Figure

32A), whilst the dentine layer in this region is comparably thinner. It appears that IT-1 had at the least reached stage 4 in Caldwell's (2007) eight-stage ontogenetic pattern for mosasaur tooth development. This means that the replacement crown had grown to the same size as the functional tooth crown that preceded it; the osteodentine root and cementum had yet to start developing but a significant portion of the crown has extended above the lingual margin of the dentary/maxilla (Caldwell, 2007). The wear pattern on the apex of IT-1 (Figure 43A') suggests that this tooth was exposed above the lingual margin of the dentary/maxilla.

Histology

Histological analysis of IT-1 revealed a thin layer of enamel surrounding a thick layer of dentine around a small pulp cavity. What was initially thought to be cementum, was later identified as sediment around the base of the crown and which had infilled the pulp cavity.

Sediment

Rogers and Schwarz (1902) wrote that the mosasaurid material was recovered just south-west of the Mzamba River mouth in the Eastern Cape (Figure 44, red arrow). Lui and Greyling (1996) did a study of the grain-size distribution and cementation of the Late Cretaceous Mzamba Formation, which stretches along the east coast of Eastern Cape and KwaZulu-Natal, SA. This is fortuitous because it provides clear information about the sediment near where the mosasaur was discovered (Figure 44, red arrow) and confirmed that the substance infilling the pulp cavity and around the base of IT-1 was sediment and not cementum.

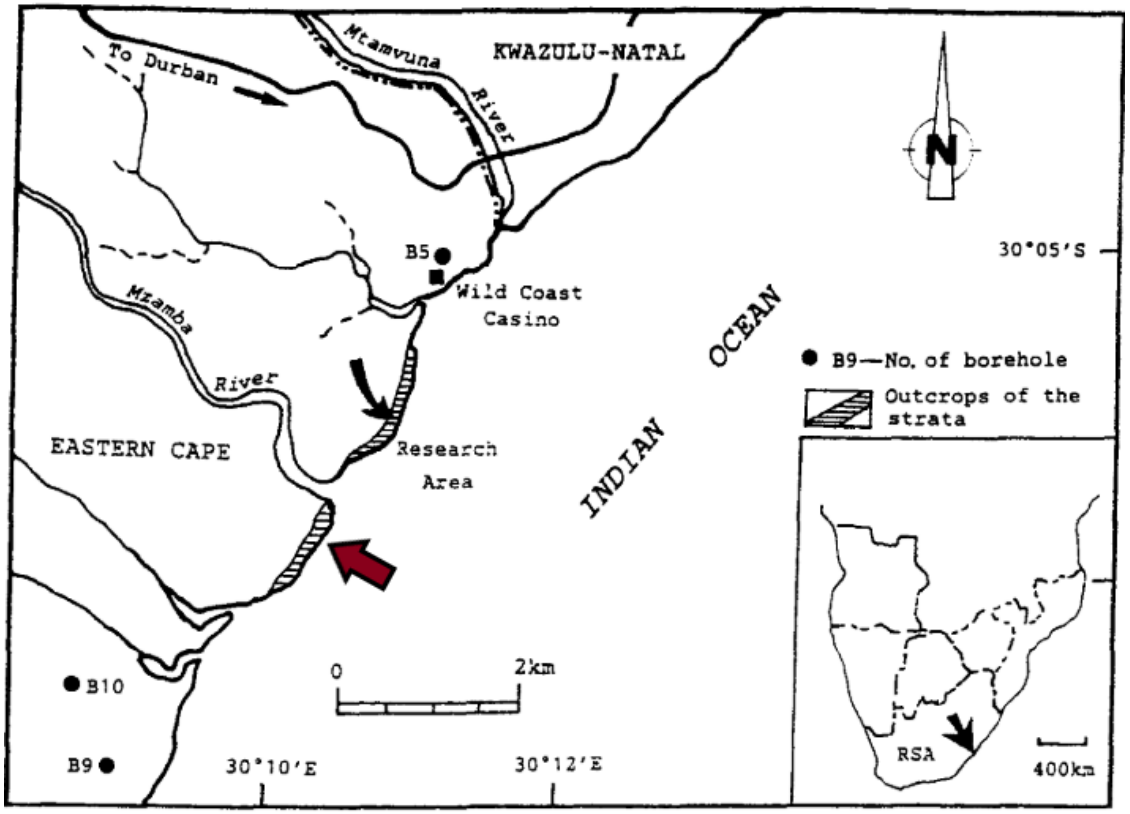

Figure 44. Locality map adapted from Lui and Greyling (1996) showing the research area of Mzamba formation and the approximate location where Rogers and Schwarz (1902) discovered the mosasaur material (red arrow).

Lui and Greyling (1996) assessed the sediment structure by thin sectioning collected samples of field outcrops and bore-hole cores (Liu and Greyling, 1996). When compared, the

micrographs of the sediment in Liu and Greyling (1996, p.92) were very similar to those of IT-1 (Figure 37D-E). They are both characterised by irregular-sized particles and possess the same rod-like structures, which are nearly exactly the same length and width as the ones measured in the sediment around IT-1(Figure 45, arrow). These rod-like structures are apparently elongated intraclasts (Liu and Greyling, 1996).

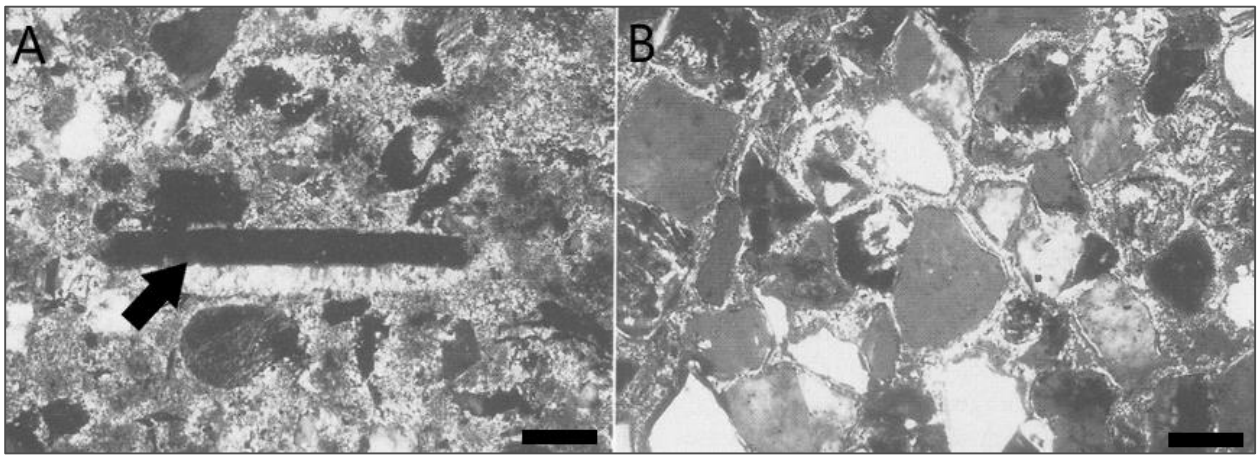

Figure 45. Micrographs of two cementation textures of the Mzamba Formation adapted from Lui and Greyling (1996). (A) Pendant sparite cement with an elongated intraclasts (arrow) that is very similar in size, shape and overall appearance to the elongated grains seen in the sediment around IT-1. (B) Variation in grain size, shape and texture of the sediment from the Mzamba formation. Scale bars: A = 100µm; B = 50µm.

Dentine

The dentine layer of IT-1 was much thicker than that of IT-2 (see Figure 32). Dentinal tubules were visible and similar to those seen in the *M. hoffmannii* tooth (Chinsamy *et al.*, 2012). However, unlike the *M. hoffmannii* tooth, no predentine was visible around the pulp cavity, which is likely due to the patchy preservation of the dentine in IT-1.

The average distance between the incremental growth lines in the dentine of IT-1 were much larger (~53.93µm) than the distance measured between the Lines of von Ebner for *M. hoffmannii*, which was approximately 10.9µm (Chinsamy *et al.,*2012). Furthermore, a study by Gren and Lindgren (2014) looked at dentine deposition rates in three mosasaur taxa and found

similar average distances between the Lines of von Ebner as Chinsamy *et al.* (2012). The average distances between Lines of von Ebner in *Dollosaurus, Platecarpus* and *Tylosaurus* were 12.2µm, 11.3µm and 15.7µm respectively (Gren and Lindgren, 2014).

This large distance between the incremental growth lines could be due to statistical error as a smaller sample size was used for the calculation in IT-1 (n=14, as opposed to n≥94 in Chinsamy *et al.* (2012) and Gren and Lindgren (2014). However, the likely cause is that the preservation of IT-1 is too poor to observe all the daily growth lines (Lines of von Ebner) and therefore the measured distances cannot be used to determine time taken for the dentine to develop.

Enamel

The average enamel thickness near the apex of IT-1 was similar to the enamel thickness noted for *P. currii* (Bardet *et al.*, 2005). The enamel is thickest at the apex, which is usually the case with durophagous mosasaurs because apical regions of the teeth undergo mechanical stress from feeding on hard prey (Bardet *et al.*, 2005; Schulp *et al.*, 2013). Apical wear is similarly noted on IT-1 (Figure 43A'), which suggests it may have had a partially durophagous lifestyle.

Histologically, several different layers were visible within the enamel (Figure 37B). To the best of my knowledge, this has not been noted in mosasaurid enamel before. Layer 2 of the IT-1 enamel was found to be birefringent under polarised light, which Cooper and Poole (1973) and Chinsamy *et al.* (2012) suggested to be indicative of prismatic enamel. The dark striations in the enamel that run perpendicular to the tooth surface slightly resemble enamel prisms; however, SEM analysis did not provide any evidence to suggest that the enamel was prismatic. A recent study by Owocki and Madzia (2020) also noted birefringent enamel in a *Mosasaurus* aff.

lemonnieri and suggested that it was because the enamel crystallites were in modules of the same type and had all had a similar orientation, not because it was prismatic.

SEM

Enamel architecture

The detailed micrographs and descriptions provided (see Chapter 3 section 3.2.1) reveal a complex array of enamel modules. These are repeatable volumes of enamel that are delimited by crystallite discontinuities or by zones of changing crystallite orientation, which produce distinct enamel types (Von Koenigswald and Sander, 1997; Sander, 2009).

Converging and diverging individual enamel crystallites formed columnar divergence/convergence units (Figure 38E and 39) that do not span the entire length of the enamel from the enamel-dentine junction to the outer enamel surface, as do enamel prisms (Sander, 2009). Similarly, Owocki and Madzia (2020) also noted columnar enamel in a *Mosasaurus* aff. *lemonnieri* tooth, with the columnar units perpendicular to the enamel-dentine junction. They indicated that the crystallites diverge from a central region without a central divergence line; however, central convergence lines were observed in IT-1 (Figure 39C).

Microunits, which are a few diverging enamel crystallites long, and a few wide (Von Koenigswald and Sander, 1997), form microunit enamel, which is a type of prismless enamel and was noted near the outer enamel surface of IT-1 (Figure 38D). No microunits were noted in the enamel of *Mosasaurus* aff. *lemonnieri* by Owocki and Madzia (2020). Another prismless enamel type that was noted is formed by groups of microunits and columnar units and is known as compound unit enamel (Figure 38E) (Sander, 2009). Enamel tubules were noted in the IT-1 enamel, these are apparently common in prismless enamel (Von Koenigswald and Sander, 1997)

and were also found in the enamel of a *Mosasaurus* aff. *lemonnieri* tooth (Owocki and Madzia, 2020).

Spherical structures found on the dentine

The spherical structures that were unexpectedly noted on the dentine of IT-1 during SEM analysis of the enamel architecture are interpreted as fossilised bacteria. The mineral replacement of bacteria that occurs during fossilisation preserves the size, shape, cellular complexity, cell wall texture, and colonial behaviour of the living organisms (Westall *et al.*, 2001). However, in order for bacteria to be well-preserved in the fossil record, a specific suite of conditions is necessary (Vinther, 2016). One of the most important conditions is the early precipitation of minerals that encapsulate the bacteria leading to rapid fossilisation (Vinther, 2016) such as fine-grained cherts (Westall *et al.*, 2001), which are apparently present in the region of Pondoland where the mosasaur remains were recovered (Susela, 2014).

The suggestion that the spherical structures on the dentine of IT-1 are fossilised bacteria is supported by the fact that the depositional environment was probably suitable for the fossilisation of such small structures, as well as the preserved morphological features of the spherical structures that characterise bacteria. These features include the uniformly spherical shape of the structures, smooth cell wall texture, small size range, evidence of cell division and aggregation in colonies all over, but not attached to the dentine (Westall *et al.*, 2001; Vinther, 2016). These characteristics have been used previously to identify the presence of fossilised bacteria (Westall *et al.*, 2001; Vinther, 2016).

The simple spherical shape, lack of flagella, filaments or any other distinguishing features only allows one to identify the bacteria as a type of cocci bacteria (Willey *et al.*, 2014). Unfortunately, the SEM micrographs do not offer much in terms of diagnostics and therefore it is

inappropriate to speculate about the precise taxonomic identification of the bacteria. EDS analysis similarly did not provide much information regarding the elemental composition of the structures as the values were too variable to draw conclusions.

In most of the SEM micrographs of the bacterial cell arrangements appear to be predominantly monococcal (occurring singly). There are a few cases where groups of individual cells appear to be attached in some way, although the irregularity of the attachment and the lack of repeated arrangements suggests that it is not indicative of distinguishable taxa. There is evidence to suggest that some of the bacterial cells were in the process of dividing and reproducing by binary fission at the time of fossilisation (Figure 46, arrows), which explains the presence of diplococcal cells (in pairs).

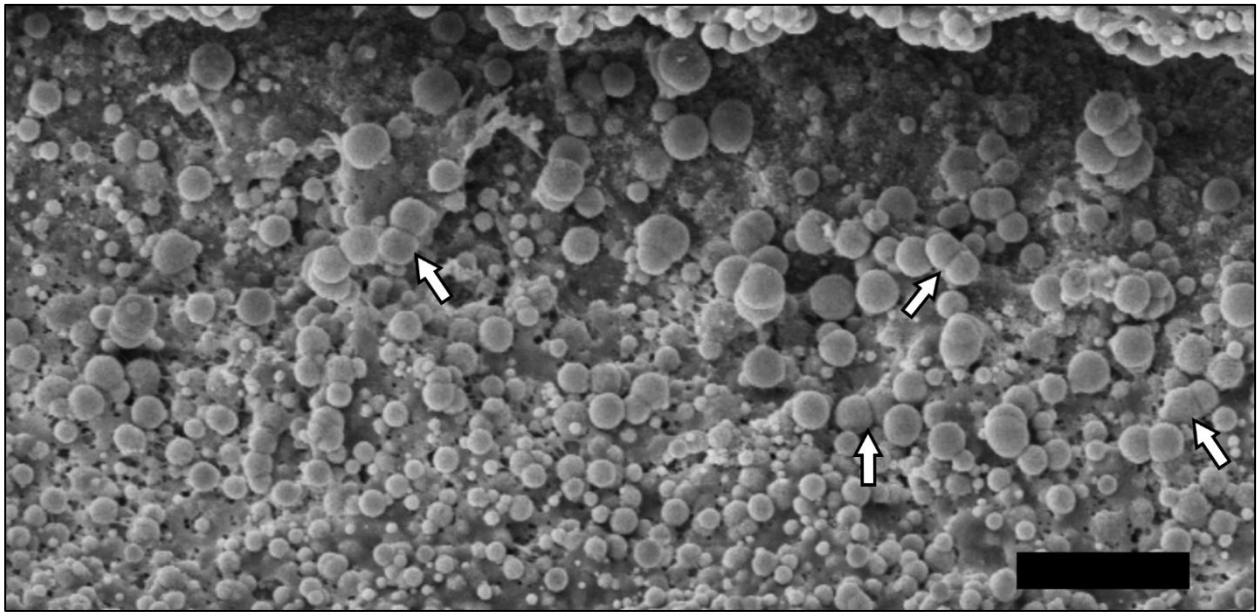

Figure 46. SEM micrograph of the suspected fossilised bacteria. The singular monococcal cells are the predominant arrangement. There are a number of diplococcal cells (in pairs) representing those cells undergoing division by binary fission (white arrows). Three-dimensional and chain arrangements of cells are visible, but are scarce and irregular. Scale bar = 5µm.

It is still unclear at which point the bacteria invaded the dentine. Knowing whether the bacteria invaded the dentine during life or after death could provide further clues as to their taxonomic identity. During life microorganisms can invade the root canal space and then

penetrate the dentine via the dentinal tubules, which was shown to be the case with *Enterococcus faecalis* (a bacterium) in infected human teeth (Al-Nazhan *et al.*, 2014). Al-Nazhan *et al.* (2014) found that in all the infected teeth, the small size of *E. faecalis* enabled it to penetrate the dentinal tubules and move through them (Al-Nazhan *et al.*, 2014). The SEM micrographs of the dentine of IT-1 clearly show the spherical structures lining the interior walls of the dentinal tubules (Figure 39D). Therefore, the first scenario for the bacterial invasion is that the microbes used the pre-existing dentinal tubules to spread throughout the dentine from the developing pulp cavity whilst the mosasaur was still alive. Upon encountering the enamel-dentine junction, the bacteria were unable to penetrate the hard enamel or the enamel provided no organic tissue for the bacteria to live off, thus explaining their absence in the enamel.

An alternative explanation, is that the bacteria invaded the dentine from the outside inwards after death. The tooth had been dislodged from the jaws during decomposition. Some of the enamel may have broken off during this process, thus exposing the underlying dentine (Figure 29). It is however unusual that histological analysis of IT-1 did not reveal any microbial damage to the dentine such as boring tunnels that would be otherwise expected had the bacteria been feeding on the dentine. Owocki and Madzia (2020) noted bioerosion in the examined *Mosasaurus* aff. *lemonnieri* tooth in the form of longitudinal microbial tunnels. These were found in the outer dentine layers and a second tunnel type was noted in the deeper core of the dentine. The microbial tunnels nearer the dentine surface had a large diameter (9.75-16.7μm), which obliterated the dentinal tubules and had also invaded the enamel in some places (Owocki and Madzia, 2020). Unlike in the current study, Owocki and Madzia (2020) did not observe the microorganisms creating these tunnels. However, they speculated that the microbial tunnels could have been made by phototrophic cyanobacteria, algae or heterotrophic bacteria based on

the location of the tunnels and the fact that they are known to metabolise collagen and the dissolved mineral matrix of dentine (Owocki and Madzia, 2020).

The lack of microborings in the dentine could indicate that the bacteria were simply using the dentine as attachment. Thus, a third scenario suggests that it could be a type of phototrophic cyanobacteria or algae that attached to the dentine whilst the tooth lay on the shallow seafloor, and then succumbed when the tooth was buried and fossilised. However, a problem with this scenario and with the identification of the cells as phototrophic cyanobacteria or algae is that these organisms are not expected to penetrate the internal structures of the tooth from the outside as this would reduce the available light needed for photosynthesis. It also does not explain why the structures were not found on the enamel.

It should also be noted that more than one of the above described scenarios could have been at play prior to fossilisation and therefore could have resulted in several different types of microorganisms on the surface of and inside the dentine. This may explain the range in size of the cells, although a variation in the size of individual bacteria within a species is possible (Willey *et al.,* 2014).

4.2.2) Oxygen isotope analysis

The results from the oxygen isotope analysis of the mosasaur tooth and shark tooth provide some evidence to suggest that CGP/1/2265 mosasaur from Pondoland was able to maintain a body temperature higher than the surrounding water. Both δO^{18}_{PO4} values for the mosasaur tooth enamel were lower than those of the shark tooth enamel, which equates to higher body temperature values. There was a difference in the mean temperature values between the mosasaur (mean = 33.21°C) and the shark (mean = 27.51°C), although this difference was not

significant ($p = 0.24$) probably due to the small sample size ($n = 4$) and also large standard deviations in the results.

Shortfalls in this investigation include the fact that it was not possible to include the δO^{18}_{PO4} values of a contemporary poikilothermic bony fish or a known endotherm with which to compare the δO^{18}_{PO4} results of the mosasaur and the shark as did Harrell *et al.*(2016). The lack of data from a poikilothermic bony fish is problematic because there is a possibility that the shark tooth was not a good ectothermic representative (see below).

By using the δO^{18}_{PO4} values of the shark to represent that of the seawater, it is assumed that the shark was a poikilothermic ectotherm. *Squalicorax* teeth have been used in similar studies as poikilothermic representatives (e.g. Clemens, 2018) and there is no direct evidence (to the best of my knowledge) to suggest that *Squalicorax* were able to thermoregulate. However, there are other members of the Lamniformes that are capable of regulating their body temperature today. The size and serrations on the cutting teeth of *Squalicorax* are indicative of a macropredatory lifestyle (Compagno, 1990; Becker and Chamberlain, 2012) and modern macropredatory sharks of the Lamnidae family are all endothermic (Bernal *et al.*, 2001). Ferrón (2017) suggested that macropredatory sharks of the extinct family Otodontidae were also endothermic and that endothermy facilitated gigantism in sharks such as *Otodus (Megaselachus) megalodon*, as opposed to gigantism being a cause for their elevated body temperatures.

The fact that the body temperatures calculated from the δO^{18}_{PO4} values of the *Squalicorax* tooth enamel were lower than those of the mosasaur may indicate differences in their ability to thermoregulate. Therefore, for the purpose of this study it is acceptable to assume the δO^{18}_{PO4} values of the shark tooth approximately represent that of the seawater.

Chapter 5: Conclusions and future research

5.1) Taxonomic conclusions of the South African mosasaurids

5.1.1) CGP/1/2265 and SAM-PK-5265 from Pondoland, SA and their relationships

In Chapter 1 (p.38) it was predicted that all the mosasaurid material from Pondoland, SA belonged to the same individual. That is the CGP/1/2265 muzzle unit (and associated isolated teeth) and the SAMP-PK-5265 frontoparietal complex and two dentary fragments. However, detailed taxonomic assessments of all the material led to a different outcome.

The robust and heavy nature of the CPG/1/2265 muzzle unit suggests affinities with the genus *Prognathodon.* It was also noted that the isolated teeth from the muzzle unit resembled those of *P. currii* (Christiansen and Bonde, 2002; Bardet *et al.*, 2005). However, there are problems associated with the *P. currii* assignment by Christiansen and Bonde (2002) and Bardet *et al.* (2005) (see Chapter 4, section 4.1.1). These issues render the assignment of CGP/1/2256 to *P. currii* unreliable (M. Caldwell, personal communication, July 2020), thus the muzzle unit and associated isolated teeth (CGP/1/2265) are assigned to cf. *Prognathodon.*

There are some characteristics of the SAM-PK-5265 frontoparietal complex that partially support its assignment to *Taniwhasaurus,* along with the associated dentary fragments (Jiménez-Huidobro, 2016; Jiménez-Huidobro and Caldwell, 2019). However, there is no evidence to suggest that the external nares invaded the frontal, or that the internarial bar overlapped the anterior tip of the frontal, which are two features that are supposedly present in all tylosaurine mosasaurs (Jiménez-Huidobro and Caldwell, 2019). For that reason, the SAM-PK-5265 frontoparietal complex is not of *Taniwhasaurus* origin, nor is it of *Tylosaurus* origin, as was first put forward by Broom (1912). Therefore, the first hypothesis of this study, which states that *Tylosaurus capensis* (Broom, 1912) is not a valid taxon, is supported.

Moreover, this feature that excludes the SAM-PK-5265 frontoparietal complex from the tylosaurines supports its assignment to cf. *Prognathodon.* A lack of overlap of the frontal by the internarial bar and an absence of narial embayment in the frontal is diagnostic for *Prognathodon* (see Appendix B). Other features supporting its mosasaurine origin include the anterior convergence of the anterior borders of the postorbitofrontal and the sinusoidal medial border of the postorbitofrontal in ventral view. When scaled against each other, the dimensions of the SAM-PK-5265 frontoparietal complex and the CGP/1/2265 muzzle unit correspond well and generate a picture of a large, heavy skull that is proportionally short, as is seen in other members of *Prognathodon.* The sheer thickness of the frontal table, even with weathering, is congruent with being a *Prognathodon*. Therefore, the proposed allocation of SAM-PK-5265 frontoparietal complex to the mosasaurine genus *Prognathodon* has led to the suggestion that SAM-PK-5265 frontoparietal complex belongs to the same individual as the CGP/1/2265 muzzle unit, which is confidently assigned to cf. *Prognathodon.*

It is tentatively suggested that the SAM-PK-5265 posterior dentary fragment also belonged to the same individual as the CGP/1/2265 muzzle unit and the SAM-PK-5265 frontoparietal complex. This is based on the overall robustness of the fragment and the size and shape of the visible tooth bases, which are comparable to the basal regions of IT-1 and IT-2 and those tooth bases visible in the muzzle unit.

Conversely, it seems less likely that the SAM-PK-5265 anterior dentary fragment belonged to the same individual as the CGP/1/2265 muzzle unit and the SAM-PK-5265 frontoparietal complex. The overall appearance of the SAM-PK-5265 anterior dentary fragment is of a more gracile mosasaurid than *Prognathodon*. The replacement tooth visible in the anterior dentary fragment possesses smooth, facetted enamel, which is not observed on the CGP/1/2265

isolated teeth. The enamel ornamentation of the replacement tooth resembles the figured teeth of *Ta. mikasaensis,* from Japan (Caldwell *et al.*, 2008). However, the replacement tooth in the anterior dentary fragment is straight, whereas *Ta. mikasaensis* has posteromedially recurved tooth crowns (Caldwell *et al.*, 2008). The suggestion by Jimenez-Huidobro and Caldwell (2019) to assign it to *Taniwhasaurus* is supported, but it cannot be identified at the species level. It is hereby referred to as cf. *Taniwhasaurus.*

Therefore, though there is still uncertainty around the relationships between the mosasaurid remains from Pondoland, it appears that there are at least two different taxa in this region, thus the second hypothesis of this study is supported.

5.1.2) Isolated partial vertebra from St Lucia, SA

Based on the fact that the mosasaurid locality in Pondoland is approximately 355km south-west of St Lucia, it was thought that the taxa from the two localities might be different. It closely resembles the dorsal vertebra of *M. hoffmannii* (NHMM 006696) (Street and Caldwell, 2017), but is too poorly preserved to confidently identify to species level. The anatomical assessment of the isolated partial vertebra from the St Lucia estuary has led to its identification *Mosasaurus* sp., cf. *M. hoffmannii*.

5.1.3) Concluding remarks and palaeobiogeographical implications

There are at least three different mosasaur taxa known from SA and a total of three individuals. Specimen SAM-PK-5265 from Pondoland, which was initially described by Broom (1912) is probably comprised of two different individuals. Two of the three elements that make up SAM-PK-5265 namely a large frontoparietal complex and a dentary fragment, belong to the same individual as specimen CGP/1/2265, which is comprised of a large muzzle unit and

isolated teeth (see Table 7, individual A). This individual has been assigned to cf. *Prognathodon* and has been dated to the End Maastrichtian using strontium isotope dating of a tooth.

The fact that the strontium isotope analysis of the CGP/1/2265 tooth dated this mosasaur to the End Maastrichtian refutes the third hypothesis that stated the strontium isotope composition of the CGP/1/2265 teeth would be reflective of the Santonian age. Furthermore, the *Prognathodon* genus is known from the Early Campanian to End Maastrichtian, and this agrees with the taxonomic assignment of the material.

Prognathodon had become very widespread by the End Maastrichtian. In Africa the genus was present in Angola, DRC, Morocco (Table 1) and now SA, but the genus has also been recovered from Antarctica (Jiménez-Huidobro *et al.*, 2017) and possibly Japan (Konishi *et al.,* 2012).

The second individual (individual B) was also recovered from Pondoland and forms a part of specimen SAM-PK-5265. It is a single left dentary fragment with a replacement tooth. Its proposed assignment is to *Ta. mikasaensis.* Strontium isotope analysis of IT-1 (CGP/1/2265) dated the Pondoland material to the End Maastrichtian, which is outside of the temporal range of *Taniwhasaurus* (Caldwell *et al.*, 2008; Polcyn *et al.*, 2014). Thus, this could indicate that: this diagnosis is incorrect; the temporal range of the genus is greater than previously thought or that the original stratigraphic age provided by Rogers and Schwarz (1902) was inaccurate, in which case this dentary fragment was recovered from different strata to the CGP/1/2265 muzzle unit. Since *Ta. mikasaensis* was recovered from upper Santonian lower Campanian deposits, it is suggested that this dentary fragment is Santonian-aged as was initially indicated, rather than it being Maastrichtian-aged as was implied by strontium isotope analysis of CGP/1/2265 with which it was initially associated.

The third individual (individual C) is represented by a single partial vertebra, which is suggested to have belonged to *Mosasaurus* sp.*,* cf. *M. hoffmannii.* Unfortunately, the geological evolution of Lake St Lucia is poorly understood, making it impossible to accurately assign this specimen to a specific age during the Late Cretaceous (Wright *et al.,* 2000). Further mosasaur fossil discoveries from Lake St Lucia could provide more concrete information regarding the species, as well as the origin and dispersal of *Mosasaurus* to the east coast of SA.

Table 7. Summary of the SA mosasaurid material with information regarding the current specimen numbers for each element; the number of skeletal elements per individual; where the elements were recovered; the age of the elements and the taxonomic assignment of each element based on this study.

Specimen	Individual	Skeletal element	Locality	Age	Taxonomic assignment
SAM-PK-5265	A	Frontoparietal complex	Pondoland	End Maastrichtian	*Prognathodon* sp.
SAM-PK-5265	A	Posterior dentary fragment	Pondoland	End Maastrichtian	cf. *Prognathodon*
CGP/1/2265	A	Muzzle unit and two isolated teeth	Pondoland	End Maastrichtian	cf. *Prognathodon*
SAM-PK-5265	B	Anterior dentary fragment with replacement tooth	Pondoland	?Santonian?	cf. *Taniwhasaurus*
NA	C	Isolated vertebra	Lake St Lucia	Late Cretaceous	*Mosasaurus* sp.*,* cf. *M. hoffmannii*

5.2) Palaeobiological conclusions

5.2.1) SA mosasaur dentition

The fourth hypothesis of this study has to do with the dentition of the SA mosasaurs and is comprised of three parts (see Chapter 1, Section 1.2.1). It was predicted that the tooth

replacement, development and histology would be like that previously described in other mosasaurids from other parts of the world.

The CGP/1/2265 muzzle unit and both SAM-PK-5265 dentary fragments supported the first part of the hypothesis by having resorption pits and replacement teeth positioned posterolingually to the functional teeth/tooth sockets. Furthermore, CT-scans of the CGP/1/2265 muzzle unit reveal vertically orientated replacement teeth in life position within the maxillae. Thus, the results support Zaher and Rieppel's (1999) argument that mosasaurids had vertically orientated replacement teeth and lizard-like of tooth development and replacement patterns.

Caldwell *et al.* (2003) used histology to show that mosasaurids had a thecodont tooth attachment condition. Histological analysis was performed on IT-1; however, IT-1 turned out to be a replacement tooth and the cementum root around which one expects to find tooth attachment tissues had not yet formed. Therefore, as suggested by Caldwell *et al.* (2003), one cannot comment on the tooth attachment condition without the assessment of the tissues associated with various methods of attachment.

The second part of the fourth hypothesis, which had to do with the tooth crown histology, is not supported. No comment could be made regarding the degree of vascularisation of the cementum because no cementum was observed. There was a thin layer of enamel surrounded by dentine, which contained incremental growth lines. However, these lines could not be used to accurately calculate the time take for a specific thickness of dentine to form as the distances between the lines were too large for them to have been deposited daily (Chinsamy et al., 2012; Owocki and Madzia, 2020).

Histology showed that the enamel of IT-1 is birefringent under polarised light. There were several distinct layers noted in the tooth enamel, the thickest of which was birefringent.

However, this birefringence cannot be used as an indicator of prismatic enamel as suggested by Cooper and Poole (1972) and Chinsamy *et al.* (2012).

SEM analysis of the enamel architecture of IT-1 supported the fifth hypothesis regarding the absence of prismatic enamel. There was no indication at any of the hierarchical levels of reptilian enamel microstructure (Sander, 2009) that the enamel of IT-1 was prismatic. Furthermore, several prismless enamel features were observed including columnar diverging/converging units, microunit enamel and compound unit enamel.

5.2.2) Fossilised bacteria in the dentine of IT-1

Colonies of cocci bacteria with smooth cell walls were identified on the dentine of tooth IT-1 during SEM analysis. Unfortunately, no diagnostic features were available to taxonomically identify the bacteria.

From the discussion presented earlier (p.137) regarding the presence of bacterial cells in the dentinal tubules, it appears that the most parsimonious explanation is that the bacteria invaded the tooth via the pulp cavity when the mosasaur was still alive. The minute size of the bacterial cells allowed them to invade the dentine via the dentinal tubules. This explains why the bacterial infection could not be detected histologically as no damage to the dentine is visible.

5.2.3) Thermoregulatory capabilities of the mosasaur and shark from Pondoland

Oxygen isotope analysis of the CGP/1/2265 mosasaur and shark tooth enamel suggest that the mosasaur could regulate its body temperature independent of the environment. Although the results were not significant, it is suggested that this could be greatly improved by having a larger sample size and by including samples from a poikilothermic fish and a known endotherm. There was scepticism around the use of *Squalicorax pristodontus* as a representative of a true ectotherm because it seems plausible that this species may also have been able to regulate its

own body temperature, as do several of its modern relatives. Despite these concerns, the mosasaur appears to demonstrate a higher body temperature than the shark in all the oxygen isotope analyses performed. It is concluded that hypothesis VI, which states that the Pondoland mosasaur (CGP/1/2265) was capable of maintaining a body temperature higher than that of the surrounding seawater, is verified by these data.

5.3) Future directions

5.3.1) Taxonomy

It is still unclear where and how mosasaurs originated in the world. The fact that most mosasaur taxa from Africa have been found in Maastrichtian–aged deposits and a lack of Early Cretaceous mosasaurid remains (see Table 1) makes it difficult to support Lingham-Soliar's (1994) suggestion that mosasaurs originated in Africa. It appears that the mosasaurids recovered from SA had dispersed there from other parts of the world. However, this could be confounded by the relative lack of fossil recovery and research, especially in the east African countries. More intensive fieldwork in central and southern Africa would undoubtedly aid in understanding the diversity, origins and dispersal of mosasaurs and other marine reptiles in and around the African continent.

Additional permission from both the Iziko Museums and the South African National Heritage Agency to perform strontium isotope dating on the SAM-PK-5265 dentary fragment could resolve some of the uncertainty around its assignment to cf. *Taniwhasaurus.* If this specimen is dated to the Maastrichtian, as is the other material from the Pondoland locality, it could indicate an incorrect diagnosis. Alternatively, if the diagnosis is correct and the specimen is Maastrichtian-aged it would extend the temporal range of the *Taniwhasaurus* genus by six

million years. If the specimen is Santonian-aged it could be the oldest representative of the genus, which could provide significant clues to its origin and dispersal.

5.3.2) Palaeobiology

The results from the investigation into the thermoregulatory capabilities of the cf. *Prognathodon* (CGP/1/2265) from Pondoland could be improved by performing additional oxygen isotope analysis on the cf. *Prognathodon* (CGP/1/2265) tooth enamel and by including contemporary poikilothermic and known endothermic representatives if these are recovered in the future. In between the poikilothermic and endothermic control groups would be a spectrum for body temperature. The position of the cf. *Prognathodon* in that spectrum would indicate its thermoregulatory capabilities. Adding more data would also improve the statistical results by increasing the sample size making it more likely to detect significant differences in body temperatures.

It would be beneficial to compare δO^{18}_{PO4} values of *Squalicorax* specimens to δO^{18}_{PO4} values of poikilothermic bony fishes from the same deposits. Testing whether these highly successful, cosmopolitan sharks were thermoregulating, as do their modern lamnid relatives, would aid in understanding the extent to which the mosasaur was able to thermoregulate, as well as provide information about the evolution of this ability in Lamniformes.

Appendix A

Diagnostic features of the six mosasaurid subfamilies (see Chapter 1, Section 1.1.1)

Halisaurinae based on Bardet et al. (2005)

Unambiguous characters:

a) Premaxilla–maxilla sutural contact vertical anteriorly, oblique at midpoint and horizontal posteriorly.
b) Contact plane between the parietal and the supratemporal oblique.
c) Preaxial ridge extending on two-thirds of the length of the radius.
d) Tibia and fibula long and slender with slightly expanded extremities.

Ambiguous characters:

e) Dorsal median ridge borne on the anterior two-thirds of the frontal.
f) Frontal with ventral boss.
g) Parietal foramen surrounded by a ventral boss.
h) Quadrate with large infrastapedial process.
i) Coalescent infra- and suprastapedial processes of quadrate.
j) Zygosphene– zygantrum complex absent.
k) Synapophyses of the cervical vertebrae extending ventrally to the ventral surface of the centrum.
l) Fused haemal spines.

Yaguarasaurinae based on Palci et al. (2013)

a) Small- to medium-sized mosasaur.
b) Posterior end of nares does not invade frontals (i.e., lack of distinct narial emargination on frontals).
c) Jugal rami form a 90◦ angle and produce a distinct posteroventral process at their junction.
d) Quadrate alar forms a shallow concavity.
e) Medial parapet of dentary (dentary medial shelf) low.
f) Tooth roots largely exposed in medial view.
g) Dentary has a projection anterior to the first tooth (reversed in *Russellosaurus*).

Tethysaurinae based of Makadi et al. (2012)

a) Medium sized (maximum 6 meters).
b) Predental maxillary rostrum absent.
c) Premaxilla-maxilla suture ends anterior to or level with the midline of the fourth maxillary tooth.
d) Nearly straight frontoparietal suture.
e) Quadrate alar concavity shallow.
f) Elongated stapedial pit (at least three times longer than wide).
g) Quadrate distal condyle is saddle-shaped.
h) Upward deflection of quadrate distal condyle absent.
i) Mandibular glenoid formed mainly by articular.
j) Cervical synapophyses extend below ventral border of centrum.
k) Dorsoventrally compressed centra in precaudal vertebrae.
l) Two sacrals with large ribs/transverse processes subcircular/oval in cross-section.
m) Facet or ilium on tip of sacral transverse processes.
n) Very elongated (two times longer than wide) pontosaur-like caudal centra.
o) Anteroposteriorly narrow scapula.
p) Ilium with posterior iliac process with compressed dorsal end bearing longitudinal grooves and ridges.
q) Spoon-shaped prearticular process overlapping the pubis.

Tylosaurinae based on Russell (1967)

a) A large edentulous rostrum anterior to the premaxillary teeth.
b) Twelve or more maxillary and dentary teeth.
c) Cranial nerves X, XI and XII leave lateral wall of the opisthotic through a single foramen.
d) No canal in the basioccipital or basisphenoid for the basilar artery.
e) Suprastapedial process of quadrate moderately large and distally pointed.
f) Dorsal edge of the surangulars rounded and longitudinally horizontal.
g) Twenty-nine or more presacral vertebrae present.
h) Length of the presacral series less than that of the postsacral series in *Tylosaurus.*
i) Neural spines of posterior caudal vertebrae at most only slightly elongated and do not form an appreciable fin.
j) Haemal arches not fused to caudal centra.
k) Appendicular elements lack smoothly finished articular surfaces.

Plioplatecarpinae based on Russell (1967)

a) Small rostrum present or absent anterior to the premaxillary teeth.
b) Twelve or more maxillary and dentary teeth.
c) Cranial nerves X, XI and XII leave the lateral opisthotic through single foramen.
d) Canal or deep groove in the floor of the basioccipital and basisphenoid for basilar artery.
e) Suprastapedial process of the quadrate large, bluntly terminated with parallel sides.
f) Dorsal edge of surangular rounded and longitudinally horizontal.
g) Twenty-nine or less presacral vertebrae present.
h) Length of presacral series less than that of postsacral.
i) Neural spines of posterior caudal vertebrae at most only slightly elongated and do not form an appreciable fin.
j) Haemal arches usually unfused to caudal centra.
k) Appendicular elements lack smoothly finished articular surfaces.

Mosasaurinae based on Russell (1967)

a) Small rostrum present or absent anterior to premaxillary teeth.
b) Fourteen or more dentary and maxillary teeth.
c) Cranial nerve X, XI and XII leave lateral wall of opisthotic through two foramina.
d) No canal or groove in the floor of the basioccipital or basisphenoid for basilar artery.
e) Suprastapedial process of quadrate distally expanded.
f) Dorsal edge of the surangular thin lamina of bone rising anteriorly to posterior surface of the coronoid.
g) At least 31, usually 42-45 presacral vertebrae present.
h) Length of the presacral series exceeds that of the postsacral series.
i) Neural spines of posterior caudal vertebrae elongated to form finished articular surfaces.
j) Tarsus and carpus is well-ossified.

Appendix B

Generic diagnosis of *Prognathodon* modified from Russell, 1967; Lingham-Soliar and Nolf (1990) and Konishi *et al.*, 2011

Medium- to large- sized mosasaur, attaining mandible length of up to 1.5 m and estimated maximum body length of around 10 m; skull massive and proportionally large, constituting nearly 15% of total body length; first set of premaxillary teeth procumbent; premaxillary-maxillary suture short, anterior edge of external naris occurring no more posteriorly than fourth maxillary tooth; frontal short and triangular, lacking narial embayment (except for *P. saturator*); posteromedian flanges (= medial sutural flanges) of frontal broadly enclosing anteromedial portion of dorsal parietal surface (except for *P. saturator*, in which a pair of long and narrowly spaced posteromedian processes forms deep interdigitation with parietal); prefrontal bearing triangular, wing-like supraorbital process; postorbital process of parietal dorsally broadly exposed, posteriorly sloping at shallow angle; parietal postorbital process long, reaching posterolateral corner of frontal; dorsal parietal field long rectangular, laterally bounded by thin, horizontal flanges; suspensorial ramus distally bifurcate; postorbitofrontal dorsally broadly exposed; posteroventral corner of jugal lacking distinct process; supratemporal bar gently arched dorsally; parietal process of supratemporal extremely long, extending to reach midpoint of suspensorial ramus or further; suprastapedial process elongate, constituting at least 50% of quadrate height; suprastapedial process broadly fused to infrastapedial process; basioccipital bearing distinct, blind-ended opening along midline of medullary floor; coronoid deep and robust; posterior border of coronoid process meeting surangular at very shallow angle (except for *P. kianda*); 11-13 maxillary teeth; 12-15 dentary teeth; marginal teeth bicarinate; marginal teeth heterodont; pterygoid tooth count low, no more than nine; anterior pterygoid teeth large, typically

exceeding last marginal teeth in size; pterygoid teeth only bearing posterior carinae; minimum of 110 vertebrae; about 40 prepygal vertebrae; zygapophyses well developed throughout prepygal series; zygosphenes and zygantra present; hemal arch fused to caudal centrum; neural and hemal spines of terminal caudal series elongate, providing skeletal support for caudal fin; this portion of tail gently bent ventrally; scapula and coracoid semi-equal in size; humerus as long as distally wide; pectoral crest separate from glenoid condyle; pectoral and deltoid crests divided; proximal end of radius narrower than that of ulna; proximal end of ulna distinctly wider than distal end; metacarpal I broad; pubic and ischiadic tubercles well developed; femur elongate; tibia distinctly longer than fibula; astragalus 'L'-shaped; phalanges flat and elongate; and hyperphalangy absent.

References

Al-Nazhan, S. *et al.* (2014) ‘ Microorganism penetration in dentinal tubules of instrumented and retreated root canal walls. In vitro SEM study ’, *Restorative Dentistry & Endodontics*, 39(4), p. 258. doi: 10.5395/rde.2014.39.4.258.

Alazem, O. and Abramyan, J. (2019) ‘Reptile enamel matrix proteins: Selection, divergence, and functional constraint’, *Journal of Experimental Zoology Part B: Molecular and Developmental Evolution*, 332(5), pp. 136–148. doi: 10.1002/jez.b.22857.

Andrews, C.W. (1911) 'Description of a new plesiosaur (*Plesiosaurus capensis*, sp. nov.) from the Uitenhage Beds of Cape Colony', *Trustees of the South African Museum.*

Antunes, M. T. (1964). 'O Neocretácico eo Cenozóico do litoral de Angola', *Junta de Investigações do Ultramar*, Lisboa, pp. 254.

Arambourg, C. (1952) 'Les vertébrés fossiles des gisements de phosphates (Maroc-Algérie-Tunisie)'. *Notes et Mémoires du Service géologique du Maroc*, 92, pp. 1-372.

Azzarolli, A., Claudio, G. de, Ficarelli, G. and Torres, D. (1972) 'An aberrant mosasaur from the Upper Cretaceous of North Western Nigeria', *Accademia nazionale dei Lincei, Classe di Scienze fisiche, matematiche e naturali*, 52, pp. 53-56.

Bardet, N. *et al.* (2005) ‘Durophagous Mosasauridae (Squamata) from the Upper Cretaceous phosphates of Morocco , with the description of a new species of *Globidens* . Durophagous Mosasauridae (Squamata) from the Upper Cretaceous phosphates of Morocco , with description of a new’, *Netherlands Journal of Geosciences*, 83(3), pp. 167–175. doi: 10.1017/S0016774600020953.

Bardet, N. *et al.* (2005) ‘A new species of *Halisaurus* from the Late Cretaceous phosphates of Morocco, and the phylogenetical relationships of the Halisaurinae (Squamata:

Mosasauridae)', *Zoological Journal of the Linnean Society*, 143(3), pp. 447–472. doi: 10.1111/j.1096-3642.2005.00152.x.

Bardet, N. *et al.* (2010) 'Reptilian assemblages from the latest Cretaceous – Palaeogene phosphates of Morocco: from Arambourg to present time', *Historical Biology*, 22(1–3), pp. 186–199. doi: 10.1080/08912961003754945.

Bardet, N. *et al.* (2015) 'Mosasaurids (Squamata) from the Maastrichtian Phosphates of Morocco: Biodiversity, palaeobiogeography and palaeoecology based on tooth morphoguilds', *Gondwana Research*. International Association for Gondwana Research, 27(3), pp. 1068–1078. doi: 10.1016/j.gr.2014.08.014.

Bardet, N., Suberbiola, X. P. and Corral, J. C. (2006) 'A Tylosaurine Mosasauridae (Squamata) from the Late Cretaceous of the Basque-Cantabrian Region', *Estudios Geológicos*, 62(1), pp. 213–218.

Bardet, N., Suberbiola, X. P. and Jalil, N. E. (2003) 'A new mosasauroid (Squamata) from the Late Cretaceous (Turonian) of Morocco Nathalie', *Comptes rendus Palevol*, 2(8), pp. 607–616. doi: 10.1016/j.crpv.2003.09.006.

Becker, M. A. and Chamberlain, J. A. (2012) '*Squalicorax* chips a tooth: A consequence of feeding-related behavior from the lowermost navesink formation (late cretaceous: Campanian-maastrichtian) of Monmouth County, New Jersey, USA', *Geosciences (Switzerland)*, 2(2), pp. 109–129. doi: 10.3390/geosciences2020109.

Bell, J. L. and Polcyn, M. J. (2005) '*Dallasaurus turneri,* a new primitive mosasauroid from the Middle Turonian of Texas and comments on the phylogeny of Mosasauridae (Squamata)', *Geologie en Mijnbouw/Netherlands Journal of Geosciences*, 84(3), pp. 177–194. doi: 10.1017/S0016774600020965.

Bengtson, P. and Lindgren, J. (2005) ‘First record of the mosasaur *Platecarpus Cope*, 1869 from South America and its systematic implications’, *Revista Brasileira de Paleontologia*, 8(1), pp. 5–12. doi: 10.4072/rbp.2005.1.01.

Bernal, D. *et al.* (2001) ‘Review: Analysis of the evolutionary convergence for high performance swimming in lamnid sharks and tunas’, *Comparative Biochemistry and Physiology - A Molecular and Integrative Physiology*, 129(2–3), pp. 695–726. doi: 10.1016/S1095-6433(01)00333-6.

Bernard, A. *et al.* (2010) ‘Regulation of Body Temperature by Some Mesozoic Marine Reptiles’, *Science*, 328(5984), pp. 1379–1382.

Beucheat, C. A. (1988) ‘TEMPERATURE EFFECTS DURING GESTATION IN A VIVIPAROUS LIZARD’, *J. therm. Biol*, 13(3), pp. 135–142.

Błażejowski, B. (2004) 'Shark teeth from the Lower Triassic of Spitsbergen and their histology'. *Polish Polar Research*, 153-167.

Broom, R. (1912) ‘On a Species of Tylosaurus from the Upper Cretaceous Beds of Pondoland’.

Budney, L. A., Caldwell, M. W. and Albino, A. (2006) ‘Tooth socket histology in the Cretaceous snake Dinilysia , with a review of amniote dental attachment tissues’, *Journal of Vertebrate Paleontology*, 26(1), pp. 138–145.

Caldwell, M. W. *et al.* (2005) ‘An unusual tylosaurine mosasaur from New Zealand : a new skull of *Taniwhasaurus oweni* (Lower Haumurian ; Upper Cretaceous)’, *Journal of Vertebrate Paleontology*, 25(2), pp. 393–401. doi: 10.1671/0272-4634(2005)025.

Caldwell, M. W. (2007) ‘Ontogeny , anatomy and attachment of the dentition in mosasaurs (Mosasauridae : Squamata)’, (1997), pp. 687–700.

Caldwell, M. W. *et al.* (2008) 'A new species Of *Taniwhasaurus* (Mosasauridae , Tylosaurinae) from the upper Santonian-lower Campanian (Upper Cretaceous) of Hokkaido , Japan', *The Society of Vertebrate Paleontology*, 28(2). doi: 10.1671/0272-4634(2008)28.

Caldwell, M. W. and Bell, G. L. (1995) *'Halisaurus* sp. (Mosasauridae) from the Upper Cretaceous (? Santonian) of East-Central Peru , and the Taxonomic Utility of Mosasaur Cervical Vertebrae Published by : Taylor & Francis , Ltd . on behalf of The Society of Vertebrate Paleontology Stable UR', 15(3), pp. 532–544.

Caldwell, M. W., Budney, L. A. and Lamoureux, D. O. (2003) 'Histology of Tooth Attachment Tissues in the Late Cretaceous Mosasaurid *Platecarpus*', *Journal of Vertebrate Paleontology*, 23(3), pp. 622–630.

Caldwell, M. W., Bundey, L. A. and Lamoureux, D. O. (2003) 'Histology of tooth attachment tissues in the Late Cretaceous mosasaurid Platecarpus', *Journal of Vertebrate Paleontology*, 23(2), pp. 483–487. doi: 10.1671/0272-4634(2003)023.

Caldwell, M. W. and Lee, M. S. Y. (2001) 'Live birth in Cretaceous marine lizards (mosasauroids)', (July). doi: 10.1098/rspb.2001.1796.

Callison, G. (1967) 'Intercranial Mobility in Kansas Mosasaurs', *The University of Kansas Palaeontological Contributions*, (November), pp. 1–15.

Canoville, A., Thomas, D. B. and Chinsamy, A. (2014) 'Insights into the habitat of Middle Permian pareiasaurs (Parareptilia) from preliminary isotopic analyses', *Lethaia*, 47(2), pp. 266–274. doi: 10.1111/let.12056.

Carlson, S. J. (1990) 'Vertebrate Dental Structures', *Skeletal Biomineralization: Patterns, Processes and Evolutionary Trends*, 5(December), pp. 235–260. doi: 10.1007/978-1-4899-5740-5.

Carroll, R. L. and Debraga, M. (1992) ‘Aigialosaurs : Mid-Cretaceous Varanoid Lizards’, 12(1), pp. 66–86.

Casey, J. P., James, M. C. and Williard, A. S. (2014) ‘Behavioral and metabolic contributions to thermoregulation in freely swimming leatherback turtles at high latitudes’, *Journal of Experimental Biology*, 217(13), pp. 2331–2337. doi: 10.1242/jeb.100347.

Chin, K. *et al.* (2008) ‘Life in a Temperate Polar Sea: A Unique Taphonomic Window on the Structure of a Late Cretaceous Arctic Marine Ecosystem’, *Proceedings of the Royal Society B: Biological Sciences*, 275(1652), pp. 2675–2685. doi: 10.1098/rspb.2008.Published.

Chinsamy, A., Tunogllf, C. and Thomas, D. B. (2012) ‘Dental microstructure and geochemistry of *Mosasaurus hoffmannii* (Squamata: Mosasauridae) from the Late Cretaceous of Turkey’, *Bulletin de la Societe Geologique de France*, 183(2), pp. 85–92. doi: 10.2113/gssgfbull.183.2.85.

Christiansen, P. and Bonde, N. (2002) ‘A New Species of Gigantic Mosasaur from the Late Cretaceous of Israel’, *Journal of Vertebrate Paleontology*, 22(3), pp. 629–644.

Clemens, M. (2018). *An Early Late Cretaceous Nodosaur from the Marine Eagle Ford Group of North Central Texas , a Test of the Endothermy in the Mosasaurs from the Late Cretaceous of Angola , and the Ontogeny of a New Pipid Frog from the Miocene of Ethiopia*. Southern Methodist University.

Cohen, K. M., Harper, D. A. T. and Gibbard, P. L. (2018) ‘ICS International Chronostratigraphic Chart’, *International Commission on Stratigraphy*, (August).

Compagno, L. J. V (1990) ‘Relationships of the Megamouth Shark, *Megachasma pelagios* (Lamniformes: Megachasmidae), with Comments on Its Feeding Habits’, *Systematics*, 5, pp. 1–2.

Cooper, J. S. and Poole, D. F. G. (1973) 'The dentition and dental tissues of the agamid lizard, *Uromastyx*', *Journal of Zoology*, 169(1), pp. 85–100. doi: 10.1111/j.1469-7998.1973.tb04654.x.

Copeland, S. R. *et al.* (2008) 'Strontium isotope ratios (87Sr/86Sr) of tooth enamel: a comparison of solution and laser ablation multicollector inductively coupled plasma mass spectrometry methods', *Rapid Communications in Mass Spectrometry*, 22. doi: 10.1002/rcm.

Diekwisch, T. G. H. *et al.* (2009) 'Amelogenin evolution and tetrapod enamel structure', *Frontiers of Oral Biology*, 13(16), pp. 74–79. doi: 10.1159/000242395.

Dorn, P., Johnson, L. and Darby, C. (1979) 'The Swimming Performance of Nine Species of Common California Inshore Fishes', *Transactions of the American Fisheries Society*, 108(4), pp. 366–372. doi: 10.1577/1548-8659(1979)108<366:tspons>2.0.co;2.

Dortangs, R. W. *et al.* (2002) 'A large new mosasaur from the Upper Cretaceous of The Netherlands', *Geologie en Mijnbouw/Netherlands Journal of Geosciences*, 81(1), pp. 1–8. doi: 10.1017/S0016774600020515.

Elewa, A. M. T. (2002) 'Paleobiogeography of Maastrichtian to early Eocene Ostracoda of North and West Africa and the Middle East', *Micropaleontology*, 48(4), pp. 391–398. doi: 10.2113/48.4.391.

Ellis, R. (2003). *Sea dragons: predators of the prehistoric oceans*. University Press of Kansas.

Erickson (1996a) 'Daily deposition of dentine in Juvenile Alligator and assessment of tooth replacement rates using incremental line counts', *Journal of Morphology*, 228(2), pp. 189–194. doi: 10.1002/(SICI)1097-4687(199605)228:2<189::AID-JMOR7>3.0.CO;2-0.

Erickson (1996b) 'Incremental lines of von Ebner in dinosaurs and the assessment of

tooth replacement rates using growth line counts', *Proceedings of the National Academy of Sciences*, 93(25), pp. 14623–14627.

Everhart, M. (2004) 'Plesiosaurs as the food of mosasaurs; new data on the stomach contents of a *Tylosaurus proriger* (Squamata; Mosasauridae) from the Niobrara Formation of western Kansas', *The Mosasaur*, 7, pp. 41–46.

Fernandez, M. and Martin, J. E. (2009) 'Description and phylogenetic relationships of *Taniwhasaurus antarcticus* (Mosasauridae , Tylosaurinae) from the upper Campanian (Cretaceous) of Antarctica', *Cretaceous Research*. Elsevier Ltd, 30(3), pp. 717–726. doi: 10.1016/j.cretres.2008.12.012.

Fernández, M. S. and Talevi, M. (2015) 'An halisaurine (Squamata : Mosasauridae) from the Late Cretaceous of Patagonia , with a preserved tympanic disc : Insights into the mosasaur middle ear', *Comptes rendus Palevol*. Academie des sciences, 14(6–7), pp. 483–493. doi: 10.1016/j.crpv.2015.05.005.

Foffa, D. *et al.* (2018) 'The long-term ecology and evolution of marine reptiles in a Jurassic seaway', *Nature Ecology and Evolution*, (September). doi: 10.1038/s41559-018-0656-6.

Friedrich, O., Norris, R. D. and Erbacher, J. (2012) 'Evolution of middle to late Cretaceous oceans-A 55 m.y. Record of Earth's temperature and carbon cycle', *Geology*, 40(2), pp. 107–110. doi: 10.1130/G32701.1.

Gomes, M. *et al.* (2017) 'Diatom-inferred hydrological changes and Holocene geomorphic transitioning of Africa's largest estuarine system, Lake St Lucia', *Estuarine, Coastal and Shelf Science*. Elsevier Ltd, 192, pp. 170–180. doi: 10.1016/j.ecss.2017.03.030.

Gren, J. A. and Lindgren, J. (2014) 'Dental histology of mosasaurs and a marine crocodylian from the campanian (Upper cretaceous) of southern sweden: Incremental growth

lines and dentine formation rates', *Geological Magazine*, 151(1), pp. 134–143. doi: 10.1017/S0016756813000526.

Grigoriev, D. V (2013) 'Redescription of *Prognathodon Lutugini* (Squamata, Mosasauridae) Переописание *Prognathodon Lutugini* (Squamata, Mosasauridae)', 317113(3), pp. 246–261.

Harrell, L. T. J., Erez-Huerta, A. P. and Suarez, C. A. (2016) 'Endothermic mosasaurs? Possible thermoregulation of Late Cretaceous mosasaurs (Reptilia, Squamata) indicated by stable oxygen isotopes in fossil bioapatite in comparison with coeval marine fish and pelagic seabirds', 59, pp. 351–363. doi: 10.1111/pala.12240.

Harrell, T. L., Pérez-Huerta, A. and Phillips, G. (2016) 'Strontium isotope age-dating of fossil shark tooth enameloid from the Upper Cretaceous Strata of Alabama and Mississippi, USA', *Cretaceous Research*, 62, pp. 1–12. doi: 10.1016/j.cretres.2016.01.011.

Hillson, S. (2005) *Teeth*. 2nd edn, *Cambridge Manuals in Archaeology*. 2nd edn. Edited by G. Barker, E. Slater, and P. Bogucki. New York: Cambridge University Press. doi: 10.1017/CBO9780511614477.

Holmes, R. (1996) 'Plioplatecarpus Primaevus (Mosasauridae) from the Bearpaw Formation (Campanian , Upper Cretaceous) of the North American Western Interior Seaway', *The Society of Vertebrate Paleontology*, 16(4), pp. 673–687.

Houssaye, A. and Fish, F. E. (2016) 'Functional (secondary) adaptation to an aquatic life in vertebrates: An introduction to the symposium', in *Integrative and Comparative Biology*. Oxford University Press, pp. 1266–1270. doi: 10.1093/icb/icw129.

Jacobs, L. L. *et al.* (2006) 'The occurrence and geological setting of Cretaceous dinosaurs, mosasaurs, plesiosurs, and turtles from Angola', 22(1), pp. 91–110.

Jacobs, L. L. *et al.* (2009) 'Cretaceous paleogeography, paleoclimatology, and amniote biogeography of the low and mid-latitude South Atlantic Ocean', *Bulletin de la Societe Geologique de France*, 180(4), pp. 333–341. doi: 10.2113/gssgfbull.180.4.333.

Jacobs, L. L. *et al.* (2016) 'Post-Gondwana Africa and the vertebrate history of the Angolan Atlantic Coast', *Memoirs of Museum Victoria*, 74(July), pp. 343–362. doi: 10.24199/j.mmv.2016.74.24.

Jiménez-huidobro, P. *et al.* (2018) 'A new species of tylosaurine mosasaur from the upper Campanian Bearpaw Formation of Saskatchewan, Canada'. Taylor & Francis, (April). doi: 10.1080/14772019.2018.1471744.

Jiménez-Huidobro, P. A. (2016) *Phylogenetic and Palaeobiogeographical Analysis of Tylosaurinae (Squamata: Mosasauroidea)*. University of Alberta.

Jiménez-Huidobro, P. and Caldwell, M. W. (2016) 'Reassessment and reassignment of the early Maastrichtian mosasaur Hainosaurus bernardi Dollo, 1885, to *Tylosaurus Marsh,* 1872', 36(3). doi: 10.1080/02724634.2016.1096275.

Jiménez-Huidobro, P. and Caldwell, M. W. (2019) 'A new hypothesis of the phylogenetic relationships of the tylosaurinae (squamata: Mosasauroidea)', *Frontiers in Earth Science*, 7(March), pp. 1–15. doi: 10.3389/feart.2019.00047.

Jiménez-Huidobro, P., Simoes, T. R. and Caldwell, M. W. (2016) 'Re-characterization of *Tylosaurus nepaeolicus* (Cope , 1874) and *Tylosaurus kansasensis* Everhart , 2005 : Ontogeny or sympatry ? Re-characterization of *Tylosaurus nepaeolicus* (Cope , 1874) and *Tylosaurus kansasensis* Everhart , 2005 : Ontogeny or sympat', *Cretaceous Research*. Elsevier Ltd, 65(May), pp. 68–81. doi: 10.1016/j.cretres.2016.04.008.

Jiménez-Huidobro, P., Simões, T. R. and Caldwell, M. W. (2017) 'Mosasauroids from

Gondwanan Continents', *Journal of Herpetology*, 51(3), pp. 355–364. doi: 10.1670/16-017.

Kauffman, E. G. and Kesling, R. V (1960) 'An Upper Cretaceous Ammonite Bitten by a Mosasaur', *Contributions from the Museum of Paleontology*, XV(9), pp. 193–248.

Kear, B. P. (2005) 'Marine reptiles from the Lower Cretaceous (Aptian) deposits of White Cliffs, southeastern Australia: Implications of a high latitude, cold water assemblage', *Cretaceous Research*, 26(5), pp. 769–782. doi: 10.1016/j.cretres.2005.04.006.

Kearney, M. and Rieppel, O. (2006) 'An Investigation into the Occurrence of Plicidentine in the Teeth of Squamate Reptiles', *American Society of Icthyologists and Herpetologists*, (3), pp. 337–350.

Von Koenigswald, W. and Sander, P. M. (1997) 'Glossary of terms used for enamel microstructures.', in *Tooth Enamel Microstructure*, pp. 267–280.

Kolodny, Y., Luz, B. and Navon, O. (1983) 'Oxygen isotope variations in phosphate of biogenic apatites, I. Fish bone apatite-rechecking the rules of the game', *Earth and Planetary Science Letters*, 64(3), pp. 398–404. doi: 10.1016/0012-821X(83)90100-0.

Kolodny, Y. and Raab, M. (1988) 'Oxygen isotopes in phosphatic fish remains from Israel: Paleothermometry of tropical cretaceous and tertiary shelf waters', *Palaeogeography, Palaeoclimatology, Palaeoecology*, 64(1–2), pp. 59–67. doi: 10.1016/0031-0182(88)90142-3.

Konishi, T. *et al.* (2011) 'New exceptional specimens of *Prognathodon overtoni* (Sqamata, Mosasauridae) from the Upper Campanian of Alberta, Canada, and the systematics and ecology of the genus', *Journal of Vertebrate Paleontology*, 31(5).

Konishi, T. *et al*. (2012) '*Platecarpus tympaniticus* (Squamata: Mosasauridae): osteology of an exceptionally preserved specimen and its insights into the acquisition of a streamlined body shape in mosasaurs.' *J. Vert. Paleontol.* 32, pp.1313–1327.

Konishi, T. *et al.* (2012) A large mosasaurine (Squamata: Mosasauridae) from the latest Cretaceous of Osaka Prefecture (SW Japan). *Paleontological Research*, 16(2), pp.79-87.

Konishi, T. *et al.* (2016) 'A new halisaurine mosasaur (Squamata : Halisaurinae) from Japan : the first record in the western Pacific realm and the first documented insights into binocular vision in mosasaurs', *Journal of Systematic Palaeontology*. Taylor & Francis, 14(10), pp. 809–839. doi: 10.1080/14772019.2015.1113447.

Konishi, T. and Caldwell, M. W. (2009) 'New material of the mosasaur *Plioplatecarpus nichollsae* Cuthbertson et al ., 2007 , clarifies problematic features of the holotype specimen', *Journal of Vertebrate Paleontology*, 25(2), pp. 417–436. doi: 10.1671/039.029.0225.

Konishi, T., Jiménez-Huidobro, P. and Caldwell, M. W. (2018) 'The smallest-known neonate individual of Tylosaurus (Mosasauridae, Tylosaurinae) sheds new light on the tylosaurine rostrum and heterochrony', *Journal of Vertebrate Paleontology*. Taylor & Francis, 38(5), pp. 1–11. doi: 10.1080/02724634.2018.1510835.

Kornhuber, A. A. (1893) '*Carsosaurus Marchesettii*, a new fossil lacertilian from the Cretaceous formation of Karst near Komen', (July), pp. 1–18.

Leblanc, A. R. H., Caldwell, M. W. and Bardet, N. (2012) 'A new mosasaurine from the Maastrichtian (Upper Cretaceous) phosphates of Morocco and its implications for mosasaurine systematics', 32(1). doi: 10.1080/02724634.2012.624145.

Lécuyer, C. (2004) 'Oxygen Isotope Analysis of Phosphate', in de Groot, P. A. (ed.) *Handbook of Stable Isotope Analytical Techniques*. Elsevier B.V., pp. 482–496. doi: 10.1016/B978-044451114-0/50024-7.

Lécuyer, C. *et al.* (2007) 'High-precision determination of18O/16O ratios of silver phosphate by EA-pyrolysis-IRMS continuous flow technique', *Journal of Mass Spectrometry*,

42(1), pp. 36–41. doi: 10.1002/jms.1130.

Lécuyer, C. *et al.* (2013) ‘Calibration of the phosphate δ18O thermometer with carbonate-water oxygen isotope fractionation equations’, *Chemical Geology*. Elsevier B.V., 347, pp. 217–226. doi: 10.1016/j.chemgeo.2013.03.008.

Lee, M. S. Y. (1997) ‘On snake-like dentition in mosasaurian lizards’, *Journal of Natural History*, 31(2), pp. 303–314. doi: 10.1080/00222939700770151.

Lindgren, J. *et al.* (2009) ‘Skin of the Cretaceous mosasaur *Plotosaurus*: Implications for aquatic adaptations in giant marine reptiles’, *Biology Letters*, 5(4), pp. 528–531. doi: 10.1098/rsbl.2009.0097.

Lindgren, J. *et al.* (2011) ‘Landlubbers to leviathans : evolution of swimming in mosasaurine mosasaurs’, *Paleontological Society*, 37(3), pp. 445–469.

Lindgren, J., Jagt, J. W. M. and Caldwell, M. W. (2007) ‘A fishy mosasaur: The axial skeleton of Plotosaurus (Reptilia, Squamata) reassessed’, *Lethaia*, 40(2), pp. 153–160. doi: 10.1111/j.1502-3931.2007.00009.x.

Lindgren, J. and Siverson, M. (2005) *‘Halisaurus sternbergi,* a Small Mosasaur with an Intercontinental Distribution’, *Journal of Paleontology*, 79(4), pp. 763–773.

Lindgren, J., Caldwell, M.W., Konishi, T., Chiappe, L.M. (2010) 'Convergent Evolution in Aquatic Tetrapods: Insights from an Exceptional Fossil Mosasaur.' *PLoS ONE,* 5(8). doi:10.1371/journal.pone.0011998

Lindgren, J., Kaddumi, H. and Polcyn, M. (2012) 'Soft tissue preservation in a fossil marine lizard with a bilobed tail fin.' *Nat Commun,* 4(2423). doi.org/10.1038/ncomms3423

Lingham-Soliar, T., Nolf, D. (1990) 'The mosasaur Prognathodon (Reptilia, Mosasauridae) from the Upper Cretaceous of Belgium.' *Bulletin van het Koninklijk Belgisch*

Instituut voor Natuurwetenschappen.

Lingham-Soliar, T. (1991) 'Mosasaurs from the upper cretaceous of Niger', *The Palaeontological Association*, 34(3), pp. 653–670.

Lingham-Soliar, T. (1992a) 'A New Mode of Locomotion in Mosasaurs : Subaqueous Flying in *Plioplatecarpus marshi*', *The Society of Vertebrate Paleontology*, 12(4), pp. 405–421.

Lingham-Soliar, T. (1992b) 'The tylosaurine mosasaurs (Reptilia, Mosasauridae) from the Upper Cretaceous of Europe and Africa', *Bulletin de l'Institut Royal des Sciences Naturelles de Belgique: Sciences de la Terre*, 62, pp. 171–194.

Lingham-Soliar, T. (1994) 'First Record of Mosasaurs from the Maastrichtian (Upper Cretaceous) of Zaire', *Paläontolgische Zeitschrift*, 68(1), pp. 259–265.

Lingham-Soliar, T. (1996) 'The first description of Halisaurus (Reptilia Mosasauridae) from Europe, from the Upper Cretaceous of Belgium', *Bulletin - Institut Royal des Sciences Naturelles de Belgique: Sciences de la Terre*, 66(1967), pp. 129–136.

Lingham-Soliar, T. (1998) 'A new mosasaur Pluridens walkeri from the Upper Cretaceous , Maastrichtian of the Iullemmeden Basin , southwest Niger', 18(4), pp. 709–717. doi: 10.1080/02724634.1998.10011100.

Lingham-Soliar, T. (2002) 'First occurrence of premaxillary caniniform teeth in the Varanoidea : Presence in the extinct mosasaur *Goronyosaurus* (Squamata : Mosasauridae) and its functional and paleoecological implications', 35, pp. 187–190.

Liu, K. W. and Greyling, E. H. (1996) 'Grain-size distribution and cementation of the Cretaceous Mzamba Formation of Eastern Cape , South Africa : a case study of a storm-influenced offshore sequence', *Sedimentary Geology*, 107, pp. 83–97.

Longinelli, A. and Nuti, S. (1973). Revised phosphate-water isotopic temperature scale.

Earth and Planetary Science Letters, 19(3), pp. 373-376.

Longrich, N. R. (2016) 'A new species of *Pluridens* (Mosasauridae : Halisaurinae) from the upper Campanian of Southern Nigeria', *Cretaceous Research*. Elsevier Ltd, 64, pp. 36–44. doi: 10.1016/j.cretres.2016.03.013.

Makadi, L., Caldwell, M. W. and Osi, A. (2012) 'The First Freshwater Mosasauroid (Upper Cretaceous , Hungary) and a New Clade of Basal Mosasauroids', *PLoS ONE*, 7(12), pp. 1–16. doi: 10.1371/journal.pone.0051781.

Mao, F., Wang, Y. and Meng, J. (2015) *A systematic study on tooth enamel microstructures of Lambdopsalis bulla (multituberculate, mammalia) - Implications for multituberculate biology and phylogeny*, *PLoS ONE*. doi: 10.1371/journal.pone.0128243.

Martin, J. E. and Fernandez, M. (2007) 'The synonymy of the Late Cretaceous mosasaur (Squamata) genus *Lakumasaurus* from Antarctica with Taniwhasaurus from New Zealand and its bearing upon faunal similarity within the Weddellian Province', *Geological Journal*, 42(January), pp. 203–211. doi: 10.1002/gj.

Massare, J. A. (1987) 'Tooth Morphology and Prey Preference of Mesozoic Marine Reptiles', *Journal of Vertebrate Paleontology*, 7(2), pp. 121–137.

Massare, J. A. (1988) 'Swimming Capabilities of Mesozoic Marine Reptiles : Implications for Method of Predation', *Paleobiology*, 14(2), pp. 187–205.

Mateus, O. *et al.* (2011) 'Cretaceous amniotes from Angola : dinosaurs, pterosaurs , mosasaurs , plesiosaurs , and turtles Amniotas cretácicos de Angola : dinosaurios , pterosaurios , mosasaurios , plesiosaurios y tortugas', *Actas de V Jornadas Internacionales sobre Paleontología de Dinosaurios y su Entorno*.

Mateus, O. *et al.* (2019) 'The Fossil Record of Biodiversity in Angola Through Time : A

Paleontological Perspective : Science & Conservation : A Modern Synthesis Chapter 4 The Fossil Record of Biodiversity in Angola Through Time : A Paleontological Perspective', (January). doi: 10.1007/978-3-030-03083-4.

Maxwell, E. E. and Caldwell, M. W. (2003) 'First record of live birth in Cretaceous ichthyosaurs: Closing an 80 million year gap', *Proceedings of the Royal Society B: Biological Sciences*, 270(SUPPL. 1), pp. 104–107. doi: 10.1098/rsbl.2003.0029.

Maxwell, E. E., Caldwell, M. W. and Lamoureux, D. O. (2011) 'Tooth histology in the cretaceous ichthyosaur *Platypterygius australis*, and its significance for the conservation and divergence of mineralized tooth tissues in amniotes', *Journal of Morphology*, 272(2), pp. 129–135. doi: 10.1002/jmor.10898.

McArthur, J. M., Howarth, R. J. and Shields, G. A. (2012) 'Strontium Isotope Stratigraphy', *The Geologic Time Scale 2012*, 1–2, pp. 127–144. doi: 10.1016/B978-0-444-59425-9.00007-X.

McGowran, B. and Moore, A. C. (1971) 'A Reptilian Tooth and Upper Cretaceous Microfossils from the Lower Quarry at Needs Camp, South Africa', *African Journal of Geology*, 74(2), pp. 103–105.

Motani, R. (2010). 'Warm-blooded "sea dragons"?', *Science*, 328(5984), 1361-1362.

Novas, F. E. *et al.* (2002) '*Lakumasaurus antacticus ,* n . gen . et sp ., a new mosasaur (Reptilia , Squamata) from the Upper Cretaceous of Antarctica', *Rev. Asoc. Paleontol. Argent*, 39(2), pp. 245–249.

Owen, R. (1845) *Odontography, or, a treatise on the comparative anatomy of the teeth, their physiological relations, mode of developement, and microscipic structure, in the vertebrate animals*, *Oxford University*. London: Bailliere.

Owocki, K. and Madzia, D. (2020) 'Predatory behaviour in mosasaurid squamates inferred from tooth microstructure and mineralogy', *Cretaceous Research*. Elsevier Ltd, 111. doi: 10.1016/j.cretres.2020.104430.

Palci, A., Caldwell, M. W. and Papazzoni, C. A. (2013) 'A new genus and subfamily of mosasaurs from the Upper Cretaceous of northern Italy', *Journal of Vertebrate Paleontology*, 33(3), pp. 599–612. doi: 10.1080/02724634.2013.731024.

Páramo-Fonseca, M. E. (2000) '*Yaguarasaurus columbianus* (Reptilia , Mosasauridae), a Primitive Mosasaur from the Turonian (Upper Cretaceous) of Colombia', *Historical Biology*, 14(1), pp. 121–131. doi: 10.1080/10292380009380560.

Pearce, J. (2012) 'Control, politics and identity in the Angolan civil war', *African Affairs*, 111(444), pp. 442–465. doi: 10.1093/afraf/ads028.

Petters, S. W. (1978) 'Maastrichtian-Paleocene Foraminifera from NW Nigeria and their Paleogeography', *Acta Palaeontologica Polonica*, 23(2), pp. 131–154.

Polcyn, M. J. *et al.* (2008) 'The oldest North American mosasaurs (Squamata: Mosasauridae) from the Turonian (Upper Cretaceous) of Kansas and Texas with comments on the radiation of major mosasaur clades', *Proceedings of the Second Mosasaur Meeting*, pp. 137–155.

Polcyn, M. J. *et al.* (2010) 'The North African Mosasaur *Globidens phosphaticus* from the Maastrichtian of Angola', *Historical Biology*, 22(1), pp. 175–185. doi: 10.1080/08912961003754978.

Polcyn, M. J. *et al.* (2012) 'Description of new specimens of *Halisaurus arambourgi* BARDET & PEREDA SOBERBIOLA , 2005 and the relationships of halisaurinae', *Bulletin de la Societe Geologique de France*, 183(2), pp. 123–136. doi: 10.2113/gssgfbull.183.2.123.

Polcyn, M. J. *et al.* (2014) 'Physical drivers of mosasaur evolution', *Palaeogeography, Palaeoclimatology, Palaeoecology*. Elsevier B.V., 400, pp. 17–27. doi: 10.1016/j.palaeo.2013.05.018.

Polcyn, M. J. and Bell, J. L. (2005) '*Russellosaurus coheni* n. gen., n. sp., a 92 million-year-old mosasaur from Texas (USA), and the definition of the parafamily Russellosaurina', *Geologie en Mijnbouw/Netherlands Journal of Geosciences*, 84(3), pp. 321–333. doi: 10.1017/S0016774600021107.

Pucéat, E. *et al.* (2010) 'Revised phosphate-water fractionation equation reassessing paleotemperatures derived from biogenic apatite', *Earth and Planetary Science Letters*. Elsevier B.V., 298(1–2), pp. 135–142. doi: 10.1016/j.epsl.2010.07.034.

Ramos, F. C., Wolff, J. A. and Tollstrup, D. L. (2004) 'Measuring 87Sr/86Sr variations in minerals and groundmass from basalts using LA-MC-ICPMS', *Chemical Geology*, 211(1–2), pp. 135–158. doi: 10.1016/j.chemgeo.2004.06.025.

Reguero, M. *et al.* (2019) 'A pathological scapula in a mosasaur from the upper Maastrichtian of Antarctica : Evidence of infectious arthritis and spondyloarthropathy', 100, pp. 1–4. doi: 10.1016/j.cretres.2019.03.024.

Rey, K. *et al.* (2017) 'Oxygen isotopes suggest elevated thermometabolism within multiple permo-triassic therapsid clades', *eLife*, 6, pp. 1–25. doi: 10.7554/eLife.28589.

Rogers, A. W. and Schwarz, E. H. L. (1902) 'Annual Report of the Geological Commission 1900'.

Le Roux, P. J. (2010) 'Lithium isotope analysis of natural and synthetic glass by laser ablation MC-ICP-MS', *Journal of Analytical Atomic Spectrometry*, 25(7), pp. 1033–1038. doi: 10.1039/b920341a.

Rubilar-Rogers, D. *et al.* (2016) '*Kaikaifilu hervei* gen. et. sp. nov., a new large mosasaur (Squamata , Mosasauridae) from the upper Maastrichtian of Antarctica', *Cretaceous Research*, 70, pp. 209–225. doi: 10.1016/j.cretres.2016.11.002.

Russell, D. a (1967) *Systematics and Morphology of American Mosasaurs*, *Bulletin 23 of the Peabody Museum of Natural History Yale University*. New Haven, Connecticut.

Sander, P. M. (2009) 'Prismless enamel in amniotes: terminology, function, and evolution', *Development, Function and Evolution of Teeth*, (January 2000), pp. 92–106. doi: 10.1017/cbo9780511542626.007.

Schulp, A. S. *et al.* (2008) 'a New Species of *Prognathodon* (Squamata , Mosasauridae) From the Maastrichtian of Angola , and the Affinities of the Mosasaur Genus Liodon', *3 Proceedings of the Second Mosasaur Meeting Fort Hays Studies Special Issue*, 1853(May 2014), pp. 1–12.

Schulp, A. S. *et al.* (2013) 'Two rare mosasaurs from the Maastrichtian of Angola and the Netherlands', *Netherlands Journal of Geosciences*, 92(1), pp. 3–10. doi: 10.1017/S001677460000024X.

Schulp, A. S., Bardet, N. and Bouya, B. (2009) 'A new species of the durophagous mosasaur *Carinodens* (Squamata, Mosasauridae) and additional material of *Carinodens belgicus* from the Maastrichtian phosphates of Morocco', *Geologie en Mijnbouw/Netherlands Journal of Geosciences*, 88(3), pp. 161–167. doi: 10.1017/S0016774600000871.

Scotese, C. R. (2014) 'Atlas of Late Cretaceous Maps, PALEOMAP Atlas for ArcGIS, volume 2, The Cretaceous, Maps 16 – 22, Mollweide Projection, PALEOMAP Project, Evanston, II.', *PALEOMAP Project, Evanston, IL.*, 2(October). doi: 10.13140/2.1.4691.3284.

Shimada, K. and Cicimurri, D. J. (2005) 'Skeletal anatomy of the Late Cretaceous shark,

Squalicorax (*Neoselachii: Anacoracidae*)', *Paläontologische Zeitschrift*, 79(2), pp. 241–261. doi: 10.1007/bf02990187.

Simões, T. R. *et al.* (2017) 'Mosasauroid phylogeny under multiple phylogenetic methods provides new insights on the evolution of aquatic adaptations in the group', *PLoS ONE*, 12(5), pp. 1–20. doi: 10.1007/s11663-018-1204-0.

Solé, F. *et al.* (2019) 'Reassessment of historical sections from the Paleogene marine margin of the Congo Basin reveals an almost complete absence of Danian deposits', *Geoscience Frontiers*. Elsevier Ltd, 10(3), pp. 1039–1063. doi: 10.1016/j.gsf.2018.06.002.

Soliar, T. (1988) 'The Mosasaur Goronyosaurus from the Upper Cretaceous of Sokoto State, Nigeria', *Palaeontology*, pp. 747–762.

Stern, D. N. and Crompton, A. W. (1995) 'A study of enamel organization, from reptiles to mammals', *Aspects of dental biology: palaeontology, anthropology and evolution*, (January), pp. 1–25.

Sternberg, C. H. (1918) 'Explorations of the Permian of Texas and the Chalk of Kansas, 1918', *Transactions of the Kansas Academy of Science*, 30(April 1919-Feb 1921), pp. 119–120.

Stewart, R. F. and Mallon, J. (2018) 'Allometric growth in the skull of *Tylosaurus proriger* (Squamata: Mosasauridae) and its taxonomic implications', *Vertebrate Anatomy Morphology Palaeontology*, 6, p. 75. doi: 10.18435/vamp29339.

Street, H. P. and Caldwell, M. W. (2017). Rediagnosis and redescription of *Mosasaurus hoffmannii* (Squamata: Mosasauridae) and an assessment of species assigned to the genus *Mosasaurus. Geological Magazine*. doi: 10.1017/S0016756816000236.

Strong, C.R.C. Caldwell, M.W., Konishi, T. and Palci, A. (2020) 'A new species of longirostrine plioplatecarpine mosasaur (Squamata: Mosasauridae) from the Late Cretaceous of

Morocco, with a re-evaluation of the problematic taxon '*Platecarpus' ptychodon*', *Journal of Systematic Palaeontology,* 18(21), pp.1769-1804. doi: 10.1080/14772019.2020.1818322

Susela, Z. (2014) *Stratigraphy and sedimentology of the Mzamba Formation in the Eastern Cape*.

Torii, S. (1998) 'Origin of enamel prisms and Hunter-Schreger bands in reptilian enamel', *Connective Tissue Research*, 38(1–4), pp. 45–51. doi: 10.3109/03008209809017019.

University of KwaZulu-Natal (n.d) ' KwaZulu-Natal Geological Map and Cross Sections', *Geology Education Museum.* Viewed 2 June 2020 at www.stec.ukzn.ac.za/GeologyEducationMuseum/KZNGeology/KZNGeologyMap.aspx

Veizer, J. *et al.* (1999) '87Sr/86Sr, δ13C and δ18O evolution of Phanerozoic seawater', *Chemical Geology*. Elsevier Science B.V., 161(1), pp. 59–88. doi: 10.1016/S0009-2541(99)00081-9.

Vinther, J. (2016) 'Fossil melanosomes or bacteria? A wealth of findings favours melanosomes: Melanin fossilises relatively readily, bacteria rarely, hence the need for clarification in the debate over the identity of microbodies in fossil animal specimens J. Vinther', *BioEssays*, 38(3), pp. 220–225. doi: 10.1002/bies.201500168.

Visser, I. N. *et al.* (2010) 'First record of predation on false killer whales *(Pseudorca crassidens)* by killer whales (*Orcinus orca*)', *Aquatic Mammals*, 36(2), pp. 195–204. doi: 10.1578/AM.36.2.2010.195.

Webb, P. W. (1982) 'Locomotor Patterns in the Evolution of Actinopterygian Fishes ' body form pertinent to locomotor me- (a) a recurring fusiform carnivore-type ysis of locomotor patterns in actinopte- patterns can be discussed under two cate-', *Society*, 342 (December 1980), pp. 329–342.

Westall, F. *et al.* (2001) ‘Early archean fossil bacteria and biofilms in hydrothermally-influenced sediments from the Barberton greenstone belt, South Africa’, *Precambrian Research*, 106(1–2), pp. 93–116. doi: 10.1016/S0301-9268(00)00127-3.

Whitenack, L. B. and Motta, P. J. (2010) ‘Performance of shark teeth during puncture and draw: Implications for the mechanics of cutting’, *Biological Journal of the Linnean Society*, 100(2), pp. 271–286. doi: 10.1111/j.1095-8312.2010.01421.x.

Wiffen, J. (1980) ‘Moanasaurus , a new genus of marine reptile (Family Mosasauridae) from the Upper Cretaceous of North Island , New Zealand’, 8306. doi: 10.1080/00288306.1980.10424122.

Wiffen, J. (1990) ‘New mosasaurs (reptilia; family mosasauridae) from the upper cretaceous of North Island, New Zealand’, *New Zealand Journal of Geology and Geophysics*, 33(1), pp. 67–86. doi: 10.1080/00288306.1990.10427574.

Willey, J. M., Sherwood, L. M. and Woolverton, C. J. (2014) *Prescott’s Microbiology*. 9th edn, *Journal of Microbiology & Biology Education*. 9th edn. New York: McGraw-Hill. doi: 10.1128/jmbe.v11.i1.154.

Williston, S. W. (1904) ‘The relationships and habits of the mosasaurs’, *Journal of Geology*, 12(1), pp. 43–51.

Wright, C. I., Miller, W. R. and Cooper, J. A. G. (2000) ‘The Late Cenozoic evolution of coastal water bodies in Northern Kwazulu-Natal, South Africa’, *Marine Geology*, 167(3–4), pp. 207–229. doi: 10.1016/S0025-3227(00)00032-3.

Zdansky, O. (1935) 'The occurrence of mosasaurs in Egypt and Africa in general', *Bull. Inst. Egypte,* 17, pp 83-94.

Zaher, H. and Rieppel, O. (1999) ‘Tooth Implantation and Replacement in Squamates,

with Special Reference to Mosasaur Lizards and Snakes', *American Museum of Natural History*.